The Design of a Flexible Friction-Based Transport Mechanism

A Bio-Inspired Transport Mechanism for Tissue Transport in Minimal Invasive Medical Interventions

E. P. de Kater

TU Delft

The Design of a Flexible Friction-Based Transport Mechanism

A Bio-Inspired Transport Mechanism for Tissue Transport in Minimal Invasive Medical Interventions

by

E. P. de Kater

to obtain the degree of Master of Science in Mechanical Engineering and Biomedical Engineering
at the Delft University of Technology,
to be defended publicly on Monday January 20, 2020 at 15:00.

Student number:	4315588	
Project duration:	April 15, 2019 – January 20, 2020	
Thesis supervisors:	Dr. Ir. A. Sakes	TU Delft
	Prof. Dr. Ir. P. Breedveld	TU Delft
Thesis committee:	Dr. Ir. A. Sakes	TU Delft
	Prof. Dr. Ir. P. Breedveld	TU Delft
	Ir. J. Spronck	TU Delft
	Ir. F. Trauzettel	TU Delft

This thesis is confidential and cannot be made public until January 20, 2022.

An electronic version of this thesis is available at `http://repository.tudelft.nl/`.

TU Delft

Preface

In the second last year of secondary school I was not sure what my next step would be. Studying, yes, but there were so many interesting options, so many universities and even more different studies. How could I ever be sure to make the right decision? As part of your graduation, all students had to do a project related to one of the subject they were graduating in. You could decide the topic yourself, which for me, having difficulties with decision making, was quite a challenge. I liked biology, mathematics and physics, but I also wanted to design something. In the end, instead of making a decision for one of the subjects, I just combined all the subjects in one project: The design of a solar panel that would follow the sun in a similar fashion as a sunflower does. This project was not only very challenging and fun to do, it also helped me with my first problem; deciding what to study. Without knowing it I had done a project in bio-inspired design which happened to be a masters of mechanical engineering. My path was clear again, I would do a bachelors mechanical engineering and then a masters in bio-inspired design. However during my masters, the design of medical instruments was also very interesting. Just like my final project at secondary school, I did not choose one masters, I decided to combine them both in a double degree. This combination of masters fitted perfectly for this graduation project as it combines both fields that I am most interested in: bio-inspired design and the design of a medical instrument. In the future I hope to help improve the world by working on project in which I can combine my interests once again. So far this combination of different interests has led to great projects that will hopefully increase the gross national happiness.

E. P. de Kater
Delft, December 2019

Abstract

Background: During minimally invasive procedures, tissue damage can be limited by using smaller incisions and by using naturally occurring body orifices to reach the intervention site. During these procedures the need can arise to transport tissue. Think of a biopsy or the removal of polyps. This calls for a tool that can transport tissue and is also flexible such that the tool can be introduced via natural occurring body orifices. Currently either suction based techniques or forceps are used for these procedures. However, both show sub-optimal behaviour. Friction-based transport, which is based on the egg laying principle of parasitoid wasps, is not prone to these sub-optimal behaviour modes but is not yet used in flexible systems. **Methods:** A mechanical analysis was conducted to generate an overview of the challenges that arise in flexible friction-based transport. This resulted in a list of requirements based on which possible concept solutions were analysed. The most promising design for a flexible friction-based transport mechanism has a flexible shaft that consists of a number of wire ropes in combination with ring magnets. This shaft was manufactured and validated by transporting gelatin tissue phantoms with different material properties with the shaft in straight and in a curved position. After validation of the flexible shaft, an ergonomic handle was designed resulting in the final prototype. This final prototype was also tested by transporting gelatin tissue phantoms. **Results:** From the results can be concluded that the flexible shaft is able to transport tissue phantoms with different material properties while in straight and curved (R=59mm) position. The final prototype is showed that continuous transport was possible from the tip of the flexible shaft to the end of the handle with the shaft in straight and in curved position. The position of the shaft (straight vs. curved) did not result in a significant difference in the transport rate. **Discussion and Conclusion:** It can be concluded that friction-based transport is possible in a flexible tool. The mean transport rate in straight position (2.3 ± 0.29 mm/cycle) is comparable to the transport rate of a rigid friction-based transport mechanism with comparable dimensions. This new flexible friction-based transport mechanism shows great potential to be beneficial for a number of medical procedures.

Keywords

Flexible - Friction-based – Transport - Bio-inspired – Minimally invasive

Glossary

Blades: The translating parts that move is a certain sequence such that tissue can be transported trough the lumen. In the flexible friction-based transport mechanism the blades consist of 3-4 galvanised wire ropes.

Catheter: Soft tube used in medical interventions.

Degree of freedom (DoF): Number of independent parameters that define the orientation of the system.

Endovascular intervention: Medical intervention that is performed by reaching the intervention site by introducing the tools through the blood vessel system.

Final prototype: The newly designed flexible friction-based transport mechanism consisting of a flexible shaft and a handle that allows the used to employ the transport mechanism by continuously rotating the sling.

Flexible shaft: The flexible part of the newly designed flexible friction-based transport mechanism. Through the flexible shaft tissue can be transported in a friction-based manner.

Friction-based transport: Transport method based of friction that is inspired by the egg-laying principle of the parasitoid wasp. Substances can be transported trough a tubular structure that is formed formed by a number of blades by small translating motions of these blades in a certain sequence.

Laparoscopic procedure: Medical intervention that is performed by targeting the intervention site by introducing the tools via small incisions. Also known as key hole surgery or minimal invasive surgery.

Lumen: Inside space of a tubular structure. In the case of the flexible friction-based transport mechanism the lumen is the space formed by the blades through which the tissue is transported.

Morcellator: Surgical instrument that separates tissue for easy transport during laparoscopic interventions.

Ovipositor: Tubular organ through which eggs are transported. Insects that lay their eggs in hard materials such as wood, use the ovipositor to drill in the wood.

Research prototype: The prototype consisting of the flexible shaft and a cone-structure that is used to validate the performance of the flexible shaft.

Rigid friction-based transport mechanism: The endo-tubular friction carrier designed by I. van de Steeg [17]. This rigid laparoscopic device uses friction-based transport to be able to transport tissue.

Tissue: A cellular organism. Multiple tissues together form a organ. There are four main types of tissue: epithelial, connective, muscular and nervous tissue.

Contents

1 Introduction

1.1. Background

1.1.1. Transport mechanisms in nature

The transport of goods and substances is of vital importance in everyday life. Not only in man-made machines but also in nature the transport of resources is of great importance. Life is not possible without the intake of food, water and air, the distribution of these resources and the excretion of waste products. An example of such a transport mechanism is the in- and outflow of air during respiration in mammals. The in- and outflow of air is realised by volume changes in the lungs. Such transport mechanisms in nature can be used as a source of inspiration when designing new transport mechanisms. For example, the transport mechanism used during breathing, is also used in man-made pistons. Furthermore, roller pumps that transport fluids through tubes by compression of the wall, show a similar working principle as occurs during peristalsis; a widely used transport method to move substances through tubular organs. There are, however, also a number of transport methods in nature that are not yet commonly used in industry, but might result in a more efficient man-made transport mechanism. An example is the transport method used by wasps to transport their eggs. Parasitic wasps transport their eggs through a long tubular structure called the ovipositor using friction modulation. The mechanism used by these wasps is not widely used in man-made transport mechanisms and could, therefore, be an interesting mechanism to explore for transport of substances through man-made tubular structures.

Transport mechanism of the wasp ovipositor

Wasps have a special body part, the ovipositor, that allows them to lay eggs in a variety of materials [2], [4]. The materials range from vegetable materials, such as tree bark or leaves, to living hosts. The ovipositor generally consists of two ventral valves and two dorsal valves that are fused together, see Figure 1.1. The two ventral valves and the fused dorsal valve can slide over one another. Together the valves form the oviduct; the duct through which the eggs are transported. The surface of the oviduct is covered with small scales that are hypothesised to provide a rough surface that aids the movement of the egg through the oviduct [4]. Surrounding the valves is the ovipositor sheath; a flexible structure. During oviposition the ovipositor is extended, and becomes slightly unsheathed [2]. The eggs are transported through the oviduct by sliding the valves back and forward with respect to one other [2], [4].

The exact motion of the valves during transport of the eggs along the ovipositor is not fully known but the following motion sequence is hypothesised. 1) All the valves move distally simultaneously. Due to the friction between the egg and the oviduct wall, the egg will move in the distal direction, along with the valves, see Figure 1.2 A. 2) Once the valves have reached their most distal position, they will alternately (one by one) move back to their proximal position, see Figure 1.2 B. It is hypothesised that the orientation of the scales that cover the oviduct results in anisotropic friction between the egg and the valves, preventing the backwards motion of the egg. Instead, the scales and friction with the two static valves hold the egg in place while the other valve moves proximally, see Figure 1.2 C and D. 3) This cycle is repeated until the egg reaches the tip of the ovipositor. The wasp can, during the oviposition, slightly bend the ovipositor for repositioning [2].

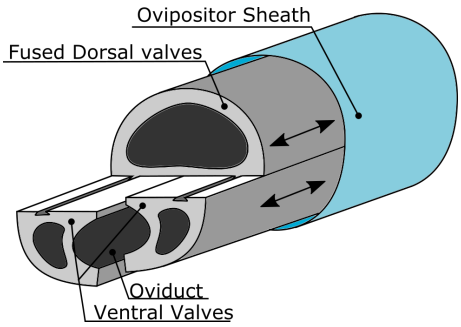

Figure 1.1: Schematic representation of an ovipositor. The fused dorsal valves and the two ventral valves can slide with respect to one other.

Though the working principle of the ovipositor is similar in different insects, there are slight differences between the characteristics of the ovipositor, depending on the host material in which the eggs are deposited [4]. The ovipositors of parasitic insects have a smaller diameter, most likely to limit injury to the host. The eggs of these species are elongated to fit through the small oviduct, which results in high stresses in the valves during the transport of the eggs. To withstand these high stresses, the valves of the ovipositors of parasitic insects are more closely interlocked [4]. Insects that oviposit in clay, or other soft material, have ovipositor valves that are less closely interlocked, as the stresses occurring during oviposition are lower [4].

1.1.2. Ovipositor inspired transport mechanism

Rigid friction-based transport

The mechanism used to transport eggs along the ovipositor has interesting features that could be beneficial in man-made transport mechanisms. The egg is isolated from its surroundings during transport. Depending on the application of the transport mechanism, this isolation can be a big advantage. Furthermore, the valves of the ovipositor only make small movements, while the egg can be transported over a much longer distance. In the master thesis of I. van de Steeg [17] the development of the endo-tubular friction-based carrier is discussed. This transport mechanism that is intended to be used during laparoscopic medical procedures, is based on the wasp ovipositor. As in the ovipositors of wasps, the transport is friction-based and uses small movements of blades that function in a similar fashion as the valves in the wasp ovipositor. The transport mechanism is designed in such a way that the tissue is isolated from its surroundings during transport. In the thesis of I. van de Steeg it is shown that friction-based transport has the potential of becoming a reliable means of transport compared to the transport mechanism commonly used during laparoscopic procedures [17]. From now on the endo-tubular friction carrier will be referred to as the 'rigid friction-based transport mechanism'.

Working principle of rigid friction-based transport mechanism

The rigid friction-based transport mechanism described, consists of six blades surrounding the central circular lumen, see Figure 1.3 A. The blades are in contact with the tissue and are held together by the outer tube. The blades function as the valves of the ovipositor. Where the valves of the wasp ovipositor have scales that provide the required friction difference, the rigid friction-based transport mechanism uses the difference in contact area to create the required friction difference. The contact area is an indicator for the generated friction, assuming at least one of the surfaces is not rigid. By moving the blades in a certain sequence, the resulting friction causes the transported tissue to move uni-directionally. The blades are actuated by an axially rotating motor. The axially rotating motion of the motor is transformed to an axially translating motion of the blades by a barrel cam. Depending on the design of cam used, the motion sequence of the blades can be altered. The six blades can be actuated in such a way that five blades move forward and one moves backwards. The friction between the blades and the transported tissue cause the tissue to be transported along with the five forward moving blades, as these have in total a larger contact surface. It is also possible to change the cam in such a way that four blades move forward while two blades move backwards. The forward moving blades will still have a larger surface, resulting in the tissue moving forward.

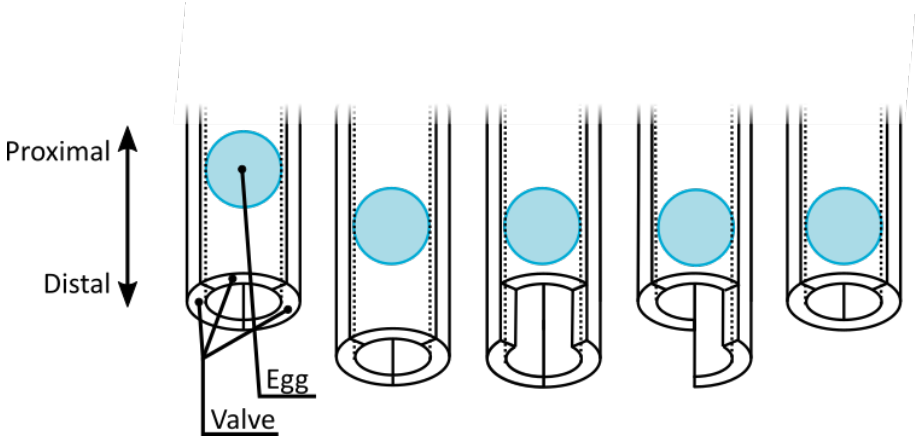

Figure 1.2: Schematic representation of the movement of the valves during oviposition. Scales cover the walls of the valves that form the oviduct. The orientation of the scales generate higher friction between the egg moving proximally with respect to the valve than the egg moving distal with respect to the valve. to motion sequence of the valves during oviposition is assumed to be as follows. The valves move distally. Due to the friction between the egg and the walls of the valves introduced by the scales, the egg is transported along with the valves. once the valves reach their most distal position, one of the valves start to move proximally. The scales prevent the egg from moving along with this single moving valve. Instead the egg remains stationary. Subsequently, the other valves will move proximally one-by-one, while the egg will again be prevented from moving along with the moving valve, due to the scales.

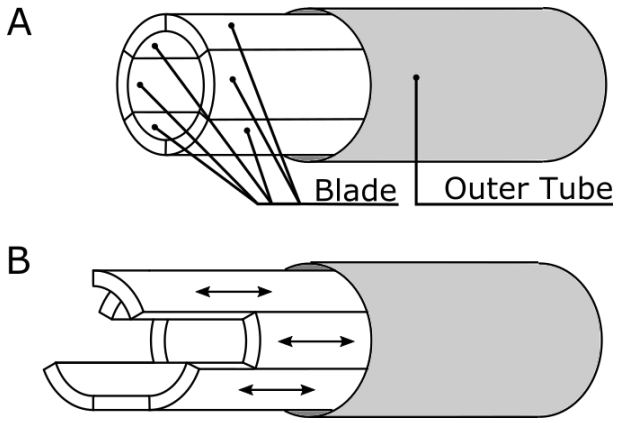

Figure 1.3: Schematic representation of the rigid friction-based transport mechanism. A: The rigid friction-based transport mechanism consists of six blades that can slide with respect to each other and an outer tube that keeps the blades together. B: the blades make translating motions. Depending on the sequence of the blades tissue can be transported forward or backwards through the tubular mechanism.

Application of the rigid friction-based transport mechanism

The rigid friction-based transport mechanism is intended to be used in the medical field during Minimally Invasive Surgery (MIS). During MIS, an instrument enters the body via a small incision. Compared to the conventional open surgery, in which a big incision is used, MIS is associated with a faster recovery of the patient and a lower mortality [12]. Since the instrument is introduced via a small incision, the tip of the instrument is not at the place where the intervention is needed. To bridge the distance between the incision and the intervention site, laparoscopic instruments often have a rigid and slender shaft. The rigid friction-based transport mechanism also has this typical slender shaft, similar to other laparoscopic surgery tools.

1.1.3. Current transport mechanisms used in the medical field

During MIS, tissue damage is limited by using slender surgical tools that are introduced via a small incision. To limit tissue damage it is, for some procedures, possible to use natural body orifices to reach the target site. For example during endovascular procedures, the procedure site is reached via the vascular system. For these kind of procedures, the surgical tools used need a certain degree of flexibility to be able to move trough these natural occurring body-orifices. Currently when tissue needs to be removed during these interventions, either suction is used, or the tissue parts are grasped and are subsequently removed. Each of the currently

used transport mechanisms will be discussed.

Transport by suction

A catheter is a tubular medical device that is inserted in a body cavity, vessel or duct to deliver or drain liquids and gases. Transport through an aspiration catheter happens based on pressure difference (suction). Some fluids can be transported by relatively low pressure differences. A problem associated with transport of solids or highly viscous fluids is that bigger pressure differences are required to transport the substance. This pressure difference can potentially damage healthy surrounding tissue, due to the stresses that are applied on this surrounding tissue. Furthermore, the catheter can get clogged making further transport impossible. One of the great advantages of aspiration catheters is that they can be made with a high flexibility, which makes it is possible to use them for procedures such as endo-vascular interventions.

Transport by grasping

Solid structures can be transported by the use of forceps. The to be transported part is grasped with the forceps and can subsequently be transported by moving the forceps. This method can be used to transport solid parts, but liquids and gasses cannot be grasped and can, therefore, not be transported this way. Also, only one part can be transported at the time. Therefore, the transport is relatively slow when multiple parts have to be transported. Also using the forceps multiple times for the transport of different tissue parts can lead to contamination. Another problem that can occur during transport is that the transported tissue slips from the forceps. The part must be grasped again leading to an increase in transport time. There are also advantages of transport by forceps. This transport method is, in contrast to the aspiration catheter, not prone to clogging.

1.1.4. Friction-based transport compared to current systems

It is thought that the rigid friction-based transport mechanism could be used as an alternative for the currently used transport mechanisms during MIS. Each of the currently used transport methods is associated with sub-optimal functioning modes. For example, aspiration has the disadvantage that the required pressure difference can potentially damage surrounding healthy tissue. By using friction-based transport mechanisms, as is the case in the rigid friction-based transport mechanism, this problem is resolved. Furthermore, the substances can be transported continuously and it is possible to transport multiple pieces at the same time. This makes the transport of the rigid friction-based transport mechanism faster than the conventional grasping devices. The use of the rigid friction-based transport mechanism can thus eliminate a number of the sub optimal functioning modes that are present in the transport systems that are currently used. However, one limiting factor of the rigid friction-based transport mechanism is the fact that the mechanism is rigid. Therefore, it cannot be used for minimally invasive procedures that used natural existing orifices such as endo-vascular procedures. A device with both the advantages of friction-based transport while still having the flexibility of the aspiration catheter is not yet existing.

1.2. Goal

The goal of this study is to design, manufacture and test a flexible friction-based transport mechanism inspired by the ovipositor of the wasp. The transport mechanism will consist of a handle and a flexible shaft through which tissue can be transported in a friction-based manner. The transport mechanism is intended to be used in the medical field to transport tissue during MIS. Friction-based transport eliminate sub-optimal behaviour present in the now used transport mechanism in medical devices. Adding flexibility to friction-based transport mechanism has not been done before and would allow this device to be used in a broader range of applications.

1.3. Content

This report will start with a mechanical analysis in which the challenges are identified that arise during friction-based transport especially when the mechanism has to be flexible. First there will be focused on the design and validation of the flexible shaft. In Chapter 3, a description of the design process is given, in which first the requirements for the flexible shaft are set, followed by a concept generation and a description of the final chosen concept. In Chapter 4, the experimental set-up that is used to validate the newly designed flexible shaft will be discussed and in Chapter 5, the results of the experiments will be presented. In Chapter

6, the design and validation of the final prototype will be discussed. This final prototype consists of the already validated flexible shaft with a handle that is newly designed. This report will end with a discussion and conclusion in Chapter 7 and Chapter 8. respectively.

2

Mechanical Analysis flexible friction-based transport

In this chapter the challenges of flexible friction-based transport will be discussed. First, in Section 2.1, the challenges that arise by friction-based transport will be discussed. These challenges are primarily based on observation of rigid friction-based transport mechanism as described by I. A. van de Steeg [17]. In Section 2.2 the challenges that might arise by adding flexibility to a friction-based transport mechanism will be discussed.

2.1. Challenges friction-based transport

2.1.1. Challenges associated with the transported tissue

A to-be-transported tissue has one of the following phases: gas, liquid or solid. Friction between the transported tissue and the blades is what makes friction-based transport possible. Friction is not fully understood on microscopic level. Based on experimental data it is suggested that the origin of friction is the formation and rupture of microscopic bonds at contact points between the two surfaces [7]. Two perfectly rigid surfaces in 2D would only have two contact points, see Figure 2.1 A. If one or both surfaces are not fully rigid, the number of contact points will increase, see Figure 2.1 B. This increase in contact surface will lead to the formation of more micro-bonds, and will increase the friction. The blades of the transport mechanism are assumed to be fully rigid. The transported tissue must not be fully rigid, to generate the needed friction. It would however be possible to transport rigid solid particles that are surrounded by a non-rigid tissue. The surrounding tissue can be transported causing the solid particles to move along with the surrounding tissue.

Friction can also occur between a liquid and a solid. In such a case the friction is depended on the characteristics of the fluid, such as the viscosity. The viscosity of a liquid indicates how 'fluid' the liquid is. Liquids with a high viscosity (such as honey) are less fluid and flow more slowly than very fluid liquids (such as water). A higher viscosity means there is a higher resistance to flow. For Newtonian fluids the viscosity is independent of the shear rate. This is not the case for Non-Newtonian fluids, such as blood and saliva, as their viscosity

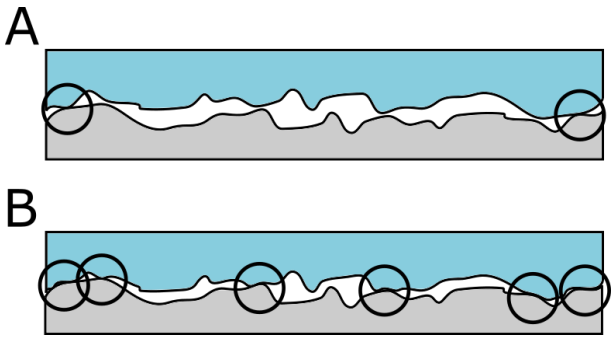

Figure 2.1: Schematic representation of the contact point between two solids. A: To completely rigid solids will only have two contact point in 2D. B: If at least one of the two solids is somewhat elastic, there will be more contact points, leading to more friction between the two solids.

is dependent on the applied shear rate. These non-Newtonian fluids can either be shear thickening or shear thinning. The viscosity of shear thickening fluids increases with the application of shear rate. The opposite is the case for shear thinning fluids. Transporting a non-Newtonian fluid by friction can be challenging. The translating motion of the blades will introduce a shear rate in the transported material and will, therefore, influence the viscosity of the material. A challenge that can arise when transporting a liquid is the leaking of the tissue between the blades, as shown in Figure 2.2. This leads to more friction between the blades and will, therefore, impede the blade movement and thus harm the transport. Gasses cannot be transported with a friction-based transport mechanism as gasses flow very easily, and will not generate enough friction with the blades of the transport mechanism. The flexible friction-based transport mechanism is intended to be used for the transport of tissues that are highly viscous fluids and non-rigid solids. These tissues require a big pressure differential when transported with the currently used aspiration catheter which can lead to damage of surrounding tissue as the pressure differential is also applied to the surrounding tissue causing high strains.

2.1.2. Challenges associated with friction generation

Friction generation

Friction-based transport uses the friction between the transported tissue and the translating blades of the mechanism. This is possible due to the difference in friction between back and forward motion. When the blades move forward a high friction between the blade and the tissue is needed. Due to this high friction, the tissue will move along with the blades. When moving the blades backwards, the tissue must not move along with the blades but move along with the other blades which are either stationary or moving forward. This is possible when the friction between the tissue and the backward moving blade is smaller than the friction between the tissue and the other blades. There are two options to create this difference in friction, see Figure 2.3. The first option is using a surface structure on the blades that leads to a higher friction in one direction that in the opposite direction. This is similar to the scales that are present in the ovipositor of a wasp, see Figure 2.3. When using this principle, a minimum of two blades is needed as one blade will move backwards while the other blade will be stationary or move forward. The second option is to create the needed friction difference by changing the contact surface between the blades and the transported tissue. Assuming that the blades have the same amount of contact surface with the transported tissue, a minimum of three blades is needed as two blades will be stationary or move forward while moving one blade backwards. Both of these options have advantages and disadvantages. The more blades, the more complicated the mechanism will become, but by using changes in contact area the Transport mechanism could be used to transport tissues in both directions, by simply changing the motion sequence of the blades. This makes it possible to use the same transport mechanism to, for instance, deliver drugs, or take biopsies. The transport rate for a friction-based transport mechanism with more blades might also be lower, as each cycle of blade movements consists of more blades that subsequently have to move. Though both options have advantages and disadvantages it was chosen to focus on using changes in contact surface to generate friction differences as this principle is already known to work in the rigid friction-based transport mechanism [17].

Tissue shape

The needed friction between the blades and the transported tissue is only existent if there is contact between the transported tissue and the blades. Ideally the contact area between the transported tissue and each of the individual blades must be equal. In Figure 2.4 A, it is shown how this ideal situation will look. This might not be the case due to the size and shape of the transported tissue. If the transported tissue is too big, no transport is possible because there will be no contact between the translating blades and the transported tissue as it will not fit in the lumen, see Figure 2.4 B. A tissue that is too small will fit in the lumen of the instrument, but there will be limited or no contact between the tissue and the blades, see Figure 2.4 C. This will, depending

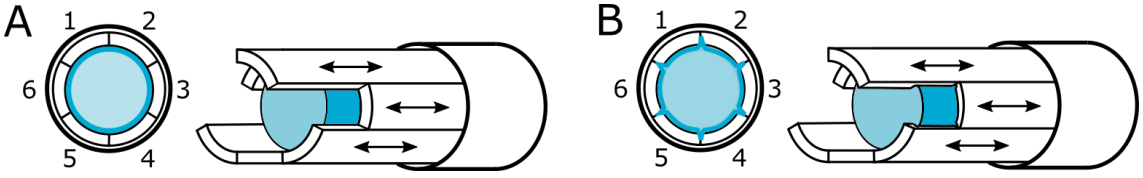

Figure 2.2: Schematic representation of the transported tissue moving between the blades. A: Representation of the transported tissue when no leaking occurs. B: Representation of the leaking of the transported tissue. This can lead to the loss of biopsy material, contamination and the complicating the blade movement.

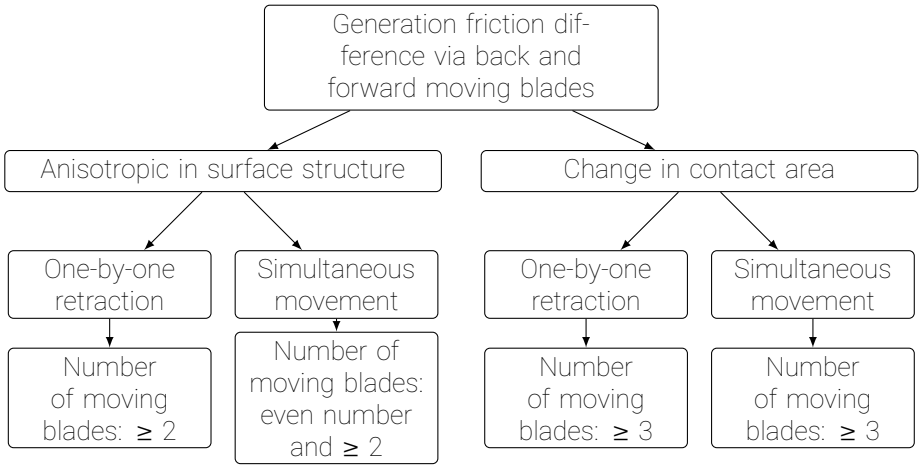

Figure 2.3: Flowchart of the solutions to generate the needed friction difference between the transported tissue and the translating blades.

on how small the tissue part is, complicate the friction-based transport. It is also possible that the tissue part has a different shape than the lumen through which it is transported. Due to this different shape, the contact area between each of the blades and the transported tissue is different, as is schematically shown in Figure 2.4 D. The transport mechanism is not capable of separating the tissue that must be transported from the surrounding tissue. Therefore it is assumed that the transport mechanism is used in combination with a device that will separate and mince the tissue that must be transported such as a morcellator that will separate the tissue from its surroundings, grind it and feed it to the transport mechanism. This would result in the transported tissue to conform to the lumen of the transport mechanism and thus ensure that there is equal contact between each of the blades and the transported tissue.

Collapse of the lumen

Depending on the forces acting on the translating blades, the blades might collapse inwards. In the rigid friction-based transport mechanism, the blades form a lumen due to their shape. This shape-lock is not very strong, and only a small force is needed to make the blade collapse inwards. This will lead to narrowing of the lumen, see Figure 2.5 A. The narrowing of the lumen could result in clogging of the transport mechanism as the transported tissue might not fit through this narrowing. This will mainly be a problem during the transport of solids and very viscous fluids as these will not easily deform. Elastic solids will deform to fit through the narrowed lumen, but due to this change in shape, new stresses will be introduced that will lead to unequal friction generation between the transported tissue and each of the blades. This can complicate the transport as friction-based transport is built on the assumption that there is equal friction between the

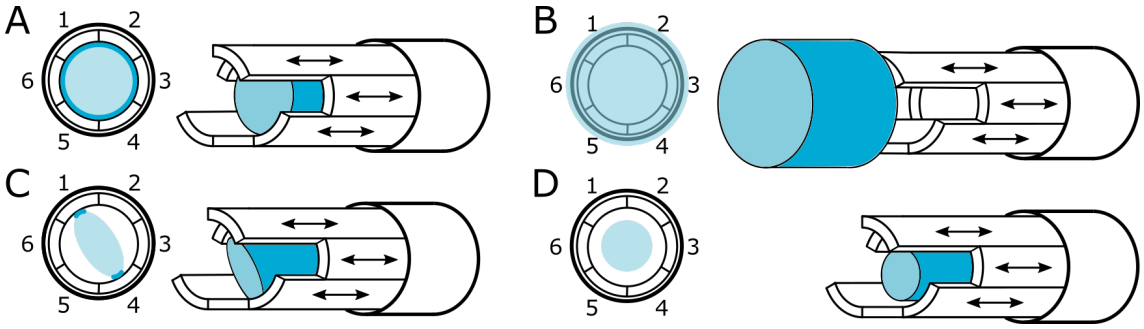

Figure 2.4: Schematic representation of the the effect of the size and shape of the transported tissue on the contact surface. A: Transported tissue part is shaped to the size of the lumen. In this perfect scenario, there is equal contact between the transported part and each of the surrounding blades. B: Tissue part is bigger than the lumen which results in no contact between the blades and the transported part, making transport by friction impossible. C: Oddly shaped tissue part that results in unequal contact area between the blades and the transported part complicating transport by friction. D: The tissue part is smaller than the lumen resulting in less or unequal divided contact between the transported tissue and the blades, complicating the transport by friction.

transported tissue and each of the blades. Therefore it is of great importance that the lumen of the transport mechanism has a constant cross-section.

Gravity

Gravity could lead to unequal friction generation between the transported tissue and each of the blades. The friction present at a certain contact point is equal to a constant multiplied by the normal force. The constant depends on surface characteristics of both the transported tissue and the blade. Due to the gravity acting in one direction, a normal force will be generated at a certain point in the opposite direction leading to an increase in friction at that specific point. For friction-based transport to optimally work, the friction between the transported tissue and each of the blades must be equal, which will not be the case due to gravity acting on the mechanism. However, since the transported tissue parts will be small the normal force is also small and thus it is expected that the effect on the transport rate of a friction-based transport mechanism will be limited.

2.1.3. Challenges associated with contamination during transport

The transported tissue should not be able to get in contact with its surroundings during transport. This could potentially lead to contamination, tumour seeding and infection. Furthermore, the flexible transport mechanism can be used for the transport of a biopsy sample. For these procedures it is of great importance to capture and transport the entire tissue sample. To avoid the tissue from escaping the device and contaminating the surroundings, the lumen through which the tissue is transported must be enclosed. There are multiple ways to achieve this. The first option is by designing the blades in such a way that they fully enclose the lumen. A number of examples of creating a closed lumen this way are shown in Figure 2.6. It can also be chosen to not enclose the lumen by the blades but by using a separate structure. This is done by the rigid friction-based transport mechanism with the outer tube, see Figure 1.3.

2.2. Challenges flexible transport

2.2.1. Challenges associated trough curves

When using a flexible transport mechanism, the transported material should also have a certain degree of flexibility. A flexible solid that is transported will deform to fit through the curved lumen, as indicated in Figure 2.7 A. The flexible friction-based transport mechanism is not intended to be used for the transport of rigid solids, as friction-based transport will not optimally work. The transport of non-homogeneous tissues that have for instance a more rigid structure surrounded by a more flexible layer could be transported. The rigid structure will not deform to the curve of the instrument and will therefore get stuck at the start of the curve, as indicated in Figure 2.7 B. This will clog the flexible friction-based transport mechanism, making further transport impossible. However, if such a non-flexible tissue part is small enough, it can still pass through the lumen, as shown in Figure 2.7 C. Whether or not a more rigid tissue part surrounded by a flexible layer can fit through a curved flexible transport mechanism depends on the bending radius of the transport mechanism, its inner diameter and the dimension of the rigid tissue part. A schematic representation of a curved flexible transport mechanism is given in Figure 2.8. The radius of curvature of the transport mechanism is indicated with $R_{curvature}\,[m]$. The diameter of the transport mechanism in indicated with $D\,[m]$. It can be observed that the bigger the diameter of the rigid tissue part is, the smaller the length of this tissue part must be to make the transport possible. The to-be-designed flexible transport mechanism is intended to be used in combination with a tissue separating device. To avoid clogging of the transport mechanism due to rigid tissue parts, this tissue separating device would not only separate the tissue from its surroundings but will

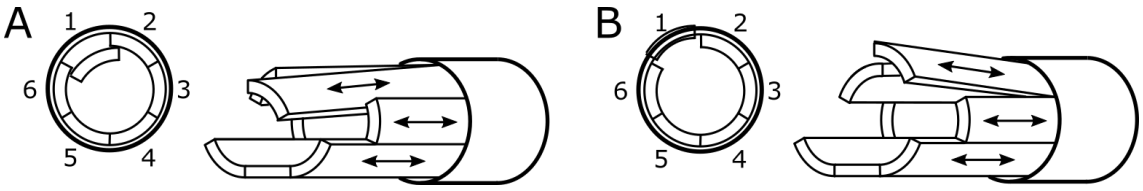

Figure 2.5: schematic representation of the effect of collapsing blades. A: Inwards falling blades lead to narrowing of the lumen which would complicate friction-based transport as there will be unequal friction between the transported tissue and each of the blades. B: Outwards movement of the blades lead to expansion of the lumen which would complicate the friction-based transport as there will be limited contact with the outward moved blade.

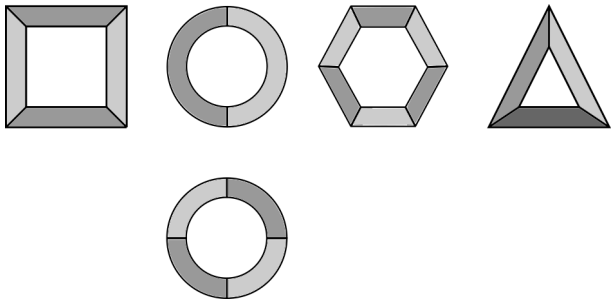

Figure 2.6: schematic representation of different cross-sections

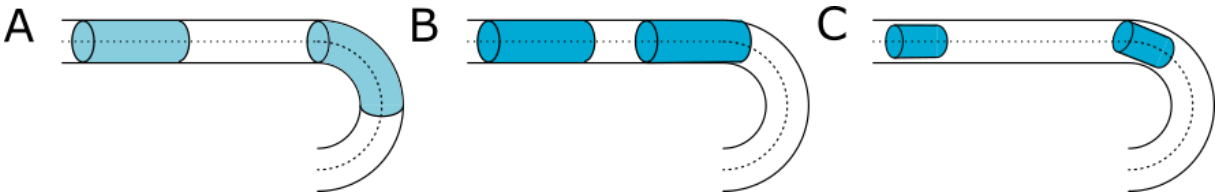

Figure 2.7: Schematic representation of the transport of solid tissue through the flexible transport mechanism. A: A flexible tissue will change shape to fit through the curved lumen. B: A Rigid tissue will not change its shape and can therefore not fit through the lumen. This will clog the transport mechanism. C: A rigid tissue part that is smaller than the lumen can fit through the curved lumen.

also grind it. This would solve the problems arising when transporting a rigid solid.

2.2.2. Challenges associated with rigidity

Flexural rigidity

The flexible transport mechanism must be able to bend, without the occurrence of plastic deformations. The forces that are applied on the transport mechanism are introduced by the organ wall. Thus, to avoid damage to the healthy organ wall, the transport mechanism must deflect or bend when a small force is applied. The deflection as a result of a certain force F, that is applied perpendicular to the longitudinal axis, as shown in Figure 2.9, can be approximated with Equation 2.1.

$$\delta = \frac{F l^3}{3 E I} \tag{2.1}$$

With δ $[m]$ is the deflection as indicated in Figure 2.9. L $[m]$ is the length of the transport mechanism. E $[N/m^2]$ is the Young's modulus. This is a material property. I $[m^4]$ is the second moment of inertia. This value is dependent on the geometry of the cross-section of the transport mechanism. A few examples of the second moment of inertia are given in Figure 2.10.

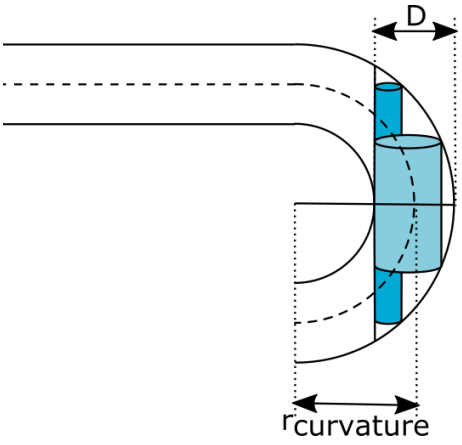

Figure 2.8: Schematic representation of a rigid tissue part that is transported through a curved lumen. The radius of curvature is indicated with $r_{curvature}$. The diameter of the lumen is indicated with D.

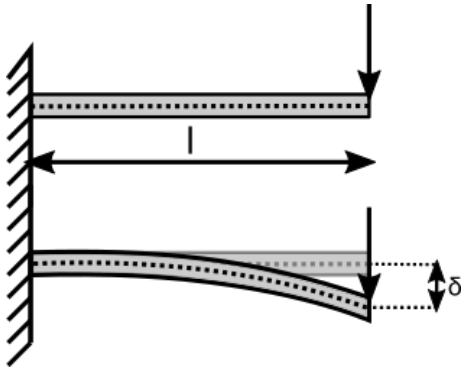

Figure 2.9: Schematic representation of beam bending. The applied force results in the deflection of the beam.

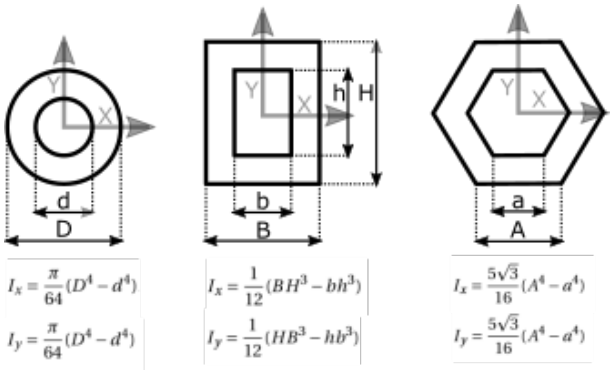

Figure 2.10: examples of the second moment of inertia.

The application of a bending moment results in curvature of the tube. The radius of this curvature can be approximated with Equation 2.2. With R $[m]$ is the radius of curvature of the tube. E $[N/m^2]$ is the elastic modulus of the material. I $[m^4]$ is the second moment of inertia around the neutral axis of the beam. M $[Nm]$ is the applied bending moment.

$$R = \frac{EI}{M} \tag{2.2}$$

To be able to bend in a 3D space, such as a human body, the flexible transport mechanism must be able to bend in all direction with the same ease, and must thus have the same flexibility in all directions. The flexibility needed depends on the application. A realistic bending radius that a colonoscope should be able to achieve is 60-90 mm [9], and an intravascular catheter can achieve a bending radius of 2.5 mm [13]. To bend this the flexible transport mechanism to this radius must require limited force as a high force would damage the organ wall. Damage to the organ wall can be minimised by choosing a material with a low elastic modulus, or designing the tube in such a way that the cross-section results in a small second moment of inertia.

Buckling

Buckling is used to describe a sudden deflection of a slender structure due to an axial load. An axial load can be introduced to the transport mechanism by, for example, the organ wall as shown in Figure 2.11 A and B. The axial load applied by the transport mechanism at the organ wall must be minimised as it could lead to the transport mechanism perforating the organ wall, see Figure 2.11 C. Buckling of the transport mechanism must be avoided as it would result in an inward collapse of the blades and will therefore obstruct transport. Instead the transport mechanism must deflect and follow the organ wall as shown in Figure 2.11 D.

The minimum buckling force F [N] that will lead to buckling can be calculated with Equation 2.3.

$$F_{buckling} = \frac{\pi^2 EI}{(Kl)^2} \tag{2.3}$$

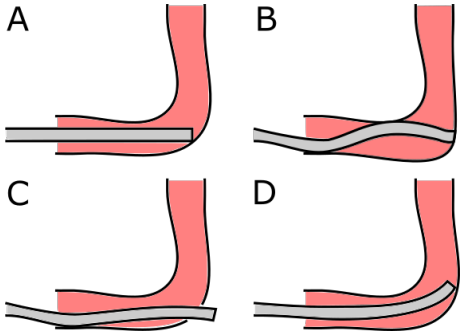

Figure 2.11: Schematic representation of Buckling. A: Initial position of the transport mechanism just in contact with the organ wall. B: Pushing the transport mechanism further in the organ will lead a force from the organ wall on the transport mechanism and an equal force from the transport mechanism on the organ wall. This could lead to buckling of the transport mechanism. C: If the organ wall cannot withstand the force exerted by the transport mechanism the organ wall can rupture. D: If the transport mechanism flexes in the correct direction, it can continue it way through the organ.

With E $[N/m^2]$, elastic modulus of the material. I $[m^4]$ is the second moment of inertia of the cross-section area and is thus depended on the geometry of the transport mechanism. K is the clamping factor and is dependent on the clamping used at the handle and the tip of the transport mechanism. Different clamping configurations and the corresponding value for K are shown in Figure 2.12. Depending on the fixation of the tip of the transport mechanism, the values for K differ between 0.5 and 2. $l[m]$ is the length of the flexible transport mechanism as indicated in Figure 2.12. This means that l is not equal to the length of the transport mechanism as a whole but equal to the distance between the tip and the part where the transport mechanism is clamped. This can for instance be the part were the transport mechanism is clamped by the blood vessel wall due to a strong curve.

To avoid buckling, the buckling force $F_{buckling}$ should be as high as possible. This can be achieved by using a material with a high elastic modulus or by designing the transport mechanism with a cross-section with a big second moment of inertia. The clamping factor and the length of the transport mechanism between the clamped points are also dependent on the surroundings of the transport mechanism and can therefore not fully be influenced by the design.

Brazier effect and kinking

Slender hollow structures such as the flexible transport mechanism and catheters are prone to Brazier buckling. Brazier buckling occurs when the flexible transport mechanism is bent. During bending tension and compression stresses occur in the transport mechanism which resist the bending moment that causes the bending. When a hollow slender structure, such as the flexible transport mechanism, is curved, the cross-section tends to flatten. This results in ovalization of the structure, see Figure 2.13 A and B. Ovalization decreases the second moment of area about the bending axis, resulting in the decrease of the flexural rigidity [5]. Once the maximal bending moment is reached it will result in a sudden collapse of the lumen, which is known as kinking. Due to this kink, the lumen is obstructed which makes transport through the lumen impossible. Not only will the kink cause problems for the transport mechanism, the process of ovalization of the lumen

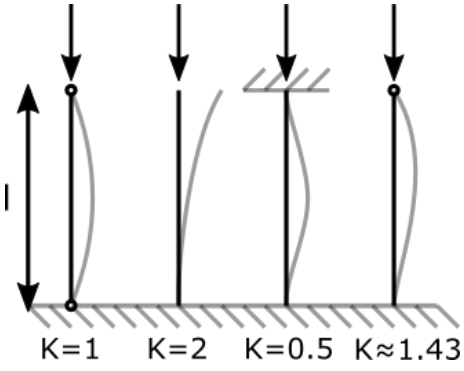

Figure 2.12: Schematic representation of clamping configurations and the corresponding value for the clamping constant K.

can also result in sub-optimal transport as ovalization would result in unequal contact forces between the tissue and each of the blades. Friction-based transport is built on the assumption that the friction between the transported tissue and each of the blades is equal. Therefore the ovalization results in complication of the transport.

The to-be-designed transport mechanism can be simplified to a catheter. The radius at which a tubular catheter will kink can be calculated with Equation 2.4. In this equation; $R_{critical}$ is the radius at which the catheter will kink. To avoid kinking the bending radius of the catheter must be smaller than $R_{critical}\,[m]$. $\nu\,[-]$ is the Poisson's ratio which is a material property. $r\,[m]$ is external radius of the catheter. $t\,[m]$ is the wall thickness and $K\,[-]$ is a constant with a value around 1 [1].

$$R_{critical} = \frac{(1-\nu^2)r^2}{Kt} \tag{2.4}$$

From this formula it can be concluded that the catheter can be made more resistant to kinking by choosing a material with a higher Poisson's ratio, by decreasing the outer radius or increasing the wall thickness. Another way to avoid kinking is by preventing the ovalization of the tube by introducing an internal spring like structure.

Torsion stiffness

Torsion is the twisting of a structure due to the application of a torque. A structure with a high torsion stiffness does not exhibit twisting after the application of a torque of one end of the structure, see Figure 2.14. By rotating one end of a torsional stiff structure an almost equal rotation at the other end will occur. This is of great importance for catheters with a pre-bent tip, as this allows the tip of the catheter to be rotated by rotating the other end of the catheter. As the to-be-designed transport mechanism will not have a pre-bent tip, torsion rigidity is not a requirement in itself. The blade movement could however be negatively affected by twisting of the structure. Twisting of the blades will result in the blades becoming partly intertwined. Translation of the blades will require more force due to the intertwined blades which is not desirable.

Cross-section trade-off

The flexural rigidity, buckling, brazier effect and the torsion rigidity are influenced by the dimension of the cross-section of the transport mechanism. The influence of geometric dimension on the flexibility of the transport mechanism is summarised in Table 2.1.

It can be seen that for the flexural rigidity the second moment of inertia must be minimised. For a tubular structure this would result in maximising $\frac{1}{D^4-d^4}$. Thus, the transport mechanism must be thin walled. However, to avoid buckling $\frac{1}{D^4-d^4}$ must be maximised and to avoid the brazier effect, $\frac{\frac{1}{2}(D-d)}{\frac{1}{4}D^2}$ must be maximised. The transport mechanism must thus have a thick wall, which is the opposite of what is needed for the flexural rigidity. This results in a trade-off between the flexural rigidity, buckling and the brazier effect prevention.

2.2.3. Challenges associated with path length and bending

When curving the transport mechanism the inner and outer curve have a different length, as can be observed in Figure 2.15. This can potentially cause problems to the functioning of the transport mechanism. The effect of this change in length can be calculated with Equation 2.5. With $\delta L\,[m]$ is the length difference between the

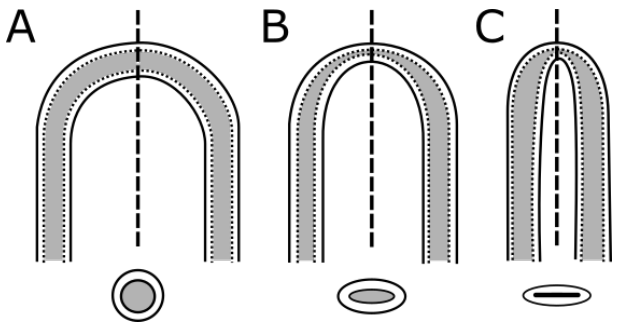

Figure 2.13: Schematic representation of Brazier buckling. A: Normal bending of a tubular structure. B: Ovalization of the structure due to the increased bending moment. C: Full kinking of the lumen. This will occur by and application of the maximal bending moment.

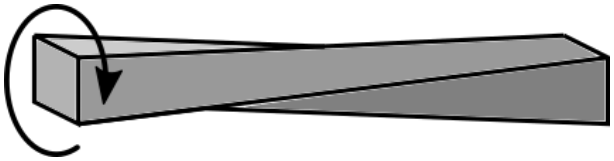

Figure 2.14: Schematic representation of torsion. If the structure is not torsion stiff enough, the applied torque results in twisting of the structure.

Table 2.1: Overview of the relation between the problems associated with flexibility and the geometry of the transport mechanism. For each of the flexibility associated problems (flexural rigidity, buckling and the brazier effect) the measure and the corresponding formula is given. For each of the formula it is stated if it must be minimised or maximised for better performance of the transport mechanism. The formula is then rewritten such that it must be maximised for better performance. To show the effect of the different geometric values of the transport mechanism on these flexibility associated problems, the to be maximised formula is given with only the geometric values.

Flexibility associated problem	**Measure**	**Formula**	**Maximise / Minimise**	**Maximise**	**Maximise geometric**
Flexural rigidity	Deflection	$\delta = \frac{FL^3}{3EI}$	Maximise	$\delta = \frac{FL^3}{3EI}$	$\frac{L^3}{I} = \frac{L^3}{\frac{\pi}{64}(D^4-d^4)}$
	Bending radius	$R = \frac{EI}{M}$	Minimise	$\frac{1}{R} = \frac{M}{EI}$	$\frac{1}{I} = \frac{1}{\frac{\pi}{64}(D^4-d^4)}$
Buckling	Buckling force	$F_{buckling} = \frac{\pi^2 EI}{KL^2}$	Maximise	$F_{buckling} = \frac{\pi^2 EI}{KL^2}$	$\frac{I}{L^2} = \frac{\frac{\pi}{64}(D^4-d^4)}{L^2}$
Brazier effect	Critical bending radius	$R_{crit} = \frac{(1-nu^2)R^2}{Kt}$	Minimise	$\frac{1}{R_{crit}} = \frac{Kt}{(1-nu^2)R^2}$	$\frac{t}{R^2} = \frac{\frac{1}{2}(D-d)}{\frac{1}{4}D^2}$

inner and outer curve. $\alpha\,[rad]$ is the degree of curvature. $d\,[m]$ is the diameter of the transport mechanism. $R\,[m]$ is the outer radius of curvature and $r\,[m]$ is the inner radius of curvature.

$$\delta L = \alpha(R-r) \tag{2.5}$$

Implementing the fact that $r = R-d$, results in Equation 2.6. This equation shows that the difference in length is not dependent on the curve radius, but only on the diameter of the transport mechanism and the degree of curvature.

$$\delta L = \alpha d \tag{2.6}$$

A flexible friction-based transport mechanism with a diameter of around 5 mm in a curve with angle $\alpha = 180^o[deg] = \pi[rad]$ will result in a length change of approximately 16 mm. This means that the tip of the blade following the inner curve will protrude 8 mm from the average while the blade following the outer curve will be depressed 8 mm from the average. The blades also must be able to make a translating motion to allow for the friction-based transport. This translating blade movement must not be harmed by the difference in path size of the different blades.

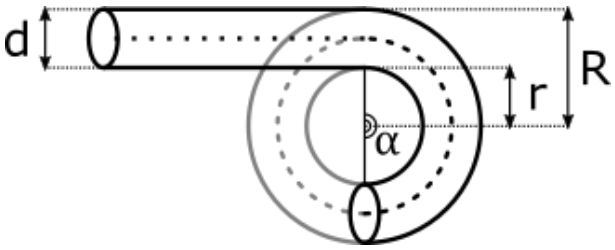

Figure 2.15: schematic representation of transport mechanism in a curve. The diameter of the transport mechanism is indicated with d, the radius of the outer curve is R and the radius of the inner curve is indicated with r.

3

Design process flexible shaft

In this chapter the design process of the flexible shaft will be discussed. The design requirements that the flexible shaft should fulfil are listed in Section 3.1. Section 3.2 discusses the design approach. For a number of challenges, possible solutions are presented. Based on these possible solutions a concept solution is described that will be discussed in Section 3.3. The final design of the flexible shaft will be presented in Section 3.4.

3.1. Design requirements flexible shaft

The requirements that the flexible shaft must fulfil are divided in three categories. 1) The geometric requirements: These requirements define the size of the flexible shaft. 2) Functional requirements: These requirements are associated with the function of the flexible shaft. 3) Medical requirements: These requirements will apply since the flexible shaft is intended to be used in a medical setting.

3.1.1. Geometric requirements

- **Length:** The flexible shaft could in the future be used in a number of medical procedures. Think of the transport of biopsy material during a colonoscopy but also as an alternative for aspiration catheters such as percutaneous aspiration catheters that are used for the removal of blood clots (thrombus) in the coronary or peripheral artery. Depending on the application the flexible shaft needs to have a certain length. Aspiration catheters have a length between 135 and 141 cm [15]. Colonoscopes are longer with a working length between 133 cm and 169 cm [6]. The flexible shaft must be able to adequate work for these length.

- **Outer diameter:** The maximal allowed outer diameter of medical instrument depends on the application of the instrument. Percutaneous guiding catheters have an outer diameter between 6 and 7 French (between 2.0 and 2.3 mm) [15]. However a colonoscope has a larger outer diameter that is normally around 12mm [8]. Therefore the outer diameter of the flexible shaft must be between 2 and 12 mm.

- **Inner diameter:** To be able to compare the data of the flexible friction-based transport mechanism to the rigid friction-based transport mechanism of I. van de Steeg [17], the inner diameter must be comparable. Therefore the inner diameter will have to be equal to 4 mm. Since friction-based transport depends on contact between the transported tissue and the blades forming the inner lumen, the lumen must have a constant diameter over the entire length of the flexible shaft.

3.1.2. Functional requirements

- **Flexibility:** The flexible shaft is intended to be used in minimal invasive medical procedures using natural body orifices, such as endovascular interventions. Flexibility of the shaft is required to be able to reach the desired location for the procedure. The flexibility of the shaft must be the same in all directions, meaning that it can bend two degrees of freedom with the same ease. Bending of the flexible shaft should not harm the transport. This means that the lumen through which the transport takes

place must not change is diameter or kink during bending. A colonoscope is able to bend with a bending radius of 60-90 mm [9]. The flexible shaft must be able to transport when being curved with a bending radius of 60 mm. Furthermore, the flexible shaft must be able to perform adequately when a torque of 1.0 Nm is applied as this is the maximum torque expected to be exerted on a colonoscope during a colonoscopy [3]. The flexural rigidity of a colonoscope is between $2.6 * 10^{-2}$ and $4 * 10^{-2}$ Nm^2 [9]. Therefore the flexural rigidity of the shaft is required to be lower than $4 * 10^{-2}$ Nm^2.

- **Lumen:** The flexible shaft must have a lumen through which the tissues can be transported. During bending, the lumen must maintain a constant diameter. A curve in the flexible shaft can lead to inwards motion of the blades resulting in the occlusion of the lumen which would harm the transport performance.Friction-based transport is built on the assumption that there is equal friction between the transported tissue and each of the blades. This can be achieved by a constant diameter of the lumen of the flexible friction-based transport mechanism even when the mechanism is curved. Therefore it is required that the lumen has a constant diameter along the whole length of the flexible shaft, independent of the curve of the shaft.

- **Friction transport in straight and in curved position:** friction-based transport uses the friction between the tissue and the translating blades to transport the tissue. A difference in friction between the forward moving blades and the backwards moving blades results in an unidirectional transport of the tissue. The flexible shaft must be able to transport soft tissue with a transport rate that is comparable to the transport rate of the rigid friction-based flexible shaft designed by I. van de Steeg which is approximately 2 mm/cycle [17]. The flexible shaft must be able to transport homogeneous and heterogeneous tissue. It is assumed that the tissue is separated from its surroundings by an second device that also grinds the tissue. Due to this only small heterogeneities are expected in the to be transported substance.

3.1.3. Medical requirements

- **Tissue separation:** The flexible shaft is expected to be used in combination with a second device that will separate the tissue form its surroundings and grind it. For now it is assumed that the transported tissue will conform to the lumen through which the tissue is transported.

- **Clean-ability:** The flexible shaft will be introduced in the human body and must therefore be sterilised before use. This means that the materials used should be able to withstand the cleaning routines used in hospitals. Furthermore, the flexible shaft must be manufactured in such a way that the individual components can be detached and cleaned easily. The flexible shaft can also be designed to be a single-use system, that will not have to be sterilised. In this case the price per piece will be more important. Since this research focuses on the development of a prototype as a proof of principle, the prototype itself does not have to fulfil the high standards regarding clean-ability as would be the case for a medical device.

- **Bio-Compatibility:** The flexible shaft will be introduced in the human body. To limit any adverse effect, the materials used should be bio-compatible, meaning that it will not lead to a response of the human body such as excessive blood clotting. Since this prototype is merely intended as a proof of principle, the prototype itself does not have to be fully bio-compatible. The flexible shaft must, however, be designed in such a way that it can be made bio-compatible with slight alterations.

- **Tissue isolation:** The transported tissue cannot have contact with the surroundings of the flexible shaft as this might lead to adverse effects such as contamination of surrounding tissue and tumour seeding. This means that the tissue must not be able to escape from the flexible shaft.

- **X-ray compatibility:** Endovascular procedures are performed under x-ray. To have a clear view on where the tip of the flexible shaft is located, the tip of the flexible shaft must be opaque on the x-ray images. Since the designed flexible shaft is intended to be a proof of principle, for now there will be no hard requirements regarding the x-ray compatibility. It should, however, be considered that future versions can be made x-ray compatible with small alterations.

3.2. Concept generation flexible shaft

Each of the set requirements must be met by the flexible shaft. A concept design is generated by comparing different options for the main parts of the flexible shaft.

3.2.1. Flexible blades

One of the main functions of the flexible shaft is that it must be flexible, while being able to transport tissues based on friction. Flexibility is used to describe the ability to bend or curve without breaking. For the flexible shaft as a whole to be flexible, the blades, that are used to transport the tissue, must also be flexible. As stated in the requirements, the flexible shaft must have the same flexibility in all directions. Flexibility in the blades can be achieved in different ways as is indicated in Figure 3.1. Either a single structure can be flexible, or the flexibility can be generated by using multiple structures that move with respect to each other. When a single structure is used, the cross-section can be constant. In this case the flexibility will be achieved by elastic deformation in the material, see Figure 3.2 A. It is also possible to change the cross-section. A thicker structure is less flexible. By incorporating parts with smaller cross-sections, the structure will bend more easily over these thinner parts that are known as compliant hinges, see Figure 3.2 B. Flexibility can also be achieved by using multiple structures. Wire ropes consist of multiple braids, and thus a wire rope consists of multiple structures. The individual braids can slightly slide with respect to each other. This allows for easier bending, and thus generates flexibility see Figure 3.2 C. The different structures can also be connected by regular joints. This way the structures can move with respect to each other, see Figure 3.2 D. Each of the ways to generate flexibility will be discussed more elaborately below.

Elastic bending

The flexibility of a structure is dependent on its second moment of inertia. The moment of inertia around the x axis can be calculate with Equation 3.1. With A is the cross-sectional area. All in Cartesian axis.

$$I_x = \int_A y^2 \, dA \tag{3.1}$$

For the blade to have the same flexibility in all directions the second moment of inertia must be the same for every axis around which the flexible shaft is bend. The second moment of inertia around an axis that is rotated with angle θ can be calculated with Equation 3.2.

$$I_{x'} = I_x \cos^2\theta + I_y \sin^2\theta - 2I_{xy} sin\theta cos\theta \tag{3.2}$$

In this equation I_y is the second moment of inertia around the axis perpendicular to the x axis and can be calculated with Equation 3.3.

$$I_y = \int_A x^2 \, dA \tag{3.3}$$

I_{xy} is the product of inertia which can be calculated with Equation 3.4.

$$I_{xy} = \int_A xy dA \tag{3.4}$$

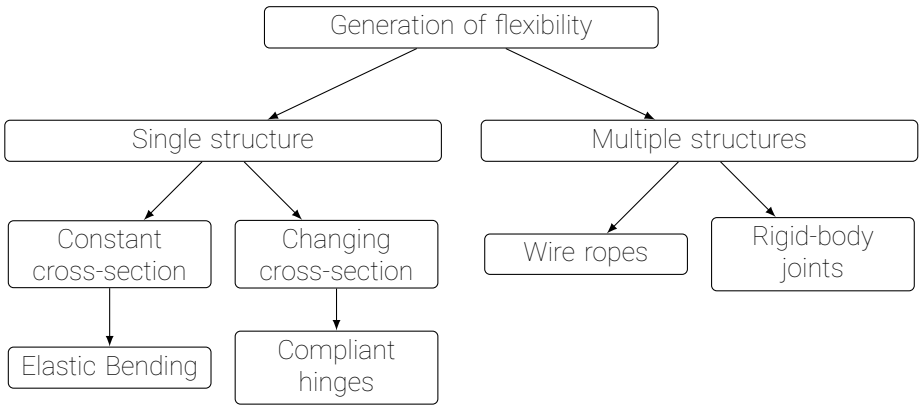

Figure 3.1: Flowchart of the solutions to generate the needed flexibility in the blades.

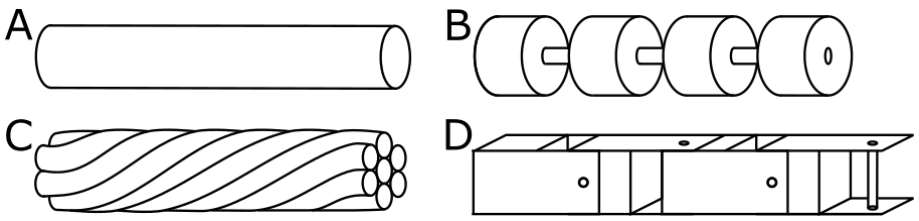

Figure 3.2: Schematic representation of the different ways to generate the needed flexibility. A: Elastic beam bending. B: Complaint hinges. C: wire ropes. D: Regular hinges

I_{xy} is equal to zero if the x or y axis is an axis of symmetry. If I_x and I_y are the same and the x or y axis is an axis of symmetry that means that $I_{x'}$ is equal to I_x for every axis through the origin. Meaning that the structure has the same flexibility in the required directions. This is the case for any regular polygon (equilateral triangle, square, regular pentagon etc.) as cross-section. These cross-sections are rotational symmetric, meaning that turning them with a certain angle ϕ results in the same shape, with $\phi \leq \pi$.
Each blade will be free to axially translate with respect to the other blades. Therefore the cross-section of the flexible shaft as a whole will consists of a number of parts. This influences the flexibility. Depending on the design, the flexibility might vary depending on the directions. The influence of having loose parts compared to one solid structure will be investigated using the beams shown in Figure 3.3. The first beam consists of one structure and has a square cross-section, see Figure 3.3 A. A square cross-section (or any other regular polygon) has the same flexibility in all directions, as $I_x = I_y$ and $I_{xy} = 0$. By cutting the beam in two halves, the cross-section will now consist of two loose parts. Although the parts are loose, they must maintain surface contact during bending. This is also the case with the blades of the flexible shaft. Intuitively, one can already see that bending the two beams as shown in Figure 3.3 B will require more force than bending the beam as shown in Figure 3.3 C. This can also be proven by using equations. The second moment of inertia for a rectangle can be calculated with Equation 3.5. This formula shows that the second moment of inertia increases with the width to the power one and with the height to the power three. This means that increasing the height increases the second moment of inertia more than increasing the width. Although the cross-sectional area and shape of the cross-section of beam A, B and C is the same, the fact that the the cross-section is cut through leads to an anisotropic flexibility.

$$I = \frac{1}{12} b h^3 \tag{3.5}$$

Compliant hinges

Compliant hinges use linkages that deform elastically to allow certain motions. These links are called flexures. The parts connected with these flexures are assumed to be rigid. This is schematically shown in Figure 3.4. Such a system can be made of one part eliminating the need for assembly which would be the case when using regular hinges. Other advantages of compliant hinges compared to regular hinges are the lack of friction loss. Furthermore, compliant hinges are compact which makes them especially useful in small systems [10]. Depending on the shape of the compliant hinge a certain motion is allowed. As explained before, the second moment of inertia, which is dependent on the geometry of the cross-section, is a measure for how easy a structure bends around a certain axis. This principle is also used when designing compliant hinges.

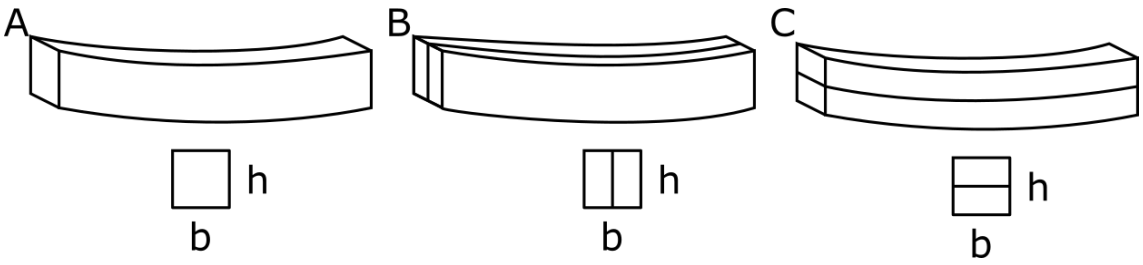

Figure 3.3: schematic representation of the bending of a beam with difference cross-sections. A: Elastic bending of a beam with a square cross-section. B: elastic bending of a beam that is cut in half, resulting in a cross-section of two rectangles that can slide with respect to each other. C: Elastic bending of a beam with the same cross-section as in case B but now 90 degrees turned.

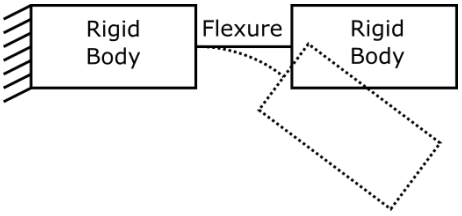

Figure 3.4: Schematic representation of a compliant hinge. The two rigid bodies are connected by a flexure. Elastic deformation of the flexure results in movement comparable to the use of a regular hinge.

A long rectangular cross-section allows for easy bending in one direction, but does not allow bending in the perpendicular direction as shown in Figure 3.5 A. Since the flexible shaft should be flexible in two directions the compliant hinges must allow for bending with two DoF. The flexures in Figure 3.5 B and C have a regular polygon as cross section. Therefore they have the same flexibility in all directions. Disadvantages of using compliant hinges is the limited force that can be transmitted through the structures. The small cross-sections of the flexures leads to limited stresses that the structure can withstand. Besides the low stress limit the flexures that allow for bending in 2 DoF are not torsion stiff.

Wire ropes

Wire ropes are made from a number of twisted strands. The number of wires and the number of strands influences the flexibility of the wire rope. Because the individual strands can slide with respect to each other, a wire rope is more flexible than a solid bar with the same cross-sectional area. The flexibility increases when using more wires and rope strands. There are also different strand and rope constructions. For instance, a 1x7 wire rope consists of one central wire that is surrounded by 6 other wires. This is a strand construction. Multiple strands can be twisted around each other to create a rope construction. For instance in a 7x7 wire rope, one central strand is surrounded by 6 other strands in which each strand has a 1x7 construction. Due to the twisted wire that comprises the wire rope, a wire rope can withstand limited compression loads compared to a solid bar of the same diameter. Due to the fact that the wire ropes comprise different strands, the wire rope becomes not only more flexible, but will also buckle at a lower compression force. This means that for the flexible shaft, that will have a small cross-section compared to its length, the translating motion of the wire ropes cannot be achieved by simply pushing and pulling the wire rope over the entire length of the flexible shaft, as a push force on the wire rope will lead to buckling of the wire rope and not the desired translating motion. There are several ways how a translating motion of a wire rope can be achieved. First of all the wire rope can be looped around the shaft. A pull force will lead to a translating motion one way and a push force will lead to a pull force at the other side of the loop. Therefore the wire rope will translate in the other direction, see Figure 3.6 A. Another option is to incorporate a spring at the tip of the flexible shaft. This spring will tension the wire rope, pulling it back in position after each actuation cycle. Introducing a pulling force that is big enough to withstand the force introduced by the spring will result in a translating motion of the wire rope in the other direction, see Figure 3.6 B. It is also possible to use a 'seesaw' as shown in Figure 3.6 C. Finally, the buckling of a wire rope can be prevented by guiding the wire. A wire rope will not buckle when it is pushed trough a tube that is slightly bigger than the wire. Such a tube would however prevent contact between the transported tissue and the wire ropes. Furthermore, the tube will decrease the flexibility of the blade. By guiding the wire not over the entire length of the wire, but rather providing regular support, the wires will still be able to bent between the support point and have contact with the transported tissue while still preventing buckling, see Figure 3.6 D. The smaller the distance between the support points, the better buckling will be prevented.

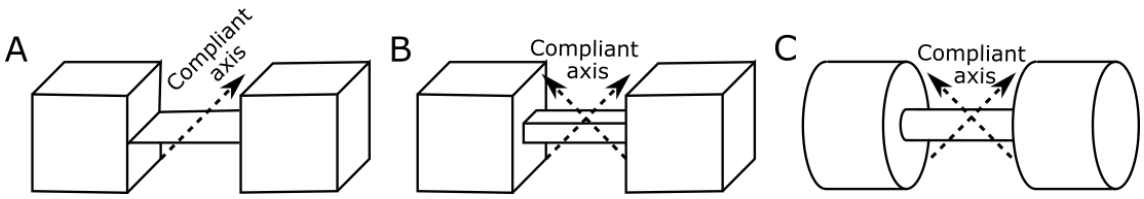

Figure 3.5: Schematic representation of different flexures. A: flexure with one compliant axis allowing bending with one DoF. B: flexure with two compliant axis which allows bending with 2 DoF. C: flexure with two compliant axis which allows bending with 2 DoF.

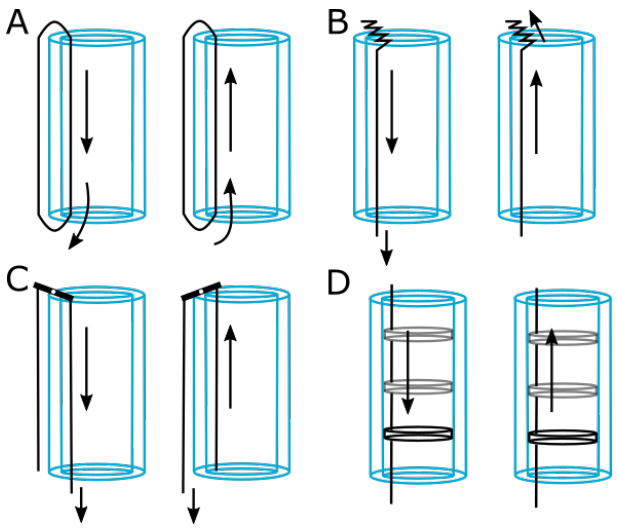

Figure 3.6: Schematic representation of possible solution to create translating motion of wire ropes. A: wire rope loop that allows pulling and pushing. B: Addition of a spring that will keep the wire rope under tension. C: Use of a lever to create the translating motion of the wire rope. D: regular support points that guide the wire. The length of the wire between the support points is short which will prevent buckling of the wire when pushed.

Rigid-body joints

The needed flexibility in the blades can also be generated by incorporating regular rigid-body joints. These joints consist of rigid structures that, based on the interlocking shape, allow for certain movements. There are different joints that allow different movements and thus result in a different DoF. Think of the hinge that allows for rotation around one axis but also the ball-and-socked joint that allows for rotation around three axes. By combining different joint more DoF can be added to a system. Using joints in this case also leads to some disadvantages. Joint are rather big and down scaling will lead to very small parts that are difficult to fabricate and might break.

3.2.2. Lumen diameter

The lumen through which the tissue will be transported must have a constant cross-section, as a narrowing of the lumen would harm the transport. Even when the flexible shaft is curved, the blades should not collapse. During transport, an axial force will be exerted on the blades to achieve the wanted translating motion. The application of this force can also lead to the blade moving inwards in the curve and thus occluding the lumen, as is indicated in Figure 3.7. To avoid this, the blades should be restricted in radial direction, while being able to make the translating motion needed to achieve the friction-based transport. To realise this, different ideas were generated and are summarised in Figure 3.8. First, the division is made based on whether or not an additional external structure is used to avoid the collapse of the blades. Secondly, a division is made based on the fixation between the blades or between the blades and the external structure. Each of the identified ideas are elaborated below.

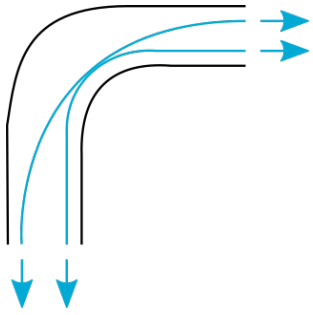

Figure 3.7: Schematic representation of the blades collapsing leading to narrowing of the lumen in the curve of the flexible shaft.

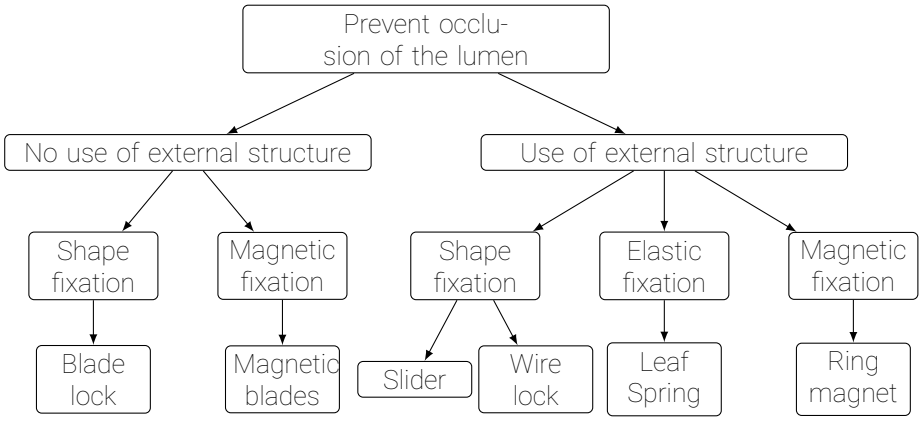

Figure 3.8: Flowchart of the solutions to prevent occlusion of the lumen.

No use of external structure

Blade lock

To maintain an open lumen the blades could be made in such a way that they interlock due to their shape, see Figure 3.9 A. This principle can be observed in the ventral and dorsal valves of the ovipositor of wasps. The interlocking shape still allows the blades to slide with respect to each other, but prevents the collapse of the blades and thus the occlusion of the lumen. Problems with this interlocking can occur during bending as this might lead to changes in the shape due to stresses. This could break the connection between the blades and thus result obstruction of the lumen. The blades could also get stuck to another, which would prohibit the translating motion of the blades that is needed to achieve the friction-based transport. Furthermore, the manufacturing of this shape will be very challenging especially for the required size.

Magnetic blades

The blades could be made of a material that is magnetic. By arranging the north and south poles of the magnets in a specific way, the blades will attract each other. This in combination with a specific shape of the blades would allow the blades to only slide with respect to each other while keeping the lumen open, see Figure 3.9 B. A problem that could arise when choosing this option is a decrease in flexibility. Magnetic materials are often brittle. By using these materials for the blades, the blades cannot easily elastically deform which will make it more difficult to bend, making the system less flexible.

With external structure

Slider

The blades can be kept at a certain distance from each other by connecting each of the blades to an outer tube as shown in Figure 3.9 C. This outer tube must be able to bend, and be kink resistant which can be achieved by a spring-like structure or a tube that is reinforced with such a spring-like structure. By connecting the blades to this outer tube using shape interlocking, the blade can still make the needed translating motion but cannot collapse and obstruct the lumen. When the flexible shaft bends, deformations in the shape lock can occur, which could allow the blades to occlude the lumen and thus harm the transport. It would also be possible that the blades get stuck and would not be able to make the translating motion needed for the friction-based transport. Also, for this shape lock, the manufacturing will be challenging due to the small size.

Wire lock

The blades can be prevented from occluding the lumen by using a structure through which the blades can be weaved, as shown in Figure 3.9 D.1. This prevents the blades from occluding the lumen but allows for contact between the blades and the transported tissue. Due to the shape of the rings, the manufacturing will be difficult. It can also be chosen to use a ringlike structure through which the blades run, as shown in Figure 3.9 D.2. A down side of this design is that there is no contact possible between the blades and the transported part where the ring is. By slightly rearranging the ring as shown in Figure 3.9 D.3, it is possible to have continuous contact between the blades and the transported tissue. The manufacturing of these rings will again be challenging, as the blades will be small to allow for the needed flexibility. For all three ideas the rings must be placed at a certain distance from each other for the flexible shaft to function adequately.

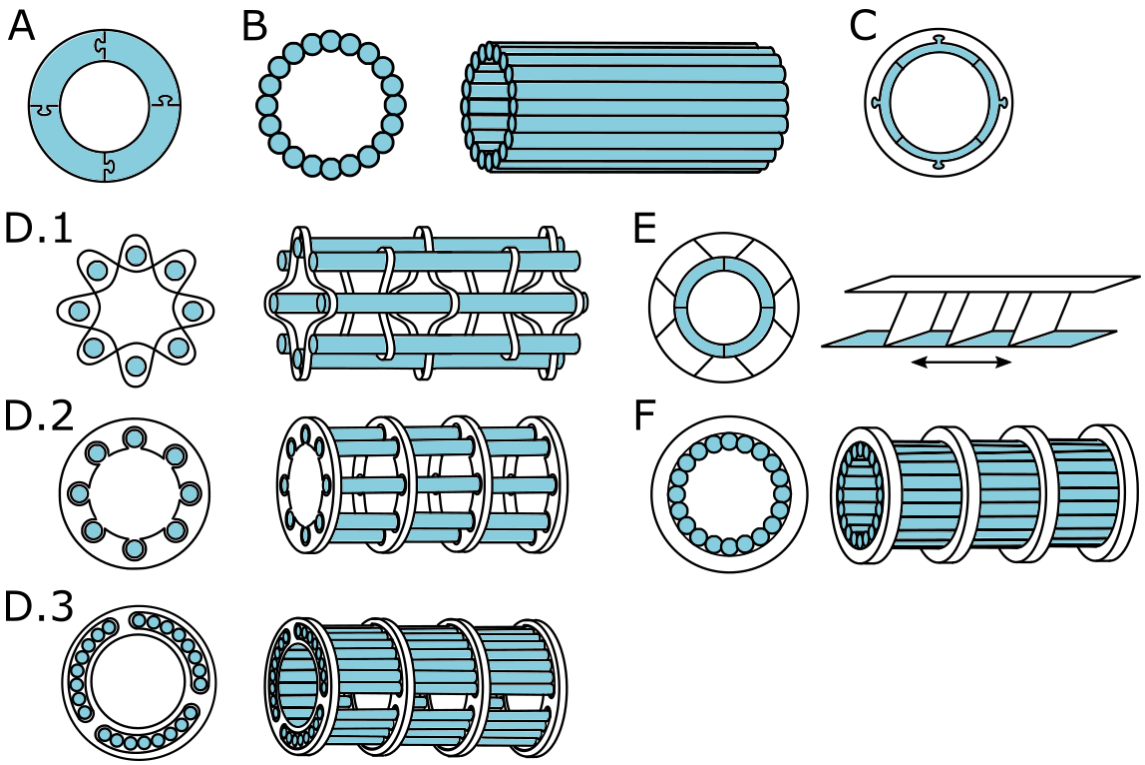

Figure 3.9: Schematic representation of different options to keep the lumen open during transport. The blades are coloured blue. A: Interlocking blades. B: Magnetic blades. C: Slider. D: Wire lock. E: Flexures. F: Ring magnet

Leaf spring
A leaf spring is a flexure that can bend. By connecting the blades to an outer tube with a leaf spring, the blades can translate in the desired direction while the blades can not collapse in or outwards, see Figure 3.9 E. The outer tube should again be flexible and kink resistant. For small displacements the motion allowed by the leaf spring can be simplified to be a straight translating motion, however for bigger movements this simplification will not hold, as the end point of the leaf spring will follow a rotational path. The blades would, during bigger motions, also move slightly up and downwards. This leads to changes in the lumen diameter. Furthermore, the leaf springs will need space and are therefore not convenient for this small-scale medical device.

Ring magnet
Blades can be prevented from occluding the lumen by using ring magnets, as shown in Figure 3.9 F. The ring magnet will only attract the blades if they contain iron, cobalt or nickel, as these materials are attracted by magnets. Furthermore, the ring magnets must be magnetised in a certain way, as shown in Figure 3.10. An advantage of this design is that the transported part will remain in contact with the blades over the full length of the flexible shaft, which is beneficial to the transport. A downside of the use of magnets is that the magnetic field of the ring magnets can interact with other systems. This could potentially harm the patient. Another disadvantage is that the strength of a magnets related to the size of the magnets. The larger the magnet the bigger the generated magnetic field. As the flexible shaft must be rather small the size of the magnet might be so small that it will not generate a magnetic field with the required strength.

3.3. Concept solution flexible shaft

It was chosen to use wire ropes for the flexible blades as these can easily be made in the required size and could even be scaled down further if needed for future designs. Furthermore, the wire ropes provide the needed flexibility in both directions. Ring magnets are used to make sure that the blades form a lumen and prevent collapse. The ring magnets would guide the wire ropes en therefore prevent buckling of the wires during compression. This would allow the wire ropes to be translated by pushing and pulling. The concept solution will be elaborated further.

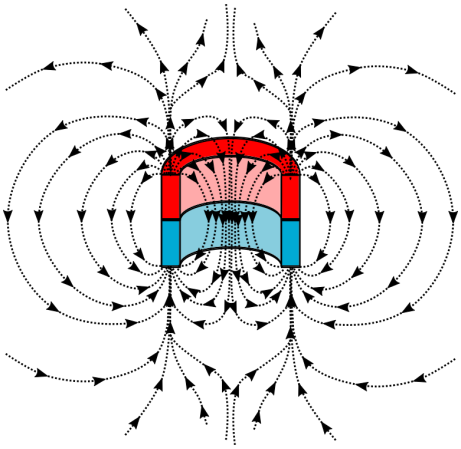

Figure 3.10: Schematic representation of the magnetisation of the ring magnet. The magnetic north and the south pole are indicated with red and blue and the magnetic field lines are shown with the doted lines.

3.3.1. Dimensions ring magnet and wire rope

The dimension for the flexible shaft are kept as similar to the rigid rigid friction-based transport mechanism by I. van de Steeg [17]. The lumen through which the transport takes place has to be 4 mm. Therefore ring magnets with a hole diameter of 5 mm were selected. The outer diameter of the ring magnets has to be as small as possible, as this will be the main factor influencing the outer diameter of the flexible shaft. The height of the ring magnets is also chosen to be as small as possible, which resulted in using the following ring magnets: Conrad Components Permanent magnet Ring N35M which is a neodymium ring magnet with an outer diameter of 10 mm, a hole diameter of 5 mm and a height of 2 mm. The blades have to be made of a material that is attracted by a magnet. Galvanised steel wire ropes fulfil this requirement and could be obtained easily. The diameter and the winding of the wire ropes are the main determinants for the flexibility of the shaft. The bigger the diameter of the wire rope the stiffer it will behave. By choosing a wire rope that consists of more strand results in a more flexible wire rope. The most flexible galvanised wire rope that could be obtained and was thus used. This was the 0.6 mm 1x7 galvanised steel wire rope by Engelmann.

3.3.2. Number of wire ropes

For the flexible shaft to function, the wire ropes must form a lumen with a constant cross-section. The more wire ropes, the more the lumen is closed of which prevents the tissue from escaping the lumen. The maximal number of wire ropes that fit the ring magnets to form a lumen can be calculated with Equation 3.6. With N is the maximal number of wire ropes that will fit. The outcome should be rounded to the closest lower integer. d_w is the wire diameter and d_{ri} is the inner diameter of the ring magnet. These variables are also schematically represented in Figure 3.11.

$$N = \frac{\pi}{sin^{-1}(\frac{D_w}{D_{ri}-D_w})} \tag{3.6}$$

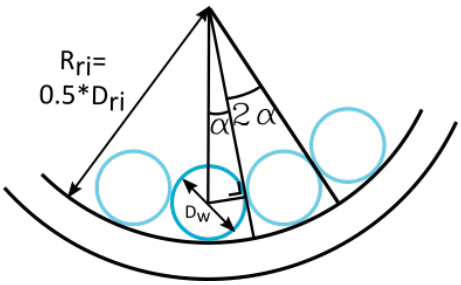

Figure 3.11: Schematic representation of the variables influencing the number of wire ropes that fit the inside of a ring magnet.D_w is the wire diameter, D_{ri} is the inner diameter of the ring and α is the angle between the tangent line that runs through the centre of the ring magnet and the contact points between the wire ropes.

For the chosen ring magnets with a hole diameter of 5 mm and blades that have a diameter of 0.6 mm, the maximum number of blades that will fit is equal to $N = \frac{\pi}{sin^{-1}(\frac{0.6}{5-0.6})} = 22.97$. This means that a maximum of 22 wire ropes will fit in the ring magnet. However since wire ropes do not have a perfectly round cross-section wire ropes actually take up less space than is assumed in this calculation. Based on physically fitting the wires in the ring magnets it was decided to manufacture the flexible shaft with 24 wires.

3.3.3. Distance between the ring magnets

The wire ropes are kept in place by ring magnets. The less distance between these rings, the smaller the chance of the wires collapsing inwards in tight curves. There is however a limit, as more rings will decrease the flexibility of the shaft. This means there is a trade-off between the flexibility of the shaft and preventing the collapse of the wires. Furthermore, the flexibility of the wire ropes influences the distance needed between the ring magnets, as the more flexible the wire ropes are, the easier they buckle and thus the better they must be guided by having the ring magnets closer together. Steel wire ropes have a minimum bending radius which is the minimal radius at which no plastic deformation will occur. Therefore the wire ropes in the flexible shaft should not be bent in a radius that is smaller than this minimum bending radius. It depends on the wire configuration what the minimal bending radius is. For a 7x7 wire rope the minimal bending radius is approximately 21 times the diameter of the wire, while for a 19x7 wire rope the minimal bending radius is approximately 12 times the wire diameter [11]. The steel wire ropes used are 1x7 and are thus less flexible that the 7x7 wire ropes. Therefore the used wire ropes have a minimal bending radius that is bigger than 25 times the wire diameter. After a physical test the minimal bending radius for the 1x7 wire rope was found to be approximately 35 times the wire diameter. The wire ropes are under tension when they are pulled backwards. In this situation the wire ropes will always take the shortest path while the bending radius of the wire rope should never be smaller than its minimal bending radius. This results in a decrease in lumen diameter, see Figure 3.12. The wire ropes are indicated with the blue lines and the minimal bending radii are indicated with the grey arcs. The horizontal grey line indicates how the wire rope will bend to follow the shortest path without having a smaller bending radius than the minimal bending radius of the wire rope. It can be observed in Figure 3.12 that, depending on the distance between the ring magnets, the lumen will decrease. The minimal lumen diameter is indicated with $min\, d_l$ and can be calculated with Equation 3.7. In this equation α is the angle between the ring and the vertical. The distance between the magnets for a certain angle α can be calculated with Equation 3.8.

$$min\, d_l = sin(\frac{1}{2}\pi - \alpha) \cdot d_l \tag{3.7}$$

$$distance_{magnet} = 2 \cdot \alpha \cdot r_{bw} + sin(\alpha) \cdot (r_{bw} \cdot d_l) - sin(\alpha \cdot r_{bw}) \tag{3.8}$$

The trade-off between narrowing of the lumen and the distance between the ring magnets which influences the flexibility of the shaft is shown in Figure 3.13. The Matlab code used to generate this plot can be found in Appendix A. From this figure can be observed that the indeed the narrowing of the lumen increases with increasing distance between the ring magnets. For a maximum decrease in lumen diameter of 5% the distance

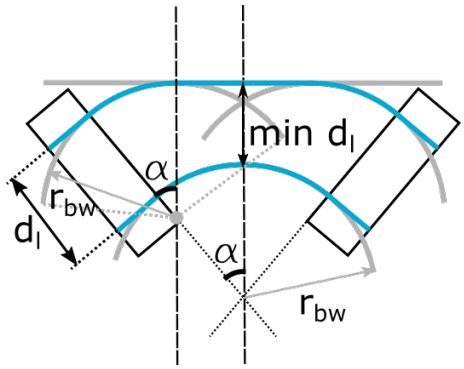

Figure 3.12: Schematic representation of the curve of the flexible shaft with the wire ropes and plates that keep the wire ropes on the required place. d_l is the lumen diameter measured from the centre of the wire rope to the centre of the opposite wire rope. r_{bw} is the minimal bending radius of the wire rope. α is the maximal angle the plates can make with respect to the vertical line without plastic deformation occurring in the wire ropes. $min\, d_l$ is the minimal lumen diameter taking into account the collapsing of the wire ropes.

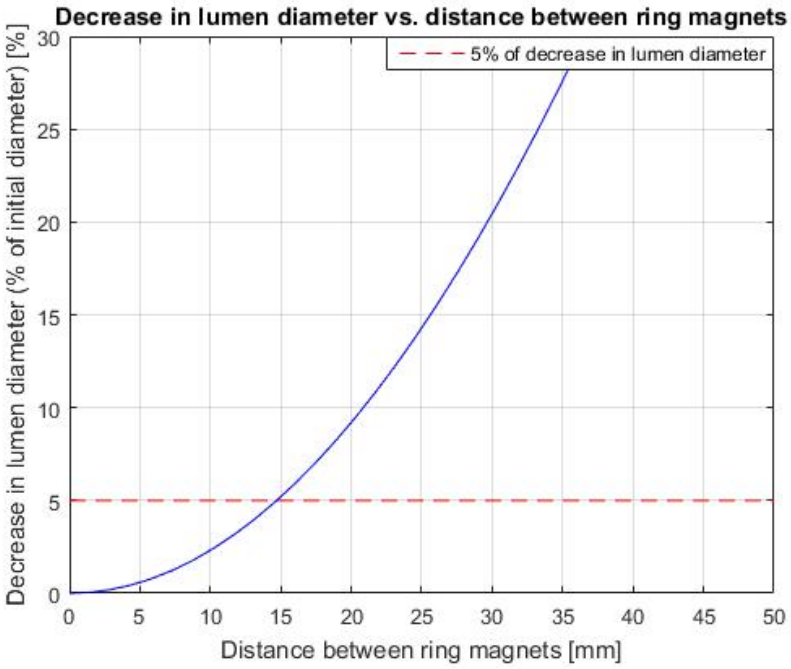

Figure 3.13: Graph showing the narrowing of the lumen as a percentage of the lumen diameter and the distance between the ring magnets.

between the ring magnets must be smaller or equal to 14.7 mm. These theoretically found values were tested in practice by using springs with 12 mm length and 30 mm length, see Figure 3.14. In this figure it can clearly be seen that a distance of 30 mm results in a non-circular lumen, which would harm the transporting abilities. Therefore it was chosen to keep the ring magnets at a maximal distance of 12 mm, as this would theoretically lead to a maximal decrease in lumen diameter of 3.3 %. In practice it was found that this distance between the ring magnets would result in the desired circular lumen.

3.3.4. Keeping the ring magnets in place

There are several ways to keep the ring magnets at the desired distance from each other. The difficulty is that the flexibility of the shaft must be preserved as well as the open lumen. In Figure 3.15 a number of possibilities to keep the magnets at the desired place are shown.

The first option is to use the magnetic repulsion between the ring magnets to keep the ring magnets at a constant distance from each other. This would not require any extra parts which is an advantage. During tests it was however found that the strength of the magnetic field decreased rapidly over the distance and thus the magnets would have a very small distance to each other. A flexible shaft of 10 cm would require over 15 magnet rings. This would not only drive up the number of parts needed and make the flexible shaft

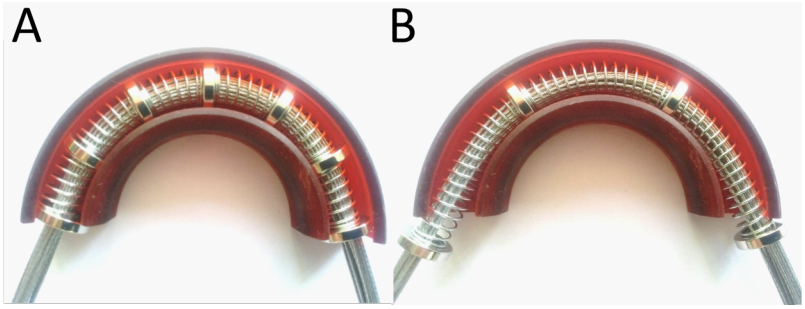

Figure 3.14: Photograph showing the change in wire rope orientation depending on the distance between the ring magnets. The ring magnets are kept at a certain place using springs with a certain length. A: spring with a length of 12 mm, which results in the wire ropes forming a circular lumen. B: Springs with a length of 30 mm, which results in a collapse of the lumen in between the ring magnets.

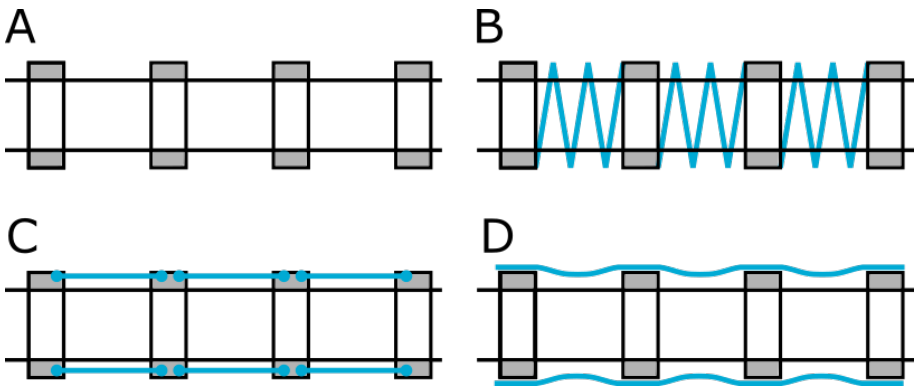

Figure 3.15: Schematic representation of different ways how the magnet rings can be kept in place. A: By magnetic repulsion between the individual ring magnets. B: By springs. C: By wire ropes. D: By a heat shrinking tube.

unnecessary heavy, it would also increase the force needed to translate the wire ropes. For more details about this test see Appendix B. Option B does not have these issues, as the springs can be chosen with any length. The springs will have to be axially stiff to prevent the magnets from moving with respect to each other. On the other hand the springs must be flexible enough to preserve the flexibility of the shaft as a whole. Since these two characteristics are connected it is not possible to find a spring that will not be pressed inwards during the translation of the blade, but does allow for easy bending. The ring magnets can also be kept at a certain place by using extra sets of wire ropes that are connected to two ring magnets (option C). The problem with this option is that wire ropes are not good in withstanding compression. The wire ropes will thus prevent the magnets from moving away from each other but will not prevent the magnets from moving closer to each other. Additionally the connection of the wire ropes to the magnets will be challenging. The last option (option D) is to use a heat shrinking tube to keep the magnets at the desired place. The heat shrinking tube shrinks around the magnets which results in a shape lock that prevents the magnets from moving with respect to each other. An extra advantage of using a heat shrinking tube is that it forms a barrier between the flexible shaft and its surroundings. This would prevent the tissue from escaping the flexible shaft during transport. A challenge that arises with this option is that the heat shrinking tube should be axially stiff as this would prevent the movement of the magnets, but it should also be flexible to allow the flexible shaft to bend. When testing the heat shrinking tube it was found that the heat shrinking tube would easily kink. This kinking occluded the lumen and prevented the wire ropes from making the required translating motion. Kinking can be avoided by adding a springlike structure. Thus by adding springs between the magnets and covering the magnets and the springs with a heat shrink, the magnets are prevented from moving, the flexible shaft is less prone to kinking and the tissue is prevented from escaping the flexible flexible shaft.

3.4. Final concept design flexible shaft

A schematic representation of the concept design can be found in Figure 3.16. The flexible shaft consists of 24 wire ropes with a 0.6 mm diameter. These wire ropes are made of galvanised steel which makes it possible to connect them with magnetic force to the ring magnets. The ring magnets are kept at 12 mm from each other by springs. The springs have a 6.5 mm inner diameter and a wire diameter of 0.6 mm. A heat shrinking tube is used to cover the whole flexible shaft to avoid tissue from escaping the flexible shaft. Furthermore, it makes the flexible shaft more stiff in axial direction, while allowing bending of the flexible shaft. An overview of all the parts and where they can be obtained is given in Table 3.1

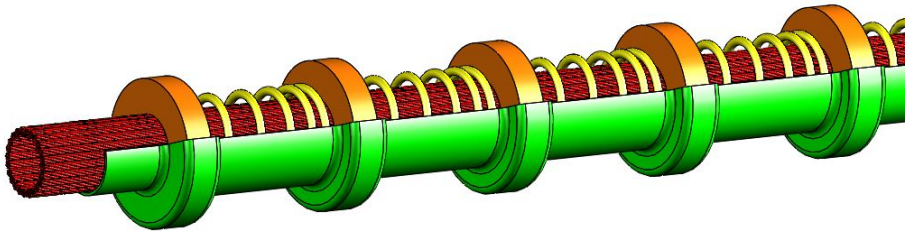

Figure 3.16: Schematic representation of the flexible shaft. The steel wire ropes (red) form a lumen due to the ring magnets (orange). The ring magnets are kept at a distance by the springs (yellow). The whole flexible shaft is covered in a heat shrinking tube (green), which keeps all the parts at the correct place and prevents tissue from escaping from the flexible shaft, while not limiting the flexibility of the shaft.

Table 3.1: Overview of the parts in the flexible shaft, their acquisition and their connection to other parts.

Part	**Details**	**Production method / Acquisition details**	**Amount**	**Connection**
1. Blade	galvanised steel wire rope d = 0.6 mm	Bought: Engelmann	24	Connected to ring magnet [2] by magnetic force.
2. Ring magnet	neodymium di = 5 mm do = 10 mm h = 2 mm	Bought: Conrad	8	Connected to blade [1] by magnetic force. Connected to heat shrinking tube [4] by shape.
3. Spring	dw = 0.5mm d = 6.5mm l = 12 mm	Bought: Het Tandhof B.V.	9	
4. Heat shrinking tube	d = 10 mm	Bought: Zwaard ijzerhandel	1	Connected to spring [3] and ring magnet [2] by shape

4

Experiment flexible shaft

In this chapter a number of experiments are discussed that are used to identify the performance of the flexible shaft. First the goal of the experiments in explained in Section 4.1, followed by the identification of the experimental variables in Section 4.2. Then the experimental facility (Section 4.3) will be discussed in as well as the experimental protocol and the used data analysis in Section 4.4 and Section 4.5 respectively.

4.1. Experimental goal

The goal of the experiment is to gain insight in the performance of the flexible shaft. Two sub-experimental goals are identified and for each of these experimental goals a separate test is designed. The first sub-goal is to see if the flexible shaft is able to transport tissue phantoms with a number of different characteristics (e.g. density and homogeneity). This will be tested during the 'Material test A' and 'Material test B'. The second sub-goal is to identify the transport performance when the flexible shaft is curved. This will be tested in the 'curve test'.

Material test A

During 'Material test A' tissue phantoms with different densities will be transported. All tissue phantoms will be homogeneous during this test.

Material test B

During 'Material test B' Tissue phantoms with different densities will be transported. All tissue phantoms will be heterogeneous during this test. The tissue phantoms are made heterogeneous by adding sesame seeds to the tissue phantom. During both 'Material test A' and 'Material test B' the transport mechanism will be in a straight position.

Curve test

The second goal is to identify the transport performance when the flexible shaft is curved which be tested by heterogeneous tissue phantoms with different densities.

4.2. Experimental variables

For each of the experiments the independent variables (the variables that are kept constant during each experiment) and the dependent variables (the variables that are measured) are identified.

4.2.1. Independent variables

Each of the tests has different independent variables.

Material test A

independent variable: Gelatin concentration.
Tissue phantoms with three different gelatin concentrations are tested S1 = 12.5 mass%, S2 = 10 mass% and S3 = 7.5 mass%.

Material test B

Independent variable: Gelatin concentration with sesame seed.
Tissue phantoms with three different gelatin concentrations are tested S1 = 12.5 mass%, S2 = 10 mass% and S3 = 7.5 mass%. Each of the tissue phantoms has approximately 5 mass% sesame seed added to generate heterogeneous tissue phantoms.

Curve test

Independent variable: Bending radius.
The flexible shaft is tested in three different curves that each have a length of 80 mm:
1) A curve angle = 0^o resulting in a bending radius of R1 = inf mm (straight).
2) A curve angle = 90^o resulting in a bending radius of R2 = 59 mm.
3) A curve angle = 180 ^{o} resulting in a bending radius of R3 = 29.5 mm.
This is done for tissue phantoms with three different gelatin concentrations S1 = 12.5 mass%, S2 = 10 mass% and S3 = 7.5 mass%.

4.2.2. Dependent variables

For each of the tests the dependent variable will be the transport rate $[\frac{mm}{cycle}]$. The transport rate is defined as the transport distance of the material per cycle. This will be determined by measuring the transported distance per 5 cycles. By measuring after 5 cycles the effect of reading errors is minimised.

4.3. Experimental facility

4.3.1. Blade manipulation

The sequence of the blade movement is the key to the friction-based transport in the flexible shaft. To be able to transport tissue phantoms, it is of great importance to move multiple blades simultaneously. Moving the blades by hand could lead to human error and thus inaccurate data. To avoid this, a research handle is designed that allows for easier manipulation of the blades. The design process of the research handle will be discussed below.

Requirements

- **Manual operation:** The blades must be operated in a manual fashion by one person. This means that the flexible shaft must be operable with a maximum of two hands. By making the flexible shaft manual operable, the system is less complicated which is desirable for a research prototype.
- **Simultaneous blade movement:** To make transport possible more than half the blades must move in the direction of transport simultaneously.

Concept design

The wire ropes form a ring with an outer diameter of 5 mm. This measure is set by the used ring magnets. Since this is small compared to human hands, direct manual manipulation of the blades is undesirable. Therefore a cone structure is used to spread the blades. The cone structure as a whole consists of an inner cone that has ridges through which the wire ropes will run and an outer cone that prevents the wire ropes from moving out of the ridges. The two cones fit together and by three screws they will be kept in place, see Figure 4.1. 24 wire ropes fit in the ring magnets. Since manipulating each of the wire ropes individually will take a lot of time, it was chosen to cluster the wires. The more clusters to more time is needed to manually operate the blades but the higher the difference in contact surface between the moving blades and the static blades will be, which will lead to a bigger friction difference and thus easier transport. This means a balance must be found. Since the rigid friction-based transport mechanism of I. van de Steeg could transport gelatin tissue phantoms with six blades, it was decided to also make six clusters of wire ropes with each four wires as this would allow for easy comparison in transport performance of the two transport mechanisms. To make it possible to manipulate one cluster of wire ropes simultaneously, sliders are used. The four wire ropes are connected to the sliders by two component glue. The sliders fit in the cavities made between the inner and outer cone. This allows the sliders and thus the wire ropes to move with a certain stroke. The size of the stroke is bound by the length of the ridge in the outer cone and the slit in the slider. It was decided to design the system in such a way that a stroke of 5 mm would be made as this is large enough to overcome the elastic behaviour of the tissue. Furthermore this is the same stroke length as is the case in the rigid friction-based transport mechanism of I. van de Steeg [17] which allows for easier comparison between the transporting

performance of the two mechanisms. The stroke size and the number of blades in the rigid friction-based transport mechanism was based on the relation between the cam design, the stroke size and the number of segments as discussed in thesis of P. Posthoorn [14]. During transport all clusters of blades must be transported simultaneously as well. This is achieved by using a 'manipulator' that allows all sliders to be pulled backwards simultaneously, see Figure 4.1. Both cones and the sliders are made by 3D printing plastic (envionTEC). 3D printing allowed for easy and fast manufacturing of the complex shapes, and since the force on the parts will be limited, the brittle structure of the 3D printed parts will not cause any problems.

Manufacturing and assembly

From now on the flexible shaft in combination with the designed handle for blade manipulation will be referred to as the research prototype. An overview of each of the parts in the research prototype and their manufacturing method can be found in Table 4.1.

4.3.2. Test setup

The setup of the research prototype during testing is schematically shown in in Figure 4.2. During testing the research prototype is placed in a designed holder that is laser cut from 5 mm PMMA. Different attachment parts were designed that allowed the flexible shaft of the research prototype to be in a straight or curved position (R = 59 mm and R = 29.5 mm). The attachment parts are placed in the table like structure. Due to the shape lock, the attachment parts cannot move with respect to the table and the research prototype.

4.3.3. Tissue phantom preparation

Gelatin

Tissue phantoms were created with three different gelatin densities using gelatin powder (Gelatin Powder Dr. Oetker, 1Kg). The tissue phantoms were made with the following mass concentrations of gelatin: 12.5 mass%, 10 mass% and 7.5 mass% as these concentrations are known to generate tissue phantoms that resemble soft tissue such as skin [18]. The gelatin was mixed with water of approximately 90^oC. The mixture was stirred until all the gelatin was dissolved in the water. The gelatin-water mixture was poured in an ice cube tray. The heterogeneous tissue phantoms were made using the same gelatin-water mixtures and adding 5 mass% of sesame seeds per tissue phantom cube. Sesame seeds were chosen to generate the heterogeneity as they have different material properties than the surrounding gelatin and are small. The gelatin tissue phantoms were cooled for a minimum of 20 hours at approximately 7^oC.

4.4. Experimental protocol

The experiment is divided in three sub-experiments ('Material test A', 'Material test B' and 'Curve test'). In 'Material test A' the transport performance for homogeneous tissue phantoms with varying densities will be identified with the flexible shaft in straight position. In 'Material test B' the transport performance for heterogeneous tissue phantoms with varying densities will be identified with the flexible shaft in straight position. In the 'Curve test' the transport performance for homogeneous tissue phantoms with varying densities will be identified with the flexible shaft in curved position (R=59 mm and R=29.5mm). A flow chart of the experiment is shown in Figure 4.3. The test as indicated in the flow chart is elaborated below and graphically shown in Figure 4.4.

The experiment set-up is shown in Figure 4.5. The test starts with cutting the gelatin tissue phantoms and introducing it to the lumen of the flexible shaft by injecting the gelatin tissue phantom between the wire

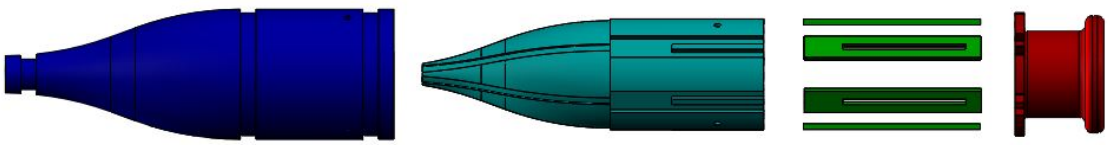

Figure 4.1: schematic representation of the handle used for the research prototype. the outer cone (dark blue) is connected to the inner cone (light blue). Six wire rope clusters run through the ridges in the inner cone and are glued to the sliders (green). The sliders can all be moved backwards simultaneously with the manipulator (red).

Table 4.1: Overview of the parts in the research prototype, their manufacturing method and their connection of other parts. With d = diameter, di = inner diameter, do = outer diameter, h= height, dw = wire diameter and l= length.

Part	**Details**	**Production method / Acquisition details**	**Amount**	**Connection**
1. Blade	galvanised steel wire rope d = 0.6 mm	Bought: Engelmann	6 (4 wire ropes per blade resulting in 24 wire ropes)	Connected to ring magnet [2] by magnetic force. Connected to slider [7] by glue.
2. Ring magnet	neodymium di = 5 mm do = 10 mm h = 2 mm	Bought: Conrad	10	
3. Spring	dw = 0.5mm d = 6.5mm l = 30mm mm	Bought: PMB shop	10	
4. Heat shrinking tube	d = 10 mm	Bought: Zwaard ijzerhandel	1	
5. Outer cone	See Appendix C	3D-printing	1	Connected to inner cone [6] by screws.
6. Inner cone	See Appendix C	3D-printing	1	Connected to outer cone [5] by screws.
7. Slider	See Appendix C	3D-printing	6	connected to blade [1] by glue.
8. Manipulator	See Appendix C	3D-printing	1	connected to slider [7] by shape.

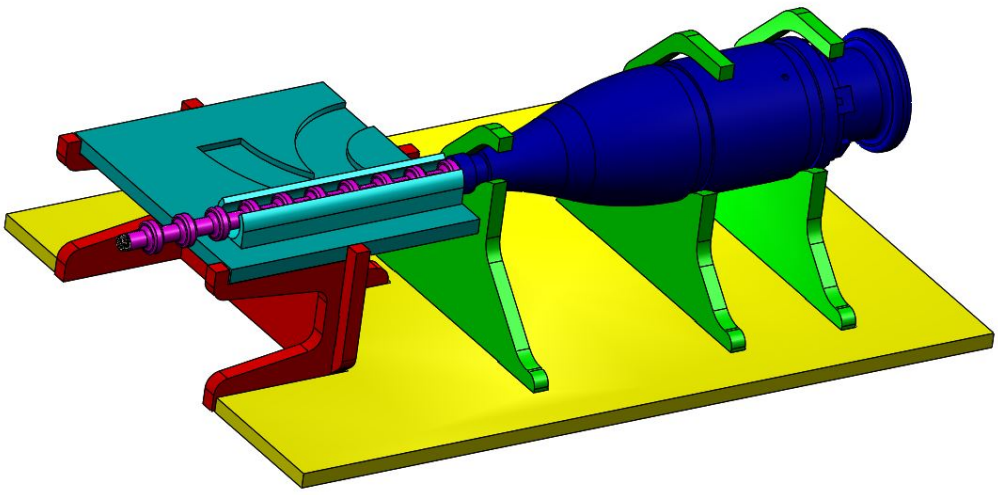

Figure 4.2: Schematic representation of the measurement set up. The handle of the research prototype (dark blue) is placed in the holders (green) that are glued to the ground plate (yellow). The tip of the research prototype (pink) can be placed in a number of curves (light blue) that can be placed on a table like structure (red). This table like structure can be sided in the ground plate (yellow).

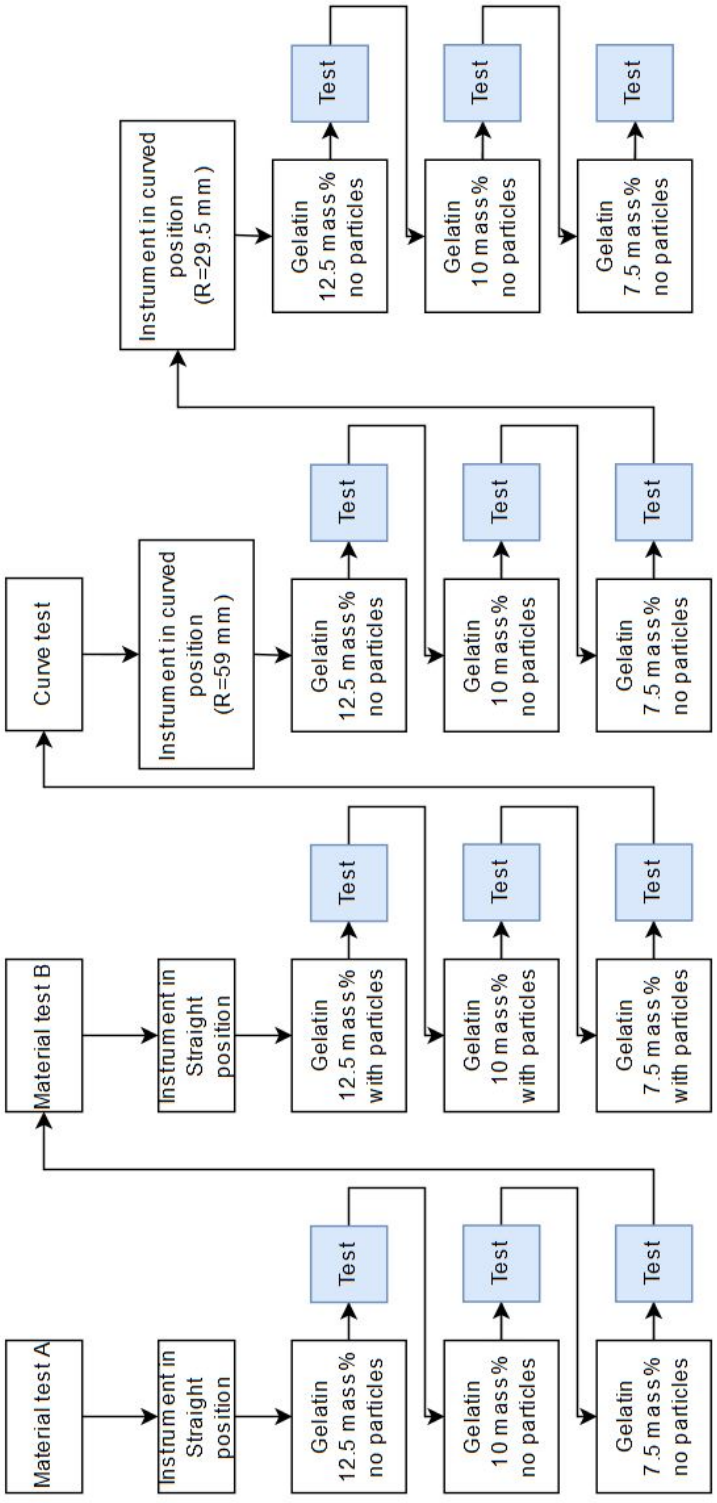

Figure 4.3: Flowchart of the different sub-experiments executed.

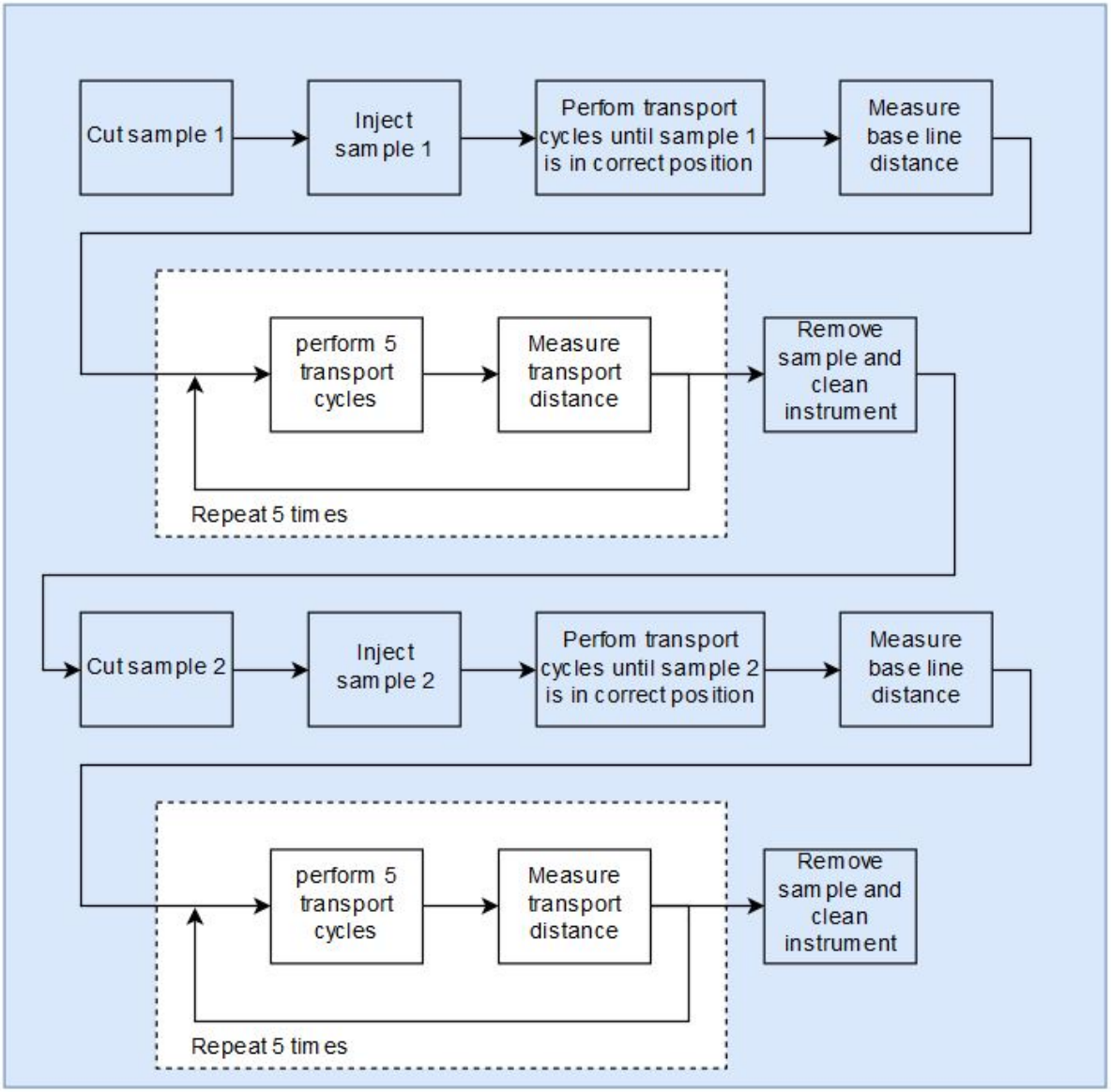

Figure 4.4: Flowchart of the test

ropes using the 3D printed cutting and injecting tool, see Figure 4.5. For each test the acquisition of the measurement data starts once the entire tissue phantom is located in the part of the flexible shaft that is covered by the heat shrink tube. Once the gelatin tissue phantom is in the correct position, this starting point is measured. The travelled distance will be measured after five cycles to limit the effect of inaccuracy due to measurement errors, by introducing a flexible plastic wire, called the transport distance measuring tool, in the lumen of the flexible shaft. One layer of masking tape was applied on this flexible plastic wire on which the transport distance could be indicated with a pen. For each type of tissue phantom, two samples were cut. These individual samples were tested by measuring the travelled distance after five cycles, five times in a row. This results in ten measurement per type of tissue phantom. After the 5 measures per sample were obtained, the tissue phantom sample is removed from the flexible shaft and the wire ropes are cleaned with a paper towel. The research prototype is put together after which the test is repeated with a new tissue phantom.

4.5. Data analysis

The transported distance per five cycles will be measured as previously described. For each of the type tissue phantoms this is repeated 10 times (5 measures per samples). The mean transport distance per cycle will be determined. Per type tissue phantom the mean transport distance as well as the standard deviation will be determined and graphically shown. The data analysis will be performed in MATLAB 2015B. The used MATLAB files can be found in Appendix A. A one-way ANOVA test will be performed to investigate if there is a significant difference in the transport rate depending on the gelatin density. A t-test will be conducted to investigate if there is a significant difference in the transport rate depending on the heterogeneity and the curve of the research prototype. A P-value smaller than 0.05 indicates that there is 95% certainty that there is a significant difference between the transport rates of the data sets.

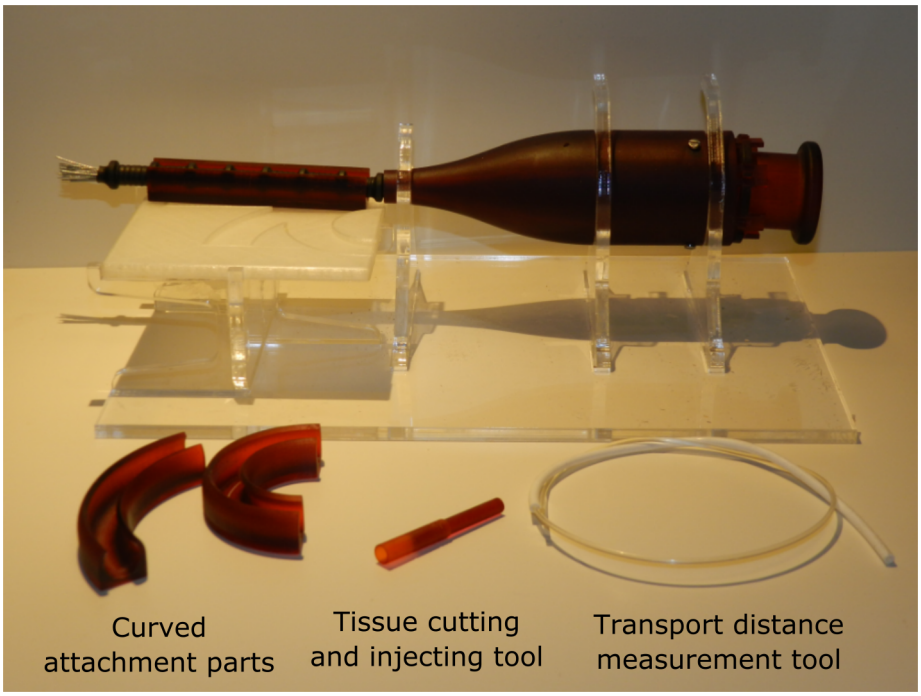

Figure 4.5: picture of the measurement setup with both the transported distance measurement tool, the tissue cutting and injecting tool and the curve attachment parts.

5

Results flexible shaft

A summary of the experimental results can be found in Section 5.1. The results regarding the density of the gelatin tissue phantoms can be found in Section 5.2. The results regarding the homogeneity of the gelatin tissue phantoms as well as the curve of the instrument can be found in Section 5.3 and Section 5.4 respectively. The raw data of the experiments can be found in Appendix D.

5.1. Summary experimental results

A graph summarising all the data found during the experiments can be found in Figure 5.1. During the experiment it was found that the transport mechanism was not able to transport substances when curved with a bending radius of 29.5 mm, therefore no measurements could be obtained with the mechanism curved with this bending radius. One-way ANOVA tests were performed to investigate the likelihood of a correlation between the transport rate and the density of the tissue phantom. A t-test was conducted to investigate the likelihood of a correlation between the transport rate and both the homogeneity and the curve of the flexible shaft.

5.2. Density tissue phantom

In Figure 5.2 a box plot summarising the results of 'Material test A' can be found. The mean transport rate for a 12.5 mass% gelatin tissue phantom was 2.71 mm/cycle with a standard deviation of 0.21 mm/cycle. The mean transport rate for a 10 mass% and 7.5 mass% gelatin tissue phantom was 2.81 mm/cycle ±0.45 mm/cycle and 2.97 mm/cycle ±0.47 mm/cycle respectively. Performing a one way ANOVA test between these three data sets resulted in a P-value of 0.35. This P-value is bigger than 0.05 and therefore there is not a statistically significant difference.

5.3. Homogeneity tissue phantom

In Figure 5.3 the data of both Material test A (in black) and B (in blue) are shown. The mean transport rate for the 12.5 mass%, 10 mass% and 7.5 mass% gelatin tissue phantoms were 2.25 ± 0.20 mm/cycle, 2.17 ± 0.28 mm/cycle and 2.4 ± 0.43 mm/cycle respectively. For each of the gelatin densities a t-test was performed to test the likelihood of a correlation between the tissue phantoms with and without sesame seeds. The P-value found for the 12.5 mass% tissue phantom was $7.5 * 10^{-4}$, for the 10 mass% gelatin tissue phantom the P-value was $2.8 * 10^{-3}$ and for the 7.5 mass% gelatin tissue phantom the P-value was $5.7 * 10^{-2}$. The P-values of the 12.5mass% gelatin and the 10 mass% gelatin had a P-value is smaller than 0.05, while for the 7.5 mass% gelatin tissue phantom the found P-value is bigger than 0.05. From this it can be concluded that there is a statistically significant difference for the 12.5 mass% and the 10 mass% gelatin tissue phantoms but not for the 7.5 mass% gelatin tissue phantom.

5.4. Curve flexible shaft

In Figure 5.4 the data of the 'Curve test' are represented in a boxplot (in blue) as well as the results of 'Material test A' (in black). The mean transport rates of the gelatin tissue phantoms with the flexible shaft in curved

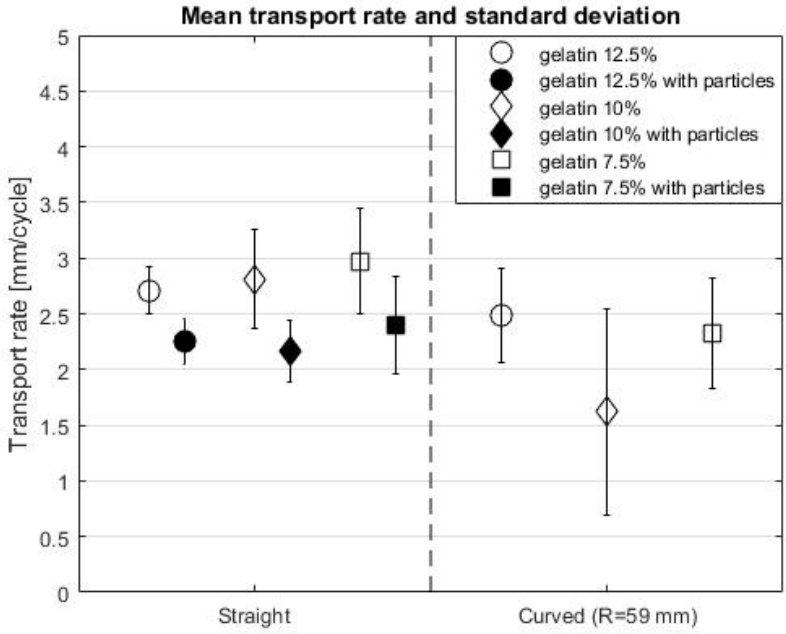

Figure 5.1: Graph showing the mean and standard deviation of the transport rate per cycle for different tissue phantoms with the flexible shaft in straight and curved position.

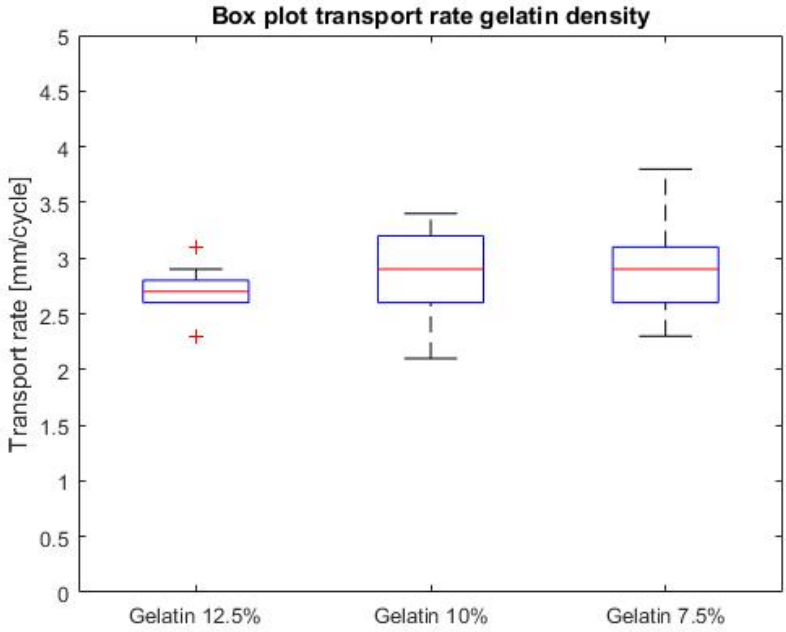

Figure 5.2: Box plot of the measured transport rate for gelatin tissue phantoms with different densities. The median is indicated with the red line. The bottom and top edge of the box indicate the 25th and 75th percentiles. Whiskers extend to the lowest and highest data point value excluding outliers that are indicated with a red '+'.

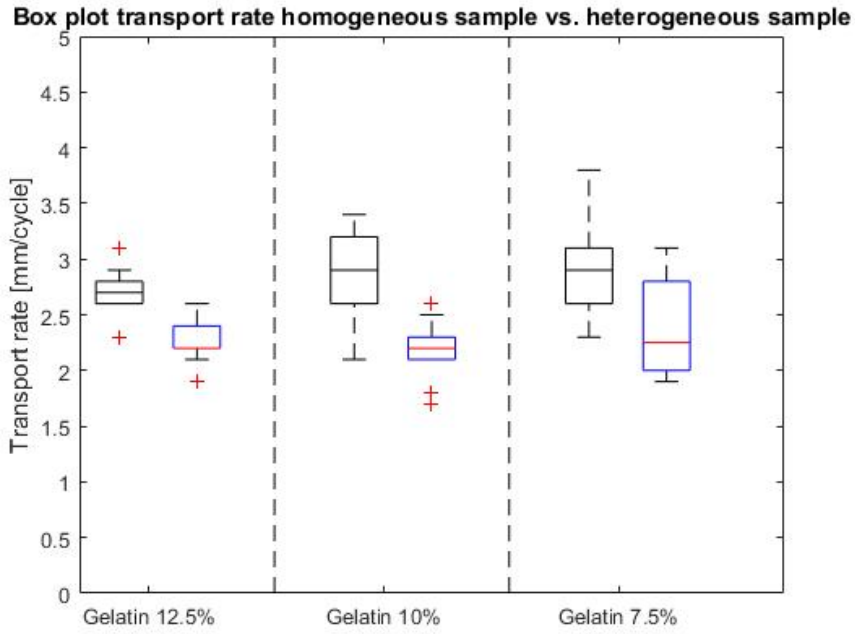

Figure 5.3: Box plot of the measured transport rate for gelatin tissue phantoms with different densities, with (in blue) and without sesame seed (in black).The median is indicated with the red line. The bottom and top edge of the box indicate the 25th and 75th percentiles. Whiskers extend to the lowest and highest data point value excluding outliers that are indicated with a red '+'.

position were 2.49 ± 0.42 mm/cycle, 1.62 ± 0.92 mm/cycle and 2.32 ± 0.49 mm/cycle for the 12.5%, 10% and 7.5% gelatin tissue phantoms respectively. The P-value found by performing the t-test for each of the gelatin densities was $2.3 * 10^{-1}$, $1.8 * 10^{-4}$ and $1.8 * 10^{-3}$ for the 12.5 mass%, 10 mass% and 7.5 mass% gelatin tissue phantoms respectively. From these values it can be concluded that there is no statistically significant difference for the 12.5 mass% gelatin tissue phantom, but there is for the 10 mass% and the 7.5 mass% gelatin tissue phantoms.

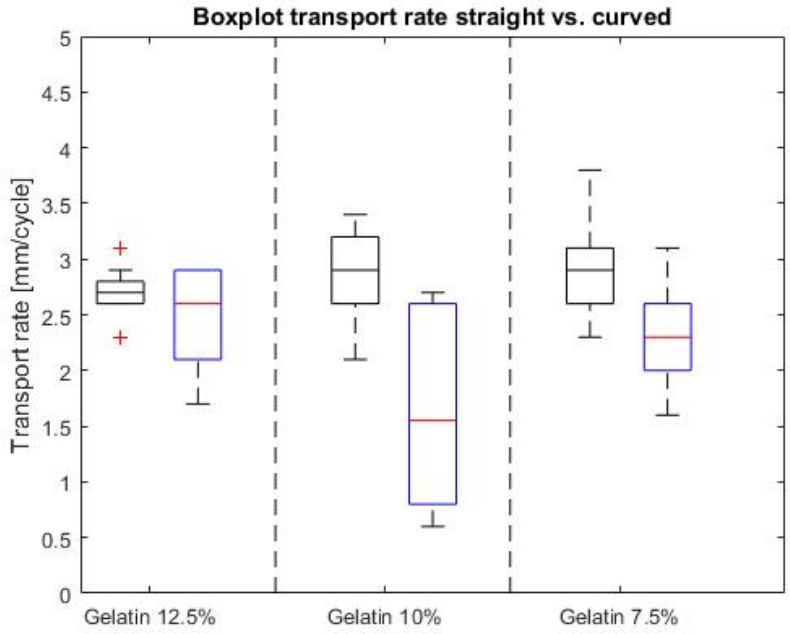

Figure 5.4: Box plot of the measured transport rate for gelatin tissue phantoms with different densities with the flexible shaft in straight (in black) and curved position (in blue). The median is indicated with the red line. The bottom and top edge of the box indicate the 25th and 75th percentiles. Whiskers extend to the lowest and highest data point value excluding outliers that are indicated with a red '+'.

6

Final prototype development and validation

In the previous chapter the results of the flexible shaft are presented. A handle is designed to make the flexible shaft easier to operate. In this chapter the design of the handle will be discussed as well as the validation of the final prototype which consist of this new handle in combination with the earlier validated flexible shaft. First the requirements that must be fulfilled by the handle are presented in Section 6.1, followed by the concept generation in Section 6.2. Then the final prototype will be discussed more elaborate in Section 6.3. Finally the handle in combination with the earlier validated flexible shaft will be tested as described in Section 6.4. The results of the test will be presented in Section 6.5.

6.1. Design requirements handle

- **Motion translation:** The user will manipulate the final prototype via the handle. By giving a certain input, the user will be able to transport the tissue. This means that in the handle the input of the user must be translated to the movement of the blades in a certain sequence.
- **Unobstructed transport:** The transport of the material must not be obstructed in the handle. This means that the tissue can be transported from the tip of the flexible shaft to the other end of the handle. The lumen through which the tissue is transported must have a constant cross-section over the entire length of the final prototype.
- **Hand held:** The final prototype must be hand held when used. No extra structure must be needed when operating this final prototype.
- **Operated by one person:** The final prototype must be able to be operated by one person. This means that a maximum of two hands can be used to hold the final prototype and give the required input to initiate the transport.
- **Manual operation:** The final prototype must be operated in a manual way. Since the final prototype is intended to be used in a medical setting, it is valuable that the final prototype is manually operated as the addition of electricity to the final prototype could make the prototype more complex. As this final prototype is intended for research only, adding complex electrical components is not desirable.

6.2. Concept generation handle

6.2.1. Motion translation

To operate the final prototype a manual input by the user must be translated to the required translated motion of the blades. There are several ways how this can be achieved. These ideas can be ordered based on the amount of automation, see Figure 6.1. The most direct way of operation is letting the user individually pull and push the blades such that the tissue can be transported. This is a discrete user input as the user is required to execute a number of discrete proceedings to generate the wanted output. Due to the number of

proceedings that must be executed, this design is prone to human error. The blade movement can be automated by using a separate structure, that actuates the blades is the correct sequence. The prototype can be actuated in a discrete way, for instance by a rotating knob, or can be made more comfortable to operate by designing it in such a way that the user can give a continuous input, for instance by rotating a sling. The final prototype can be automated further by using electrical actuation. However, since it was stated in the design requirements that the final prototype must be operated manually, electrical actuation is not an option. This means that either a discrete user input or a continuous user input must be translated to the required blade movement.
To eliminate human error as much as possible a barrel cam can be used to actuate the blades in the correct sequence. A cam is used to translate a rotational motion in a translating motion, therefore a cam can be used to translate a discrete or continuous rotational user input to the desired translating motion of the blades. A barrel-cam has a grove that wraps around the barrel, see Figure 6.2. The sliders are connected to the cam by a pin that fits the grove. furthermore, the sliders are connected to the outside world in such a way that the connection only allows for translation of the blades. By rotating the cam, the pin will follow the grove and thus the blade will translate. The shape of the grove of the cam results in a certain translating motion pattern of the blades, see Figure 6.3 The height S_b of the grove determines the stroke of the sliders and thus of the blades. Furthermore, the movement sequence of the blades is predetermined in the shape of the cam grove. The transport is friction-based. For the optimal performance the friction difference between the forward and backward moving blades must be maximised. This means that at every moment in time a maximum of one slider will move forward while all other sliders will move backwards simultaneously. The needed grove shape for this movement sequence is shown in Figure 6.3. The total horizontal length of the grove is equal to $2\pi * R_c\,[m]$ in which $R_c\,[m]$ is the cam's radius. The number of sliders and thus the number of blades that can separately be activated is $n\,[-]$ this means that the first part of the grove (downwards) has a horizontal length equal to $\frac{n-1}{n}2\pi * R_c$. The second part of the grove (upwards) has a horizontal length of $\frac{1}{n}2\pi * R_c$. For the cam to work, angle α and β should be small. Bigger angles result in more friction and thus the sliders will move less smooth. Based on previous working cams it was chosen to set a maximum angle for the angels at 30^o. This means there is a minimum radius that the cam must have in order to allow for easy actuation of the sliders. The final prototype will have six groups of wire ropes that are actuated individually, as was the case for the research prototype.This means that five blades move backwards simultaneously while one blade moves forward. The strokes of the blades will be the same as in the research prototype which is 5 mm. Taking this in account will results in a minimal cam radius of 8.3 mm. The most ergonomic way for a user to actuate the cam would be by rotating a sling, as this would allow for continuous input. Thus a rotation of the sling results in rotation of the cam which will lead to translation of the blades.

6.2.2. Continuous transport

As stated in the requirements, the final prototype must be able to transport the tissue all the way from the tip of the flexible shaft to the end of the handle continuously. Furthermore, there must be contact between the blades and the transported tissue over the entire length of the final prototype. The barrel cam as shown in Figure 6.2 will not allow for continuous transport. This means that the cam design must be changed in such

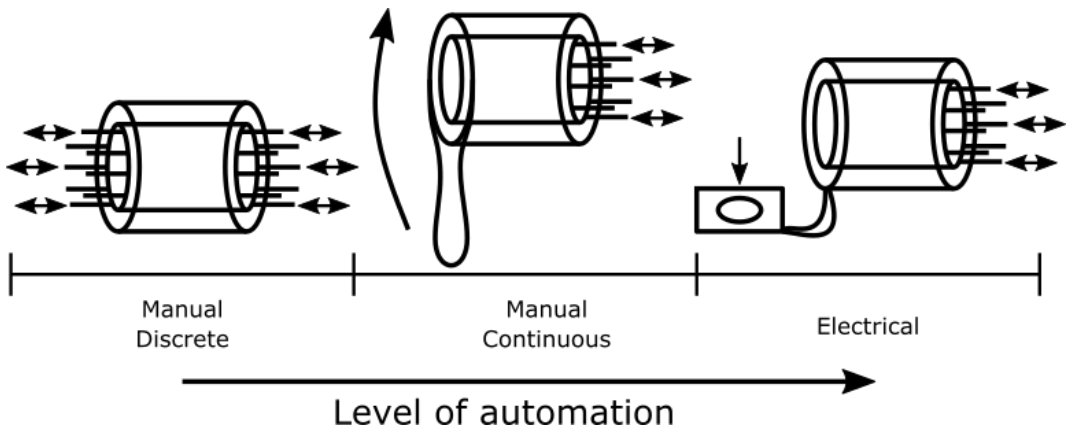

Figure 6.1: Schematic representation of different levels of automation that can be used for the handle design.

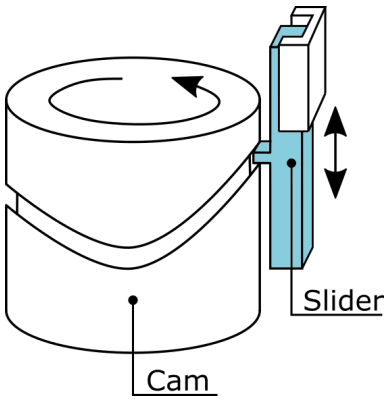

Figure 6.2: Schematic representation of a barrel-cam. The cam has a groove that influences the translating motion of the slider. The slider is connected in such a way that it can only translate. The slider has a pin that fits in the groove of the cam. By rotating of the cam the slider will make a translating motion.

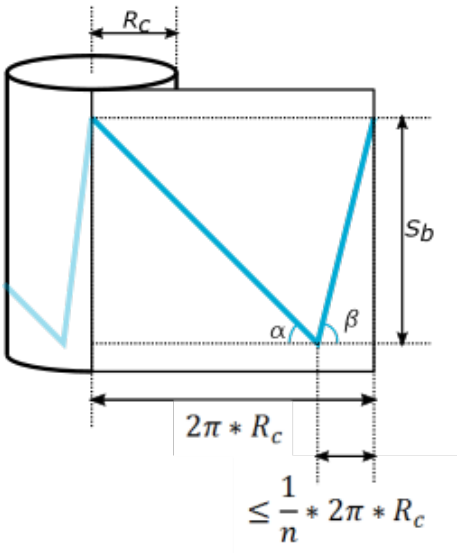

Figure 6.3: Schematic representation of the design of the cam. R_c is the radius of the cam and n is the number of pairs of blades. S_b is the stroke of the blades that is required.

a way that the cam will allow for continuous transport and contact between the blades and the transported tissue. The first option to allow for continuous transport is to add a hole in the centre of the barrel cam. The transported tissue can now go through the hole in the barrel cam from the tip to the other end of the final prototype. For this transport also contact between the blades and the to be transported tissue is needed. This means that there must be a way to connect the sliders which are at the outside of the cam to the wire ropes that need to go through the hole in the cam. A possible slider design is given in Figure 6.4 A. As can be seen, the shape of the slider is rather complicated and will, therefore, be complicated to manufacture. By creating a cam that consists of two halves, the slider can be made less complicated, while still allowing for continuous transport and contact between the blades and the transported tissue, see Figure 6.4 B. A problem that arises in this design is that the sliders can get stuck. Only one of the cam halves is actuated. The other halve will move due to the fact that the actuated cam halve pushes via the pins of the slider to the non-actuated halve. Once the pin is at a corner in the groove it will get stuck. The slides and thus the blades will not move smoothly which will complicate the transport. It can also be chosen to use one actuated cam halve and use springs to make sue the pins of the sliders follow the grove of the cam, see Figure 6.4 C. This design, however, suffers from the same problem as the design with the two halve cams, as in this case the pins can also get stuck. The springs push the pins of the sliders down thus when the pin is located at the corner, the pin gets stuck, and thus the translating of the blades will not be smooth. The last option is an inside-out cam, see Figure 6.4 D. This allows for an easy slider design, continuous transport and uninterrupted contact between the blades and the tissue. The cam is more difficult to fabricate as the grove cannot easily be produced by regular machining. However, 3D printing can be used to create such an inside-out cam in an easy manner.

6.2.3. Sliders

The sliders are connected to the blades, that consist of a number of wire ropes, which are translated in a certain sequence by the cam. The connection of the sliders to the blades can be achieved in several ways, as shown in Figure 6.5. The wire ropes can be glued to the curved slider as shown in Figure 6.5 A. It would, however, be complicated to make sure that the wire ropes are glued perfectly in line with the slider. To make sure that the wire ropes are fixated in the correct orientation, the wire ropes can each be connected individually by glueing each wire rope in a hole, see Figure 6.5 B. This will require quite some machining. Since multiple wire ropes are actuated simultaneously, the whole cluster of wire ropes can be connected by glueing them in one hole, see Figure 6.5 C. Both option B and C do not allow for contact between the wire ropes and the transported tissue. To achieve this desired contact between the transported tissue and the blades, the blades can be connected as shown in in Figure 6.5 D. This way the wire ropes can be glued in the correct orientation due to the ridges while still maintaining contact with the transported tissue.

6.2.4. Hold of the handle

In the requirements it was set that the final prototype must be hand held and must be able to be used by one person. Therefore it was decided to add a hold to the handle design. This hold can be held with one hand while the other hand is used to rotate the sling.

6.3. Final prototype design

A schematic representation of the final prototype can be found in Figure 6.6. An exploded view is given in Figure 6.7. The flexible shaft that is discussed in Chapter 3, is indicated in pink. Due to the limiting space it was chosen to have 3 wire ropes per blade, instead of the 4 wire ropes per blade as is the case in the research prototype. The tip of the handle is indicated in dark blue. In the tip an extra ring magnet, indicated in pink, is glued. The magnet makes sure that the wire ropes will form a circular lumen in the tip of handle. The slider house, which guides the sliders to make a translating motion, is indicated in light blue. The hold of the handle is indicated in green and the sliders to which the wire ropes are glued are indicated in yellow. The orange part is the cam, and due to its shape, it can easily be used to actuated the blades by rotating it. On both sides of the cam a circlip is placed which will will allow for easy rotation of the cam. Manipulation of the blades by rotating the cam results in a discrete user input which is less ergonomic than a continuous user input. therefore a sling is added, indicated in red. This sling can be used to rotate the cam with a continuous user input. An overview all the parts, their manufacturing method and the connection is given in Table 6.1.

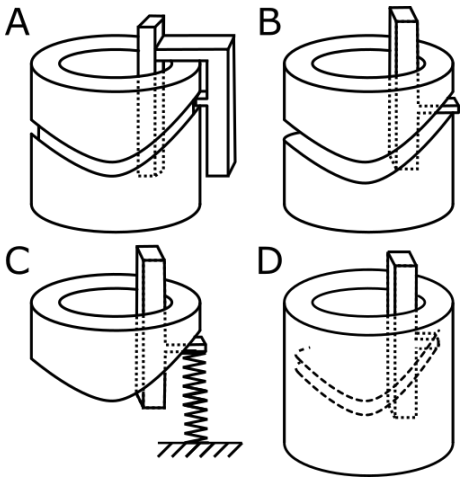

Figure 6.4: Schematic representation of different cam designs. A: Regular barrel cam with a hole. B:Two halves cam. C: Half cam with springs. D: in-side-out cam

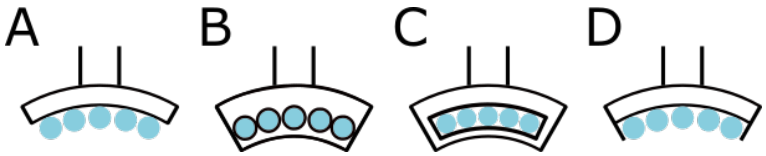

Figure 6.5: Schematic representation of different connections that can be used to connect the wire ropes to the sliders.

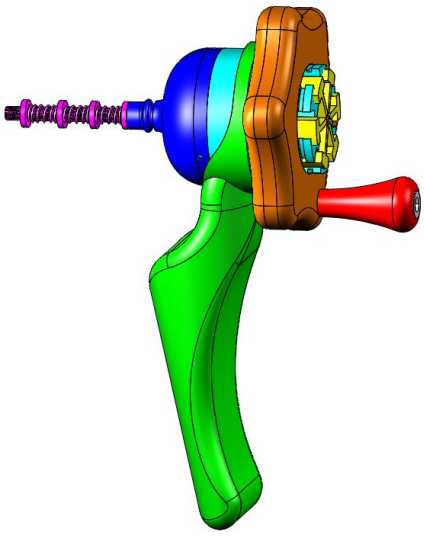

Figure 6.6: Schematic overview of the final prototype. The flexible shaft (pink) is connected to the tip (dark blue) by the heat shrink tube. The wire ropes are glued the sliders (yellow) that slide through the slider house (light blue). The final prototype is held with one hand by the hold (green) the other hand can be used to actuate the final prototype by either rotating the cam (orange) or rotating the sling (red).

Table 6.1: Overview of the parts in the final prototype, their manufacturing method and their connection of other parts.

Part	**Details**	**Production method / Acquisition details**	**Amount**	**Connection**
1. Blade	galvanished steel wire rope d = 0.6 mm	Bought: Engelmann	6 (3 wire ropes per blade resulting in 18 wire ropes)	Connected to ring magnet [2] by magnetic force. Connected to slider [7] by glue.
2. Ring magnet	neodymium di = 5 mm do = 10 mm h = 2 mm	Bought: Conrad	5	Connected to blade [1] by magnetic force. Connected to spring [3] by magnetic force.
3. Spring	dw = 0.5mm d = 6.5mm l = 12 mm mm	Bought: the Tandhof BV.	3	Connected to ring magnet [2] by magnetic force.
4. Heat shrinking tube	d = 10 mm	Bought: Zwaard ijzerhandel	1	Connected to ring magnet [2] by shape.
5. Tip	See Appendix C	3D-printing	1	Connected to slider house [6] by screws.
6. Slider house	See Appendix C	3D-printing	1	Connected to tip [5] by screws.
7. Hold	See Appendix C	3D-printing	1	
8. Slider	See Appendix C	Electrical discharge machining	6	connected to blade [1] by glue.
9. Cam	See Appendix C	3D-printing	1	
10. Sling	See Appendix C	3D-printing	1	connected to Cam [9] by screw.

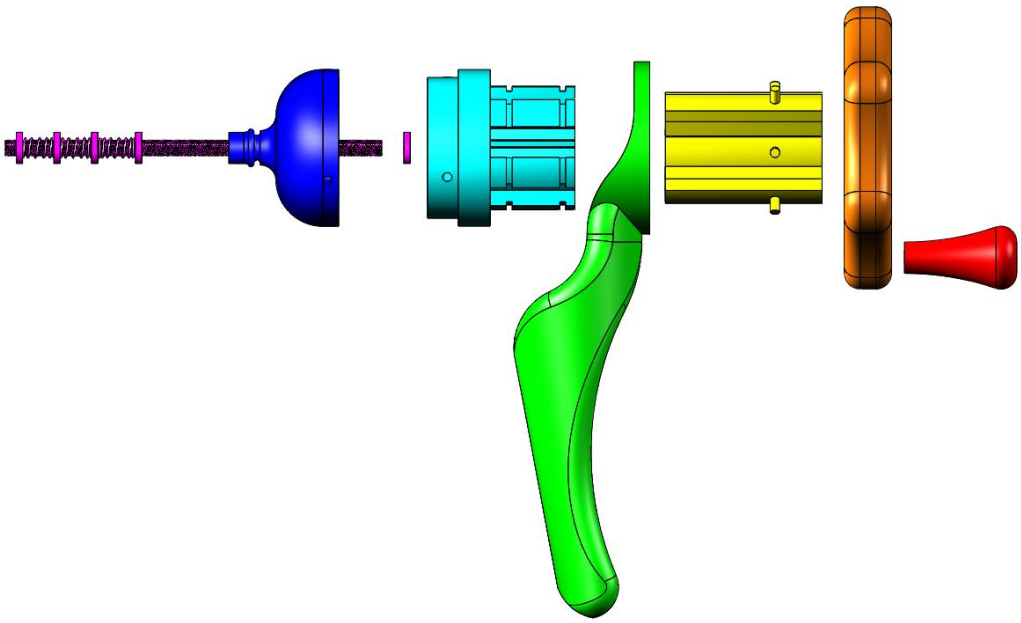

Figure 6.7: exploded view of the final prototype. The flexible shaft (pink) is connected to the tip (dark blue) by the heat shrink tube. In the tip an extra magnet (pink) is glued. The wire ropes are glued the sliders (yellow) that slide through the slider house (light blue). The final prototype is held with one hand by the hold (green) the other hand can be used to actuate the final prototype by either rotating the cam (orange) or rotating the sling (red).

6.4. Proof-of-principle experiment final prototype

To validate the performance of the new handle in combination with the validated flexible shaft the following experiment will be executed.

6.4.1. Experimental goal

The goal of the experiment is to gain insight in the performance of the newly designed handle in combination with the already validated flexible shaft. The final prototype will be tested by measuring the transport rate when transporting a gelatin tissue phantom while the flexible shaft is in straight and in curved (R=59 mm) position.

6.4.2. Experimental variables

The independent variable is the curve of the flexible shaft. The flexible shaft will be tested in straight position and in a curved position with a bending radius of 59 mm. The dependent variable is the number of cycles that is needed to transport the gelatin tissue phantom (12.5 mass% gelatin) from the tip of the flexible shaft to the end of the handle.

6.4.3. Experimental facility

The final prototype will be held with one hand and the sling will be turned with the other hand. The same curved attachment parts as used during the validation of the research prototype will be used to make sure that the final prototype is curved in the same manner.

6.4.4. Experimental protocol

The tissue phantoms will introduced to the final prototype by injecting the cut tissue phantom between the wire ropes in the same manner as during the validation of the research prototype. The number of cycles, which is equal to the number of sling rotations, needed to transport the tissue phantom all the way through the final prototype is counted. The experiment will start at the moment that the tissue phantom is fully inside the flexible shaft covered by the heat shrinking tube and will end once the tip of the gelatin tissue phantom has reached the end of the handle. The travelled distance will thus be equal to the length of the final prototype

(the flexible tip and the handle) minus the length of the tissue phantom.

6.4.5. Data analysis

The number of cycles needed to transport the gelatin tissue phantom through the final prototype will be stored. Form this the transport rate [mm/cycle] can be deducted by using equation 6.1.

$$Transportrate[\frac{mm}{cycle}] = \frac{transportdistance[mm]}{numberofcycles[cycle]} \tag{6.1}$$

Box plots of the transport rate in curved and in straight position will be generated. A t-test will be performed to investigate if there is a significant difference in the transport rate depending on the curve of the flexible shaft. A P-value smaller than 0.05 indicates there is at least a 95% certainty that there is a significant difference between the transport rates of the data sets. The data analysis will be performed in MATLAB 2015B. The used MATLAB files can be found in Appendix A.

6.5. Results final prototype

The raw data of the experiments can be found in Appendix D. Pictures showing the transport rate per cycle can be seen in Figure 6.8. A box plot summarising the results of experiment one, that compared the transport rate of the flexible shaft in straight and in curved position can be found in Figure 6.9. The mean transport rate with the flexible shaft in straight position was 2.38 mm/cycle with a standard deviation of 0.29 mm/cycle. The mean transport rate with the flexible shaft in curved position (R = 59 mm) is 2.33 mm/cycle with a standard deviation of 0.34 mm/cycle. The performance of a t-test resulted in P = 0.73. From this it can be concluded that there is no statistically significant difference in the transport rate depending on the curve of the flexible shaft.

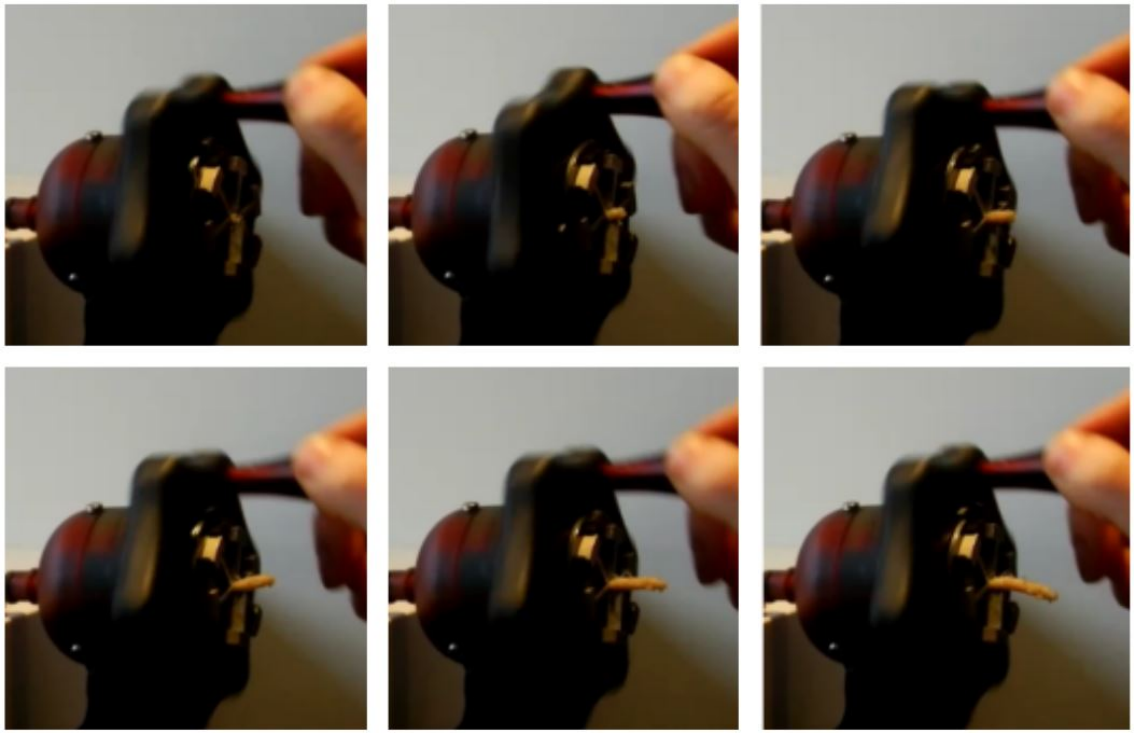

Figure 6.8: Pictures showing the transport of a tissue phantom. The pictures are taken one sling rotation (one blade movement cycle) apart.

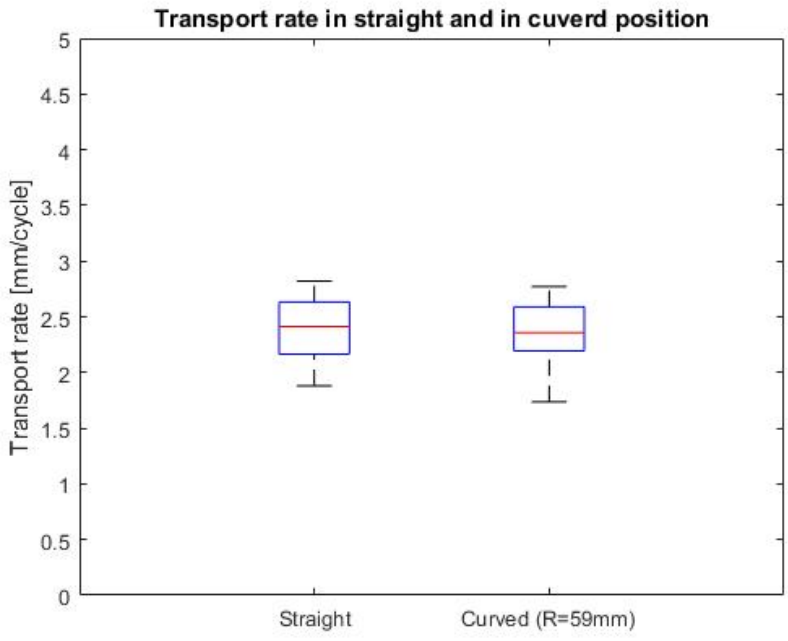

Figure 6.9: Box plot of the data obtained during the validation of the final prototype with handle. The measured transport rate [mm/cycle] is given for the flexible shaft in straight and in curved position (R=59 mm) The median is indicated with the red line. The bottom and top edge of the box indicate the 25th and 75th percentiles. Whiskers extend to the lowest and highest data point value excluding outliers that are indicated with a red '+'.

7

Discussion

7.1. Main Findings

Inspired by the ovipositor of parasitoid wasps, a flexible friction-based transport mechanism was developed (length (L) = 105 mm, outer diameter (OD) = 10.5 mm, inner diameter (ID) = 4 mm). This final prototype consists of 18 wire ropes that, due to their attraction to ring magnets, form a lumen through which tissues can be transported. In order to eliminate contact between the transported tissue and the surroundings, as well as to keep the ring magnets in place, a heat shrinking tube is used to cover the flexible shaft. The application of a torque will not influence the translating motion of the wire ropes, as the wire ropes creating the lumen can rotate freely in the hole of the ring magnet. The validation of the flexural rigidity of the flexible shaft is described in Appendix E, and is $3.7 * 10^{-3} \pm 3.2 * 10^{-4} [Nm^2]$ which is lower than the flexural rigidity of colonoscopes [9].

In a proof-of-principle experiment, it was shown that the flexible shaft is able to transport tissue phantoms with different material properties in a straight and in a curved position (R = 50.9 mm). The average transported distance per cycle was 2.4 mm. The mean transport distance per cycle was slightly higher with the flexible shaft in straight position (2.8mm) than in curved position (2.1 mm). It was also found that a stronger curve of the flexible shaft (R = 25.4 mm) would not allow for transport through the lumen. There was no significant difference found in the transport rate depending on the gelatin density of the tissue phantoms. However, there was a significant influence of the homogeneity of the gelatin tissue phantoms for the 12.5 mass% and the 10 mass% gelatin tissue phantom. There was no significant difference between the transport rate with the flexible shaft in straight and in curved position for the 12.5 mass% and the 7.5 % gelatin tissue phantoms. For the 10 mass% gelatin tissue phantom, however, a large significant difference was found. When looking at the raw data of the 10 mass% gelatin tissue phantom, it can be observed that there is a big difference between the transport rate between the first sample and the second sample that was tested. The transport rate of the first sample is 3.8 ± 0.57 mm/5 cycles while the transport rate of the second sample was measured to be 12.4 ± 1.08 mm/5 cycles. Possibly during the first sample there was no optimal contact between the wire ropes and the tissue phantom. This could explain the low transport rate measured when testing sample 1. The data obtained during the test with the first sample might therefore be unreliable. After the working principle of the flexible shaft was validated, a handle was designed resulting in the final prototype. This handle allows the user to employ the final prototype by a continuously rotation of the sling. Tissue can be transported in both directions by rotating the sling clockwise or counter clockwise. The flexible shaft with handle was validated by transporting gelatin tissue phantoms (12.5 mass%). Both in curved (R = 50.9 mm) and in straight position of the flexible shaft,the final prototype was able to transport the gelatin tissue phantoms from the distal tip of the flexible shaft all the way towards the end of the handle. The mean transport rate of the gelatin tissue phantom was 2.38 ± 0.29 mm/cycle and 2.33 ± 0.34 mm/cycle in straight and curved position, respectively. This is higher than the transport rate of the rigid friction-based transport mechanism designed by I. van de Steeg [17]. There was no statistical difference between the transport rate with the flexible shaft in curved or straight position.

7.2. Limitations of the study

7.2.1. Limitations prototype

Research prototype

During the validation of the research prototype it was found that there was a lot of friction when translating the sliders. This could be eliminated by choosing a different material for the sliders, as the 3D printed material is known to behave rubbery which results in more friction. Due to the friction it was difficult to translate all the sliders perfectly simultaneously, which might have influenced the transport performance of the prototype. Furthermore, it was found that due to reassembling of the prototype, some of the wire ropes were plastically deformed. Although the plastic deformations were limited, they could potentially lead to differences in friction between the tissue and each of the blades resulting in sub-optimal transportation performance.

Final prototype

The final prototype was found to have a small decrease in lumen diameter in the handle. This was caused by play between the sliders and the slider house and due to the thin glue layer that was applied to connect the wire ropes to the sliders. This decrease in lumen diameter could influence the transport rate. Furthermore, the sliders were designed in such a way that the three wire ropes were connected to one slider. Between these clusters of wire ropes there is a small space to limit the friction between the sliders. During testing, it was found that when transporting a tissue phantom, the tissue phantom was partly pushed out of the lumen and accumulated at the tip of the handle.

flexible shaft

The flexible shaft of both prototypes is able to transport a tissue phantom when curved with a bending radius of 59 mm, but was not able to transport a tissue phantom when it was curved with a bending radius of 29 mm, as the wire ropes did not form a closed lumen. This happens because the stored elastic energy in the wire ropes was stronger that the magnetic force of the ring magnets. Using wire ropes with a smaller diameter or stronger ring magnets is thought to result in the ability to transport tissues with the flexible shaft in a stronger curve. Another phenomenon that occurs when the flexible shaft is curved more, is the length change in the path of the wire ropes. The wire ropes at the inside of the curve span a shorter path than the wire ropes following the outer curve. This difference in distance can, depending on the diameter of the flexible shaft and the angle of curvature, be big enough to complicate the transport of tissue. This problem becomes bigger when the length of the flexible shaft increases, as this will result in bigger bending angles and thus result in bigger differences in blade length. A number of solutions are given in Appendix F

7.2.2. Limitations experiments

Tissue phantoms

The gelatin tissue phantoms used in the validation of both the research prototype and the final prototype were cut using a 3D printed tool. Although this was thought to generate tissue phantoms in the same shape as much as possible, there might have been differences in the shape of the gelatin tissue phantoms that could have resulted in friction differences between the tissue phantoms and the wire ropes and thus influencing the transport rate. Furthermore, for more accurate data on the transporting performance, experiments must be conducted using a tissue (phantom) that is more similar to the tissue that will be transported with the transport mechanism once it will be used in a medical setting. During the design process it was assumed that this transport mechanism would be used in combination with a separate device that would separate the tissue from its surroundings, grind it and feed it to the flexible transport mechanism. For accurate data on the performance of the flexible transport mechanism, the mechanism should be tested in combination with such a tissue separating device.

Measurement errors

Though precautionary measures were taken to avoid measurement errors as much as possible, the measurement set up is still prone to some measurement errors. The transported distance was measured by introducing a flexible plastic wire in the lumen until it would encounter the transported tissue phantom. Though the wire was introduced using limited force, the tissue phantom might have been pushed further in the lumen during the encounter. Also, the tissue phantom might have been deformed leading to inaccurate measurements.

Sample size
The experiments with both prototypes were conducted using two tissue samples that were both used for five subsequent measures, resulting in ten measurements per type of tissue phantom. This is a limited number of measurements. By increasing the sample size more accurate data could be obtained.

Reassembling
After each of the test, both the research prototype as well as the final prototype were disassembled for cleaning purposes. Due to this disassembling and assembling the configuration of the wire ropes could have changed, leading to differences in friction generation and thus influencing the transport rate.

7.2.3. Medical application
Cleanability and biocompatibility
The flexible transport mechanism is intended to be used in a medical setting. Before the designed final prototype can be used in a medical setting, it must either be redesigned such that it can easily be sterilised, be a single use system, or a combination of both options. In the latter option, certain parts of the transport mechanism will be single use (like the parts of the flexible shaft) and will be replaced after use, while other parts (like the hold of the handle) are sterilised to be reused. The materials used for the reusable parts must be able to withstand the sterilisation process. Most parts can be made of materials that can withstand the sterilisation process, by regular machining. The in-side-out cam design is more challenging to manufacture without 3D printing. A manufacturing method that could be used for the in-side-out cam is shown in Figure 7.1.

The flexible shaft will be introduced to the patients body and must be bio-compatible. This means that contact between the shaft and the body will not results in adverse responses of the body. The heat shrinking tube used now is not made for medical used, and is therefore not bio compatible. This is also the case for the steel wire ropes which are not certified to be used in a medical device. By replacing the parts that are not bio-compatible at this point, with certified products, the transport mechanism can be made bio-compatible. Furthermore, when using this device, it must also be considered that due to the ring magnets a magnetic field is introduced in the body. High magnetic fields with certain frequencies could influence certain pacemakers [16]. The small constant magnetic field of the ring magnets is not thought to have these effects.

Changes in diameter
The designed flexible shaft has an outer diameter of 10.5 mm which is comparable to the diameter of a colonoscope [8]. Depending on the medical procedure, the current outer diameter might be too big. Due to scaling factors it is possible that, when scaling down the flexible shaft, the performance of the shaft will change. For instance, the magnetic field strength of the ring magnets is depended on the volume of the magnets. This will results in a decrease in magnetic strength when scaling them down, which in turn might result in collapse of the lumen in tight curves due to insufficient strength. A possible solution could be to use ring magnets that have a small outer diameter but are longer (e.g. more tube-like). The ring magnets will have a smaller outer diameter, while being able to generate a magnetic field that is needed to keep the wire ropes in the correct place. The will however be a trade-off as longer the ring magnets will increase the minimal bending radii that can be reached by the flexible shaft.

Changes in length
The length of the flexible shaft as is, is too short for a number of medical procedures. Increasing the length of the shaft would lead to an increase of the number of ring magnets used. This increases the force needed to

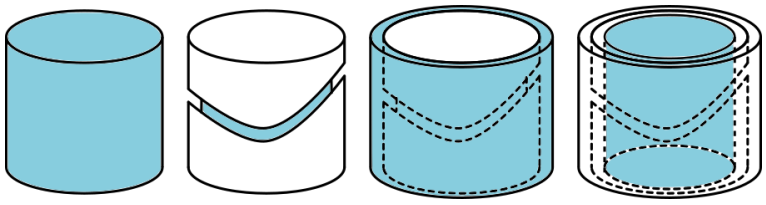

Figure 7.1: Schematic representation of a manufacturing method that could be used for the in-side-out cam. The manufacturing process will start with a cylinder. A groove with the right dimensions will be made in the same manner as during the fabrication of a regular barrel cam. Subsequently a metal tube will be glued around the barrel cam. Now a hole with the right diameter can be drilled through the centre of the barrel cam. This would result in the wanted in-side-out cam.

translate the blades. More details about the effect of the number of magnets on the force needed to translate the blades can be found in Appendix B.

7.3. Recommendations for future research

7.3.1. Redesign for better transportation performance

In this study it is shown that it is possible to transport tissue phantoms with this newly design flexible transport mechanism. It would be interesting to know if the performance of the flexible transport mechanism could be improved by changing design parameters. Think of the effect of different stroke lengths in combination with changing the number of blades and the total number of wire ropes as well as the number of wire ropes per blade. More insight in the influence of these design parameters on the transport rate in straight and curved position of the flexible shaft, could lead to improvement of the transportation performance of the flexible friction-based transport mechanism.

7.3.2. Redesign for better flexibility

The flexible shaft can be curved with a bend radius of 59 mm and even smaller but this requires a lot of force. When the transport mechanism is used in a medical setting, the force needed to bend the shaft, will be generated by the organ wall and thus the more rigid the shaft, the more tissue damage will occur. Therefore it would be valuable to redesign the flexible shaft such that it becomes more flexible. This can be done by using wire ropes that have a smaller cross-section or wire ropes that contain more strands. Furthermore, the heat shrink tube could be replaced by an other tube that allows for more easy bending.

7.3.3. Redesign for medical application

Before this transport mechanism could be used in the intended setting, more research in needed to improve the design such that it fulfils the requirements of a medical device. The cleanability of the final prototype as is, will be a challenge due to the use of glued wire ropes and the heat shrink tube. These make it impossible to fully disassemble the final prototype, which would be preferable for sterilisation. By redesigning the transport mechanism, these problems could be solved. Furthermore, the now used heat shrinking tube, as well as the galvanised wire ropes, cannot be used in a medical device. Cold drawn stainless-steel wire ropes produced by Asahi Intecc were found to have comparable attraction to the ring magnets as the galvanised wire ropes and do fulfil the requirements to be used in a medical device. Heat shrinking tubes for medical used can obtained via Nordson Medical. The performance of the flexible transport mechanism must be re-evaluated when using these new components.

7.3.4. Steerability

The transport mechanism that has been designed is flexible and can passively bend, following the curves of a tubular organ. The bending of the flexible shaft is achieved by forces that are applied by the organ wall, which could lead to damage to the organ wall. By adding steerability to the flexible shaft, this can be avoided. The shaft could be bend actively, such that the organ wall would not have to withstand high forces. The shaft could be made steerable by fixating a number of wire ropes at the tip. These wire ropes would not be used to transport, but by pulling on one these wire ropes the shaft will curve, as is schematically shown in Figure 7.2. Adding steerability to the shaft allows the transport mechanism to be used in more applications, therefore it would be valuable to know if the friction-based transport also works in combination with added steerability.

Figure 7.2: Schematic representation of actively curving the transport mechanism.

8

Conclusion

This study presents the design, manufacturing and validation of a flexible friction-based transport mechanism. The transport method used in this mechanism is inspired on the mechanism used to transport eggs along the ovipositor of parasitoid wasps. A flexible shaft using this transport mechanism was designed and validated. Th e flexible shaft was able to transport gelatin tissue phantoms with different material properties, such as density (12.5 mass%, 10 mass% and 7.5 mass% gelatin) and the presence of particles (sesame seed). Furthermore, the flexible shaft was able to transport tissue phantoms with the shaft in straight and in curved position (90^o, R=59 mm). For the final prototype, a handle, that works in combination with the flexible shaft, was designed and tested. This handle allows the user to employ the final prototype manually by continuously rotating the sling. This final prototype was able to transport a gelatin tissue phantom from the tip of the flexible shaft to the end of the handle with an average transport rate of 2.7 ± 0.3 [mm/cycle] in straight position and 2.6 ± 0.4 [mm/cycle] in curved position (R = 59 mm). These transport rates are comparable to the rigid friction-based transport mechanism that is previously designed by I. van de Steeg [17]. The test results of both prototypes support the idea that the described flexible friction-based transport mechanism could in the future be used in minimally invasive medical procedures. The flexible friction-based transport mechanism can be introduced to the intervention site via natural occurring body orifices and subsequently transport tissue form the interventions site. Before this can happen more research is needed to improve the transportation, size and flexibility of the final prototype. Furthermore, the prototype needs to be redesigned to meet the standards for a medical device, such as the cleanabilty and biocompatibility.

Acknowledgement

I would like to thank all the people that have contributed to this thesis. First of all I would like to thank my parents and my brother for always being supportive and helping me were possible, not just during this thesis, but during my entire life. Thanks to all my friends that I met somewhere along the way during my time at the TU Delft. Eva, Pepijn, Ties, Wouter, Franco, Bart, Bram, Hugo, Kim, Mats, Gregory, Miriam, Thomas, Tom and Zoe, you guys made it a lot more pleasant to go to the countless lectures, work on the assignments and study for the exams, which allowed me to start on this thesis. Working on this thesis would be very lonely if it wasn't for my 'master thesis study buddy' Hugo, so special thanks to you! This prototype would not be there, if it was not for the feedback I got from Prof. Dr. Ir. Paul Breedveld. Thank you for making me think outside the box during the design process. I would also like to thank the other members of my thesis committee: Ir. Jo Spronck and Ir. Fabian Trauzettel. During the design and manufacturing process I received a lot of help from the precision mechanics at DEMO: David Jager, Menno Lageweg and Remi van Starkenburg. I would especially like to thank David Jager, for all his time. Without the provided design and manufacturing recommendations it would not be possible to manufacture this novel prototype. Last, but most definitely not least I would like to thank Dr. Ir. Aimeé Sakes for all her help during my literature study as well as my master thesis. You were always willing to make time to help. It didn't matter if I had problems with defining the problem, the design process, the experimental set up or writing this rapport, you were always able to get me back on track whenever I got stuck. Thank you for being the best supervisor I could imagine!

A

Matlab files

A.1. Distance ring magnets

```
%% Distance magnet ring
% This script can be used to determine the relation between the distance between the ...
    magnetic
% rings and the decrease in lumen diameter.

% Made by: Esther de Kater
% Date: 19-06-2019

%% Initialisation
close all   % close all figures
clear all   % clear all data
clc         % clear command window

%% Input of data
syms alpha
d_w = 0.6;    % wire diameter [mm]
r_bw = 35*d_w;      % bending radius wire [mm]
d_l = 4.4;    % lumen diameter [mm]

%% Calculation of Δ (the decrease in lumen diameter) for every alpha

% calculate for every angle alpha
a = 0:0.01*pi:0.25*pi;
for i=1:length(a)
    alpha = a(i);
    mind_l = cos(alpha)*d_l; % minimal lumen diameter [mm]
    Δd_l = d_l-mind_l;          % decrease in lumen diamer [mm]

    d_i = 2*alpha*r_bw;     % wire rope length short
    d_o = 2*alpha*r_bw + 2*(sin(alpha)*(r_bw+d_l)-sin(alpha)*r_bw);     % wire rope ...
        length long
    d_m = 1/2*(d_i+d_o);    % distance between the ring magnets

    d_mean(i) = d_m;    % store data distance between ring magnets [mm]
    Δ(i) = Δd_l; % store data decrease lumen diameter [mm]
    Δ_per(i) = Δd_l/d_l*100; % percentual decrease in lumen diameter [%]

end

%% Plot of data
figure(1)
plot([0,80],[5 5],'r--');
hold on
plot(d_mean,Δ_per,'b')
grid on
title('Decrease in lumen diameter vs. distance between ring magnets')
ylabel('Decrease in lumen dimater (% of initial diameter) [%]')
```

```
xlabel('Distance between ring magnets [mm]')
legend('5% of decrease in lumen diamter','Location', 'Best')
xlim([0,50])
```

A.2. Data analysis research prototype

```
%%      DATA ANAYSIS tissue phantom transport research prototype        %%
% This script can be used to analyse the data of the transport performance of the
% research prototype of the flexible friction-based transport mechanism.

% Made by: Esther de Kater
% Date: 06-11-2019

%% Initialisation
close all   % close all figures
clear all   % clear all data
clc         % clear command window

%% Load test data
% data set 1: transported distance [mm] after 5 cycles for different gelatin ...
    concentrations (12,5%, 10%, 7.5%) in straight position
G12_C1 = [15.5  13  13  13.5    11.5 13 13.5    14  14  14.5];
G10_C1 = [10.5  10.5    13  13.5    14 16   15  15  16  17];
G7_C1  = [13    11.5    14  13  14 15   15.5    15  19  18.5];

% data set 2: transported distance [mm] after 5 cycles for different different ...
    gelatin concentrations (12.5%. 10%. 7.5%) in curved position
G12_C2=[8.5 13.5    14.5    11.5    10.5 14.5   14  14.5    12.5    10.5 ];
G10_C2 = [4 3   3.5 4   4.5 11  13  13.5    13  11.5 ];
G7_C2  = [15    8   9   12  10 11   10  12.5    13  15.5];

% data set 3: transported distance [mm] after 5 cycles for different different ...
    gelatin concentrations (12.5%. 10%. 7.5%) mixed with particles in straight position
pG12_C1 = [13   11  12.5    11  12 11   11  10.5    9.5 11 ];
pG10_C1 = [9    13  10.5    11  8.5 11.5    11  11  12.5    10.5 ];
pG7_C1 = [15.5  14.5    13.5    11.5    14 9.5  10.5    10  11  10];

%% Data Analysis: Get mean and standard deviation per cycle

% mean
mean_G12_C1 = mean(G12_C1./5);
mean_G10_C1 = mean(G10_C1./5);
mean_G7_C1 = mean(G7_C1./5);

mean_G12_C2 = mean(G12_C2./5);
mean_G10_C2 = mean(G10_C2./5);
mean_G7_C2 = mean(G7_C2./5);

mean_pG12_C1 = mean(pG12_C1./5);
mean_pG10_C1 = mean(pG10_C1./5);
mean_pG7_C1 = mean(pG7_C1./5);

% std
std_G12_C1 = std(G12_C1./5);
std_G10_C1 = std(G10_C1./5);
std_G7_C1 = std(G7_C1./5);

std_G12_C2 = std(G12_C2./5);
std_G10_C2 = std(G10_C2./5);
std_G7_C2 = std(G7_C2./5);

std_pG12_C1 = std(pG12_C1./5);
std_pG10_C1 = std(pG10_C1./5);
std_pG7_C1 = std(pG7_C1./5);

% data vectors
meanG = [mean_G12_C1, mean_G10_C1, mean_G7_C1, mean_G12_C2, mean_G10_C2, mean_G7_C2];
stdG = [std_G12_C1, std_G10_C1, std_G7_C1, std_G12_C2, std_G10_C2, std_G7_C2];
```

```
60
61 meanGp = [mean_pG12_C1, mean_pG10_C1, mean_pG7_C1];
62 stdGp = [std_G12_C1, std_pG10_C1, std_G7_C1];
63
64 %% plot of data
65 figure (1)
66 errorbar([0.2,1.2],[mean_G12_C1, mean_G12_C2], [std_G12_C1, ...
       std_G12_C2],'ko','MarkerSize',10)
67 hold on
68 errorbar(0.3,mean_pG12_C1, std_pG12_C1,'ko','MarkerSize',10, 'MarkerFaceColor','k')
69 errorbar([0.5,1.5],[mean_G10_C1, mean_G10_C2], [std_G10_C1, ...
       std_G10_C2],'kd','MarkerSize',10)
70 errorbar(0.6,mean_pG10_C1, std_pG10_C1,'kd','MarkerFaceColor','k','MarkerSize',10)
71 errorbar([0.8,1.8],[mean_G7_C1, mean_G7_C2], [std_G7_C1, ...
       std_G7_C2],'ks','MarkerSize',10,'MarkerSize',10)
72 errorbar(0.9,mean_pG7_C1, std_pG7_C1,'ks','MarkerFaceColor','k','MarkerSize',10)
73 plot([1 1],[0,10],'k--')
74 set(gca,'xtick',[0.5 1.5])
75 set(gca,'xticklabels',{'Straight', 'Curved (R=59 mm)'})
76 title('Mean transport rate and standard deviation')
77 ylabel('Transport rate [mm/cycle]')
78 legend('gelatin 12.5%', 'gelatin 12.5% with particles', 'gelatin 10%', 'gelatin 10% ...
       with particles',  'gelatin 7.5%', 'gelatin 7.5% with particles','Location','Best')
79 ylim([0,5])
80 set(gca, 'YGrid', 'on', 'XGrid', 'off')
81 %%
82 figure (2)
83 boxplot([G12_C1./5; G10_C1./5; G7_C1./5]','position', [1,  2, 3]);
84 hold on
85 set(gca,'xtick',[1 2 3])
86 set(gca,'xticklabels',{'Gelatin 12.5%', 'Gelatin 10%', 'Gelatin 7.5%'})
87 title('Box plot transport rate gelatin density')
88 ylabel('Transport rate [mm/cycle]')
89 ylim([0, 5])
90
91
92 figure (3)
93 boxplot([G12_C1./5; G10_C1./5; G7_C1./5]','position', [1,  2, ...
       3],'colors','k','Widths',0.2);
94 hold on
95 boxplot([ pG12_C1./5; pG10_C1./5; pG7_C1./5]','position', [1.33, 2.33, 3.33], ...
       'Widths',0.2);
96 plot([1.66 1.66],[0 10],'k--')
97 plot([2.66 2.66],[0 10],'k--')
98 set(gca,'xtick',[1.125 2.125 3.125])
99 set(gca,'xticklabels',{'Gelatin 12.5%', 'Gelatin 10%', 'Gelatin 7.5%'})
100 title('Box plot transport rate homogeneous sample vs. heterogeneous sample')
101 ylabel('Transport rate [mm/cycle]')
102 ylim([0, 5])
103
104 figure (4)
105 boxplot([G12_C1./5; G10_C1./5; G7_C1./5]','position', [1,  2, ...
       3],'colors','k','Widths',0.2);
106 hold on
107 boxplot([G12_C2./5; G10_C2./5; G7_C2./5]','position', [1.33, 2.33, 3.33],'Widths',0.2);
108 plot([1.66 1.66],[0 10],'k--')
109 plot([2.66 2.66],[0 10],'k--')
110 set(gca,'xtick',[1.125 2.125 3.125])
111 set(gca,'xticklabels',{'Gelatin 12.5%', 'Gelatin 10%', 'Gelatin 7.5%'})
112 title('Box plot transport rate straight vs. curved')
113 ylabel('Transport rate [mm/cycle]')
114 ylim([0, 5])
115
116 %% Correlation test
117 % gelatin density
118 [p_den,tbl_den,stats_den] = anova1([G12_C1./5; G10_C1./5; G7_C1./5]');
119
120 % homogeneous vs. heterogeneous
121 [h_g12h, p_g12h,tbl_g12h,stats_g12h] = ttest(G12_C1./5, pG12_C1./5);
122 [h_g10h, p_g10h,tbl_g10h,stats_g10h] = ttest(G10_C1./5, pG10_C1./5);
123 [h_g7h, p_g7h,tbl_g7h,stats_g7h] = ttest(G7_C1./5, pG7_C1./5);
```

```
% straight vs. curved
[h_g12c, p_g12c,tbl_g12c,stats_g12c] = ttest(G12_C1./5, G12_C2./5);
[h_g10c, p_g10c,tbl_g10c,stats_g10c] = ttest(G10_C1./5, G10_C2./5);
[h_g7c, p_g7c,tbl_g7c,stats_g7c] = ttest(G7_C1./5, G7_C2./5);
```

A.3. Data analysis final prototype

```
%%      DATA ANAYSIS tissue phantom transport final prototype        %%
% This script can be used to analyse the data of the transport performance of the
% final prototype of the flexible friction-based transport mechanism.

% Made by: Esther de Kater
% Date: 21-11-2019

%% Initialisation
close all   % close all figures
clear all   % clear all data
clc         % clear command window

%% Load test data
% data set 1 (gelatin sample straight): number of cycles needed to transport the ...
    tissue phantom
% trough the transport mechanism in straight position
dc1_gelatin = [65 64 56 66 71 75 73 84 60 59];

% data set 2 (gelatin sample curved): number of cycles needed to transport the tissue ...
    phantom
% trough the transport mechanism in curved position
dc2_gelatin = [71 68 57 86 64 66 72 58 61 91];

%% Other measures
length_tip = 105;    % transported length trough the heat shrink tube [mm]
length_handle = 73;  % transported length trough the handle [mm]
length_gelatin = 20; % length gelatin sample [mm]

transport_distance_gelatin = 105 + 73 - 20; %traveled distance [mm]

%% Data Analysis: Get mean and standard deviation
% mean
mean_dc1_gelatin  = mean(transport_distance_gelatin./dc1_gelatin);  % mean ...
    transported distance per cycle [mm/cycle]
mean_dc2_gelatin =  mean(transport_distance_gelatin./dc2_gelatin);  % mean ...
    transported distance per cycle [mm/cycle]


%std
std_dc1_gelatin  = std(transport_distance_gelatin./dc1_gelatin);  % mean transported ...
    distance per cycle [mm/cycle]
std_dc2_gelatin =  std(transport_distance_gelatin./dc2_gelatin);  % mean transported ...
    distance per cycle [mm/cycle]

%% Graph generation: Plot the data as mean with std. and as box plots
% figure 1: transport rate vs. straight/curve mean and std
figure(1)
errorbar(1,mean_dc1_gelatin, std_dc1_gelatin,'ko'); hold on
errorbar(2,mean_dc2_gelatin, std_dc2_gelatin,'kd')
set(gca,'xtick',[1 2])
set(gca,'xticklabels',{'Straight', 'Curved (R=59 mm)'})
xlim([0,3])
title('Transport rate in straight and in curved position')
ylabel('transport rate [mm/cycle]')

% figure 2: transport rate vs. straight/curve box plot
figure(2)
boxplot([transport_distance_gelatin ./dc1_gelatin; transport_distance_gelatin ...
    ./dc2_gelatin]'); hold on
set(gca,'xtick',[1 2])
set(gca,'xticklabels',{'Straight', 'Curved (R=59mm)'})
```

```
55 xlim([0,3])
56 title('Transport rate in straight and in curved position')
57 ylim([0,5])
58 ylabel('Transport rate [mm/cycle]')
59
60 %% Correlation test
61 % straight vs. curved
62 [h_gelatin, p_gelatin,tbl_gelatin,stats_gelatin] = ttest(transport_distance_gelatin ...
       ./dc1_gelatin, transport_distance_gelatin ./dc2_gelatin);
```

B

Number of magnets

A certain number of magnets is required to keep the steel wire ropes at the desired place. The more magnets the better the wire ropes will form a circular lumen with a constant cross-section. However, more magnets also increases the force that is required to translate the steel wire ropes. This translating motion is needed to generate the transport of tissue trough the lumen. Furthermore, the bending of the lumen might influence the required force to translate the wire ropes.

B.1. Experiment

B.1.1. Experimental goal

The goal of this experiment is to identify the influence of the number of ring magnets as well as the curve of the flexible shaft on the required pull force to translate the wire ropes.

B.1.2. Experimental variables

The independent variables in this experiment are the number of ring magnets (5, 10, 15) and the curve of the flexible shaft (straight, R = 63.66 mm, R = 31.83 mm). The dependent variable that will be measured is the maximum pull force required to translate one wire rope cluster (6 wire ropes) 2 cm.

B.1.3. Experimental facility

36 galvanised steel wire ropes (rope construction 1x7, diameter 0.45 mm) were clustered in six strings, each containing six wires. 5,10 or 15 neodymium ring magnets (di= 5mm, do = 10mm, h=2mm) were spaced over 10 cm of the steel wire ropes. Three 3D printed (ultimaker) attachment parts made of PLA were used to bend the flexible shaft in the desired predetermined curve. The maximum required pull force was saved by the used spring scale. The test setup in shown in Figure B.1.

B.1.4. Experimental protocol

The wire ropes and the required number of ring magnets were placed in the curve attachment parts. The spring scale was used to translate one cluster of 6 wire ropes 2 cm. The maximal pull force required over this 2 cm was stored.

B.1.5. Data analysis

The data analysis will be performed in MATLAB 2015B.

B.2. Results

A graphic representation of the experimental data can be found in Figure B.2. In this graph the mean required pull force as well as its standard deviation is shown.

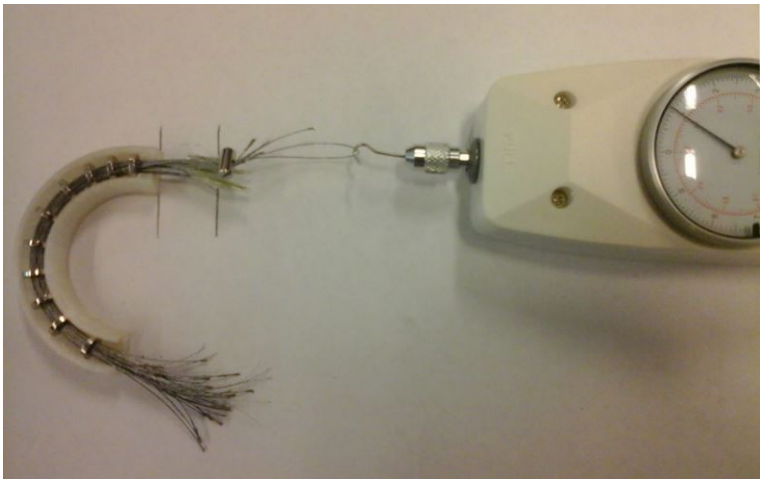

Figure B.1: Measurement setup to measure the required pull force to translate one cluster of 6 steel wire ropes.

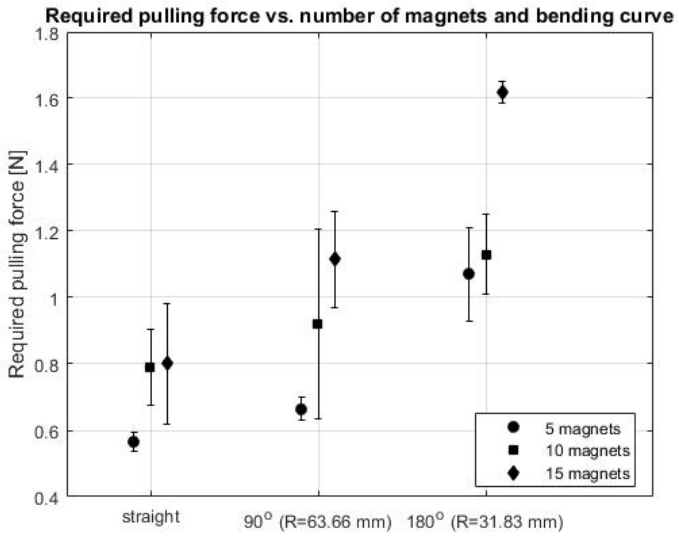

Figure B.2: Test results showing the mean of the required pull force and the standard deviation to move six steel wire ropes trough the flexible shaft with a certain number of magnets and a certain curve.

C

Technical drawings

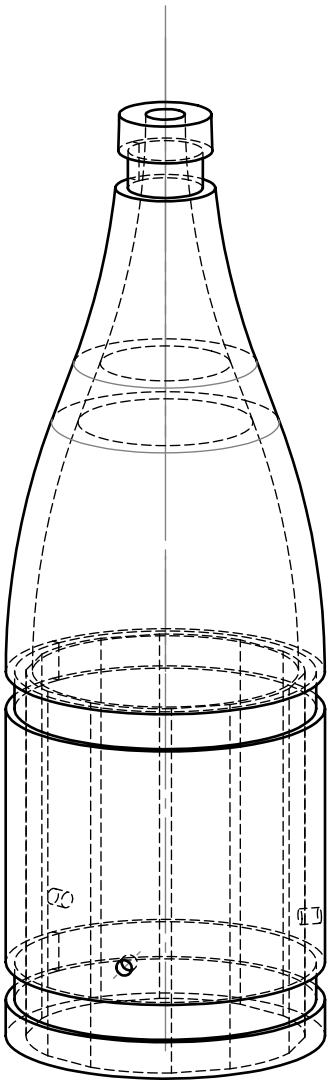

Mat.: ABS
Aantal: 1

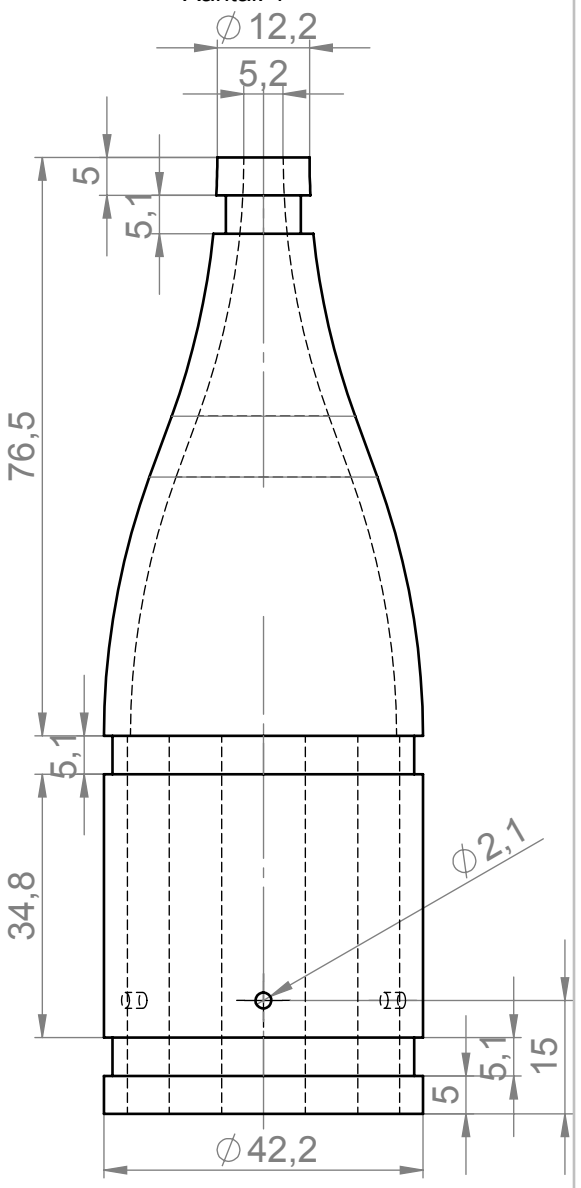

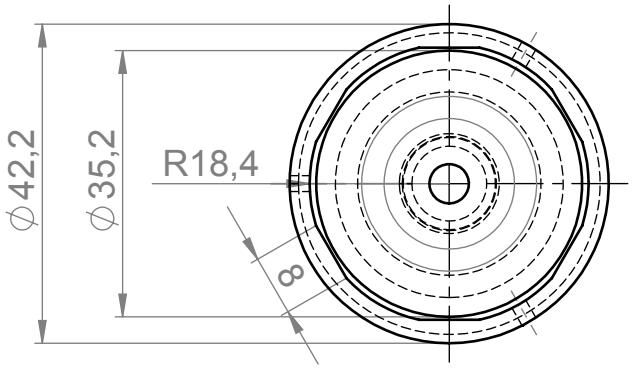

benaming	Outer cone			maateenheid	mm
				formaat	tekeningnummer
				A4	5
schaal	1:1	datum	4-12-2019	gewicht	36 gram
getekend	Esther de Kater [4315588]			groep	N.A.

TU Delft
Industrial Design Engineering

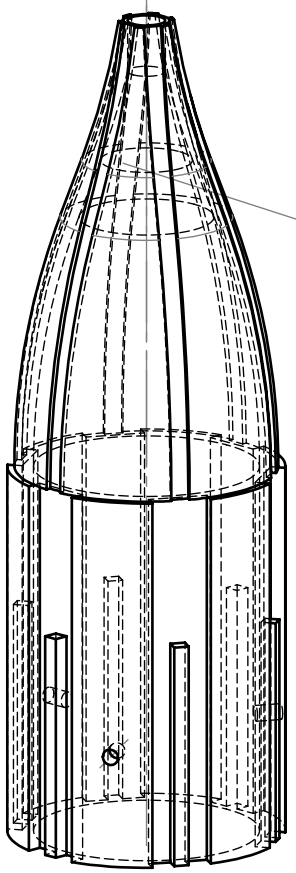

Mat.: ABS
Aantal: 1

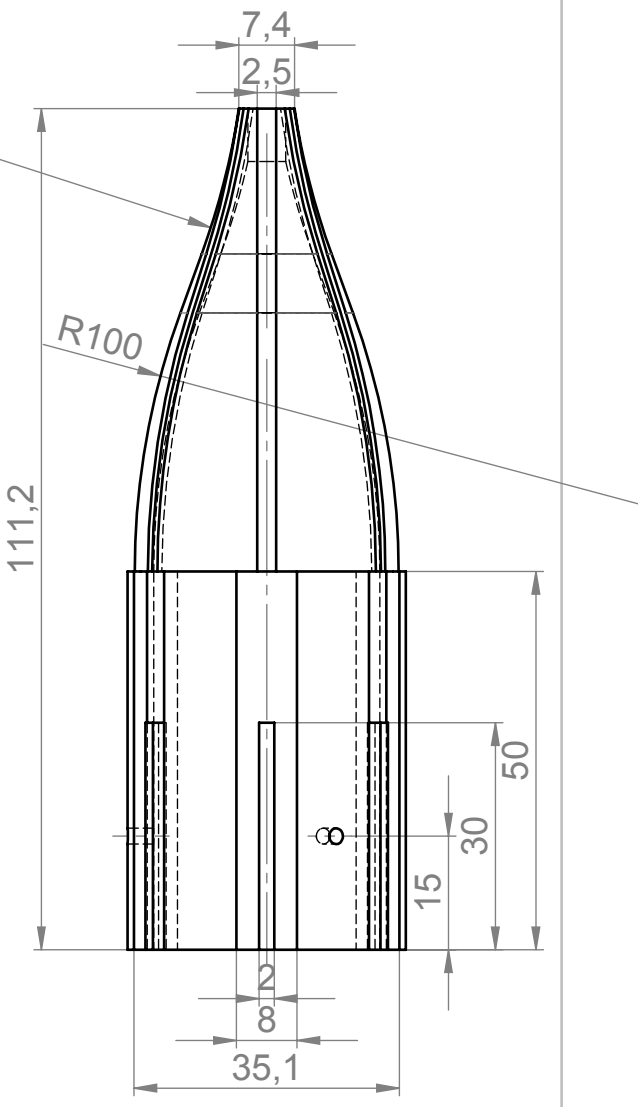

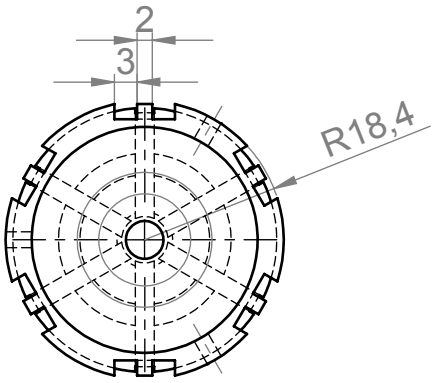

benaming: Inner cone			maateenheid: mm
		formaat: A4	tekeningnummer: 6
schaal: 1:1	datum: 4-12-2019	gewicht: 23 gram	
getekend: Esther de Kater [4315588]			groep: N.A.

TU Delft
Industrial Design Engineering

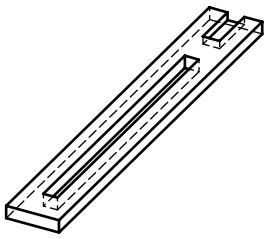

Mat.: ABS
Aantal: 6

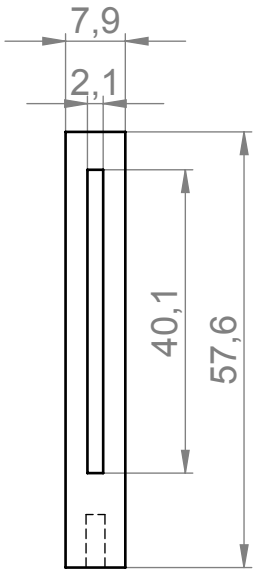

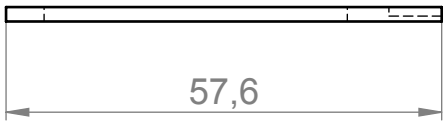

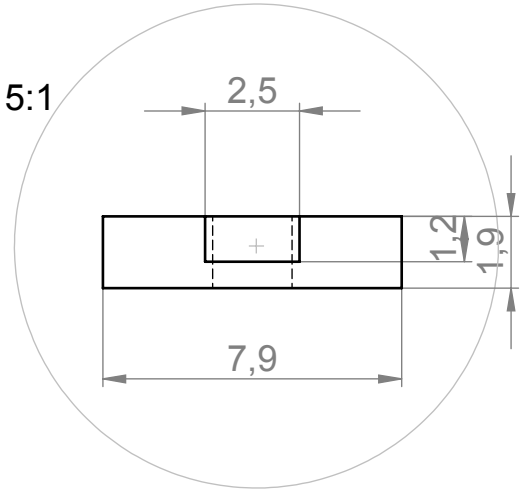

benaming Slider			maateenheid mm
		formaat A4	tekeningnummer 7
schaal 1:1	datum 4-12-2019	gewicht 1 gram	
getekend Esther de Kater [4315588]			groep N.A.
Industrial Design Engineering			

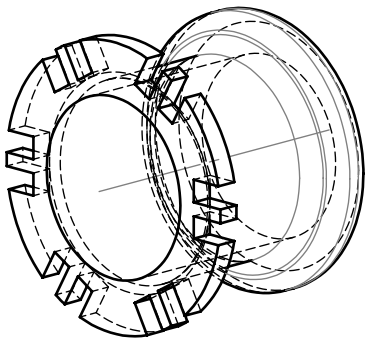

Mat.: ABS
Aantal:1

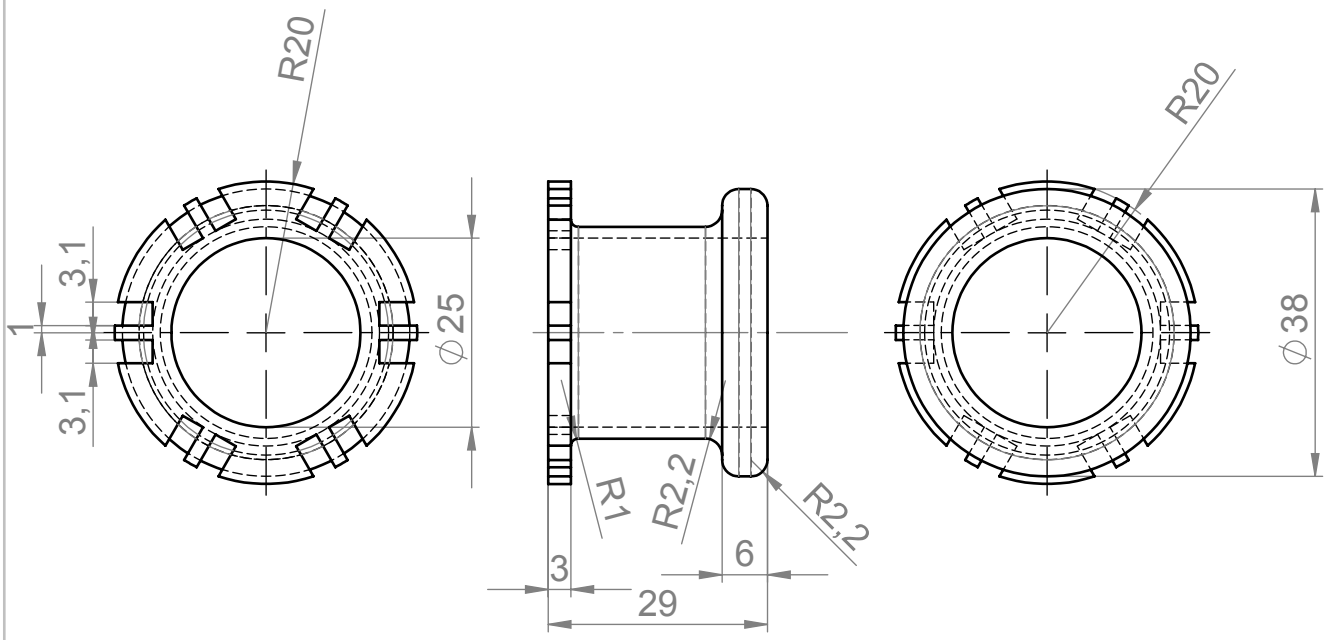

benaming Manipulator			maateenheid mm
		formaat A4	tekeningnummer 8
schaal 1:1	datum 4-12-2019	gewicht 8 gram	
getekend Esther de Kater [4315588]			groep N.A.

TU Delft
Industrial Design Engineering

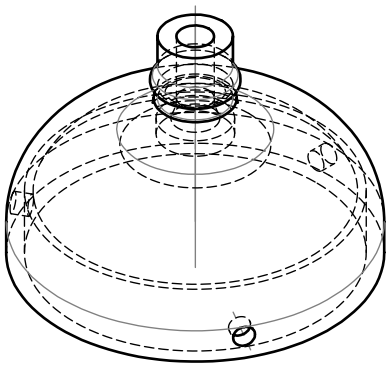

Mat.: ABS
Aantal: 1

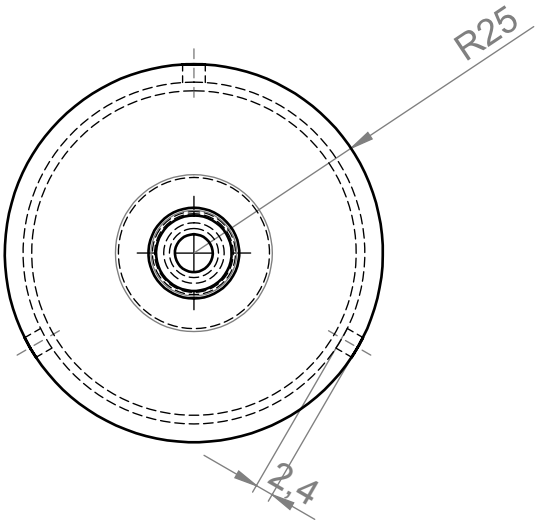

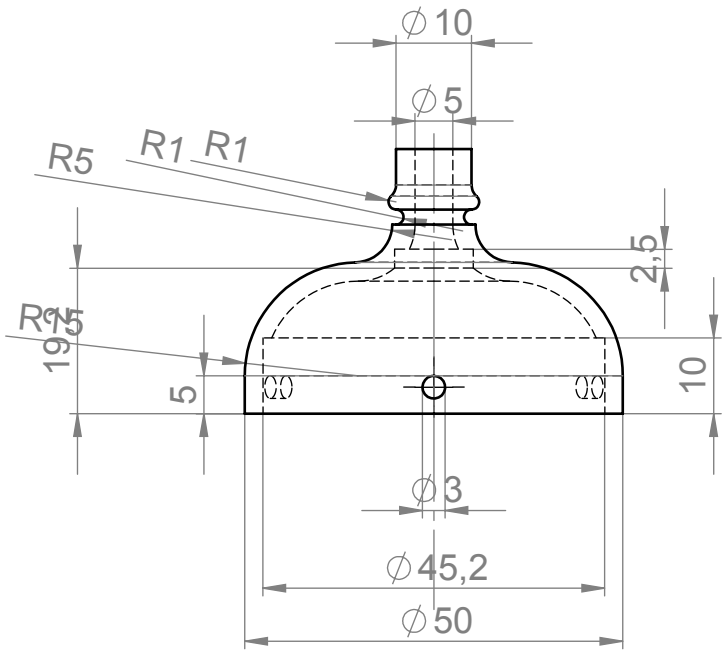

benaming Tip			maateenheid mm
		formaat A4	tekeningnummer 5
schaal 1:1	datum 4-12-2019	gewicht 10 gram	
getekend Esther de Kater [4315588]			groep N. A.
TU Delft Industrial Design Engineering			

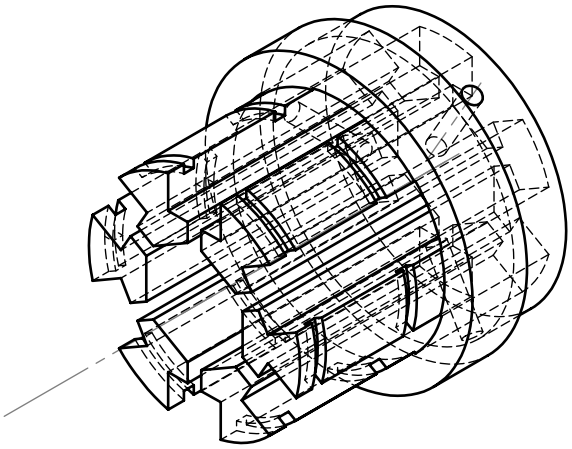

Mat.: ABS
Aantal: 1

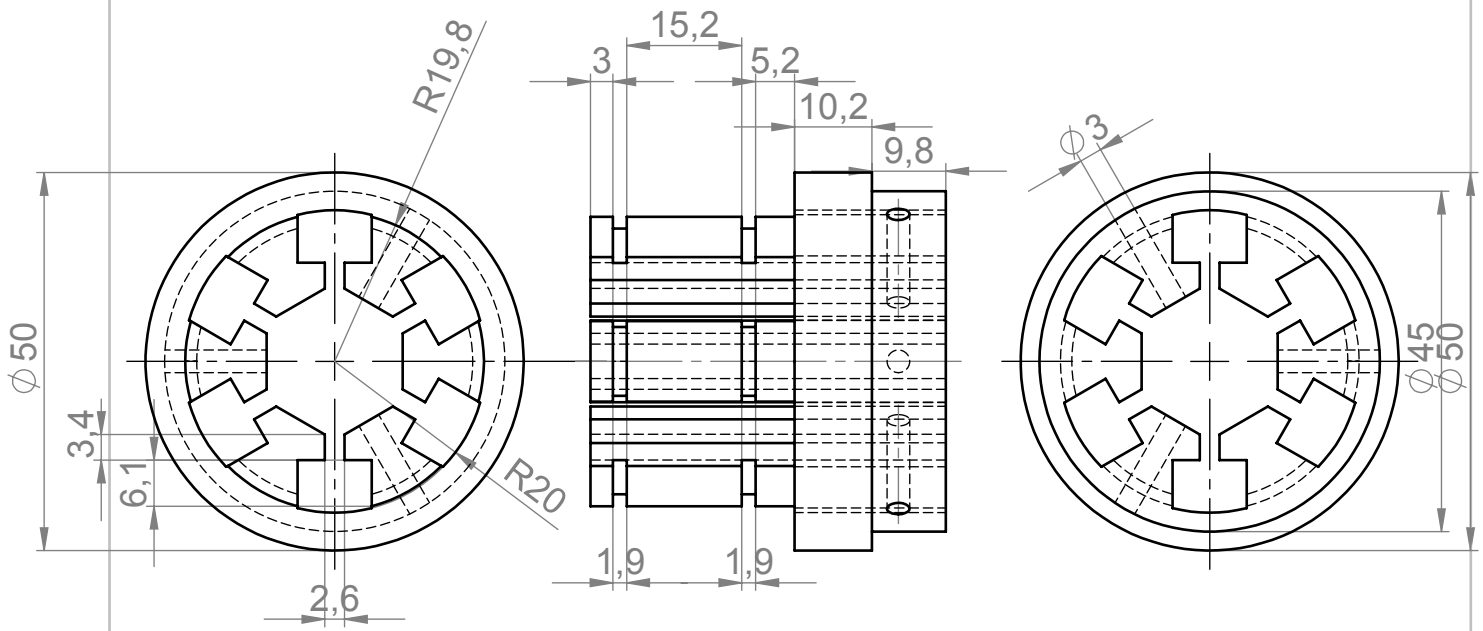

benaming Slider house				maateenheid mm	
				formaat A4	tekeningnummer 6
schaal 1:1	datum 4-12-2019	gewicht 35 gram			
getekend Esther de Kater [4315588]				groep N.A.	
Industrial Design Engineering					

Mat.: ABS
Aantal: 1

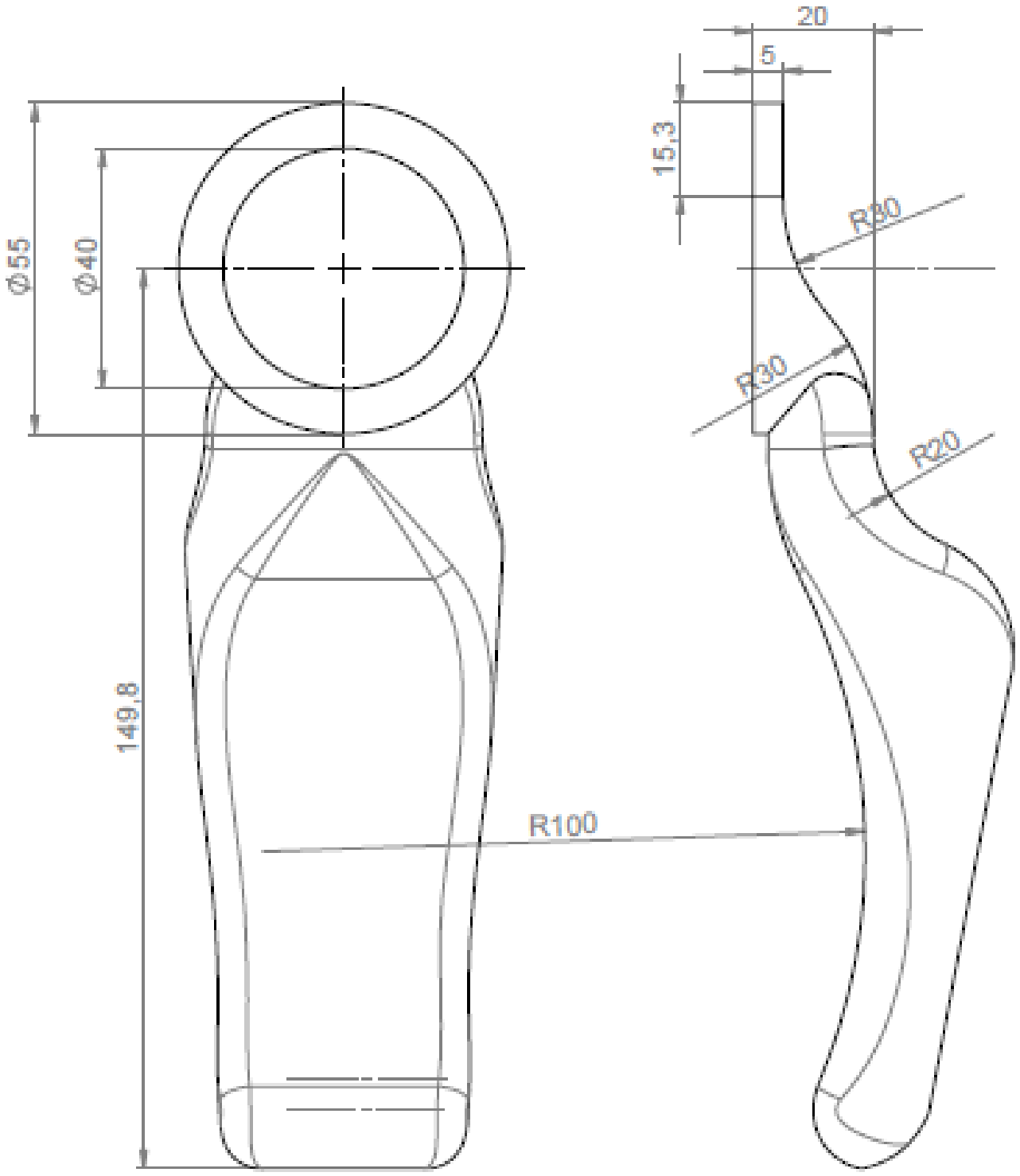

benaming: Hold			maateenheid: mm
		formaat: A4	tekeningnummer: 7
TU Delft Industrial Design Engineering	datum: 4-12-2019	gewicht: 51 gram	
	getekend: Esther de Kater [4315588]		groep: N. A.

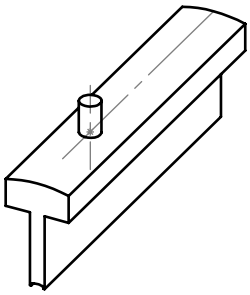

Mat.: Aluminium
Aantal: 6

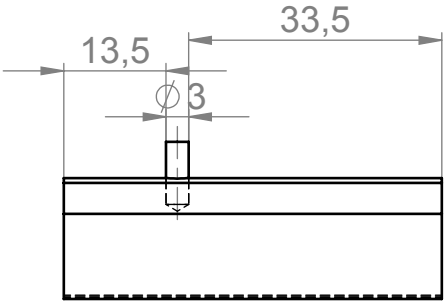

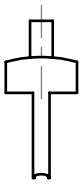

5 : 1

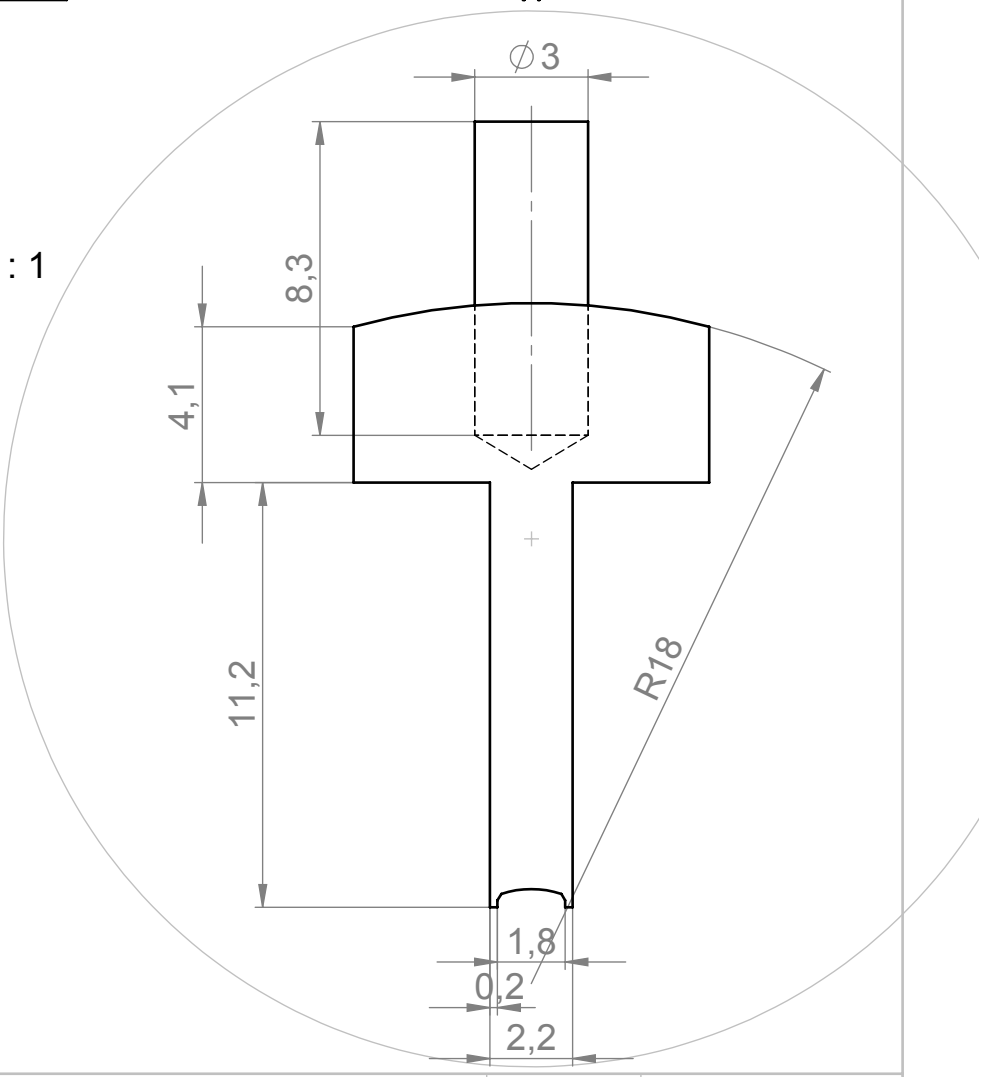

benaming Slider			maateenheid mm
		formaat A4	tekeningnummer 8
schaal 1:1	datum 4-12-2019	gewicht 0 gram	
getekend Esther de Kater [4315588]			groep N.A.

TU Delft
Industrial Design Engineering

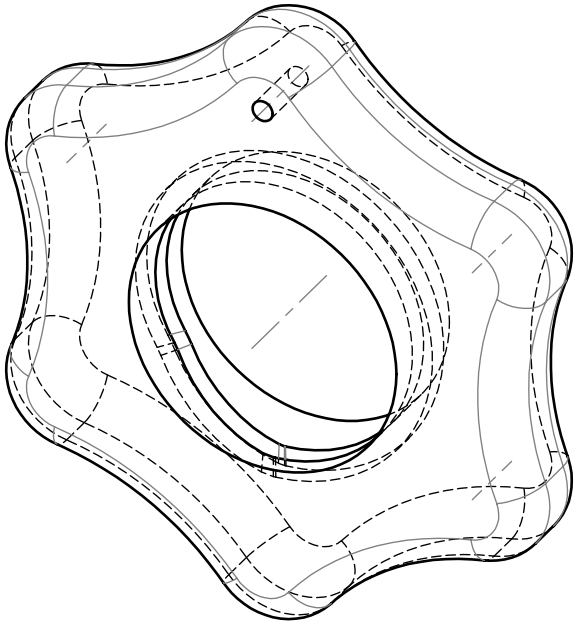

Mat.: ABS
Aantal: 1

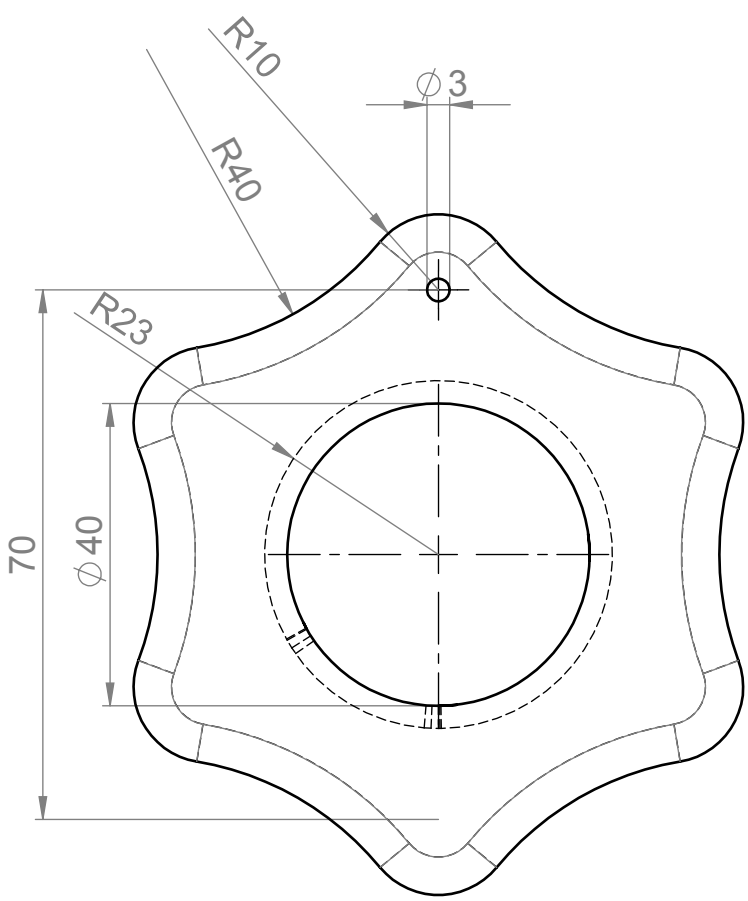

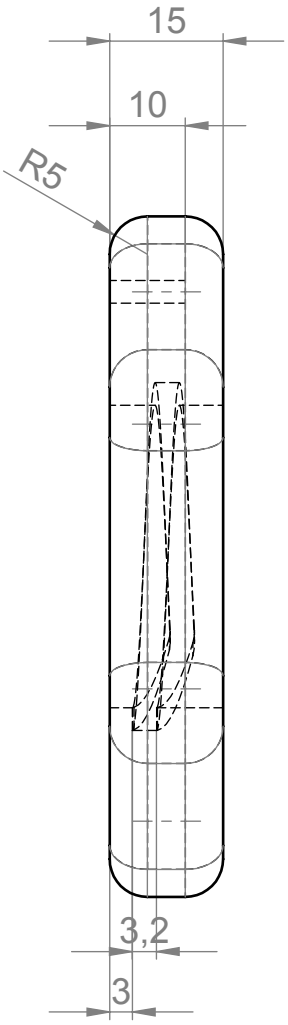

benaming Cam				maateenheid mm	
				formaat A4	tekeningnummer 9
SOLIDWORKS Student Edition. For Academic Use Only.	schaal 1:1	datum 4-12-2019	gewicht 56 gram		
TU Delft Industrial Design Engineering	getekend Esther de Kater [4315588]				groep N.A.

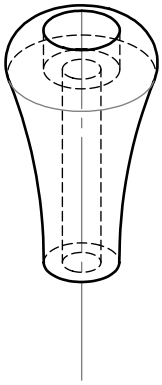

Mat.: ABS
Aantal: 1

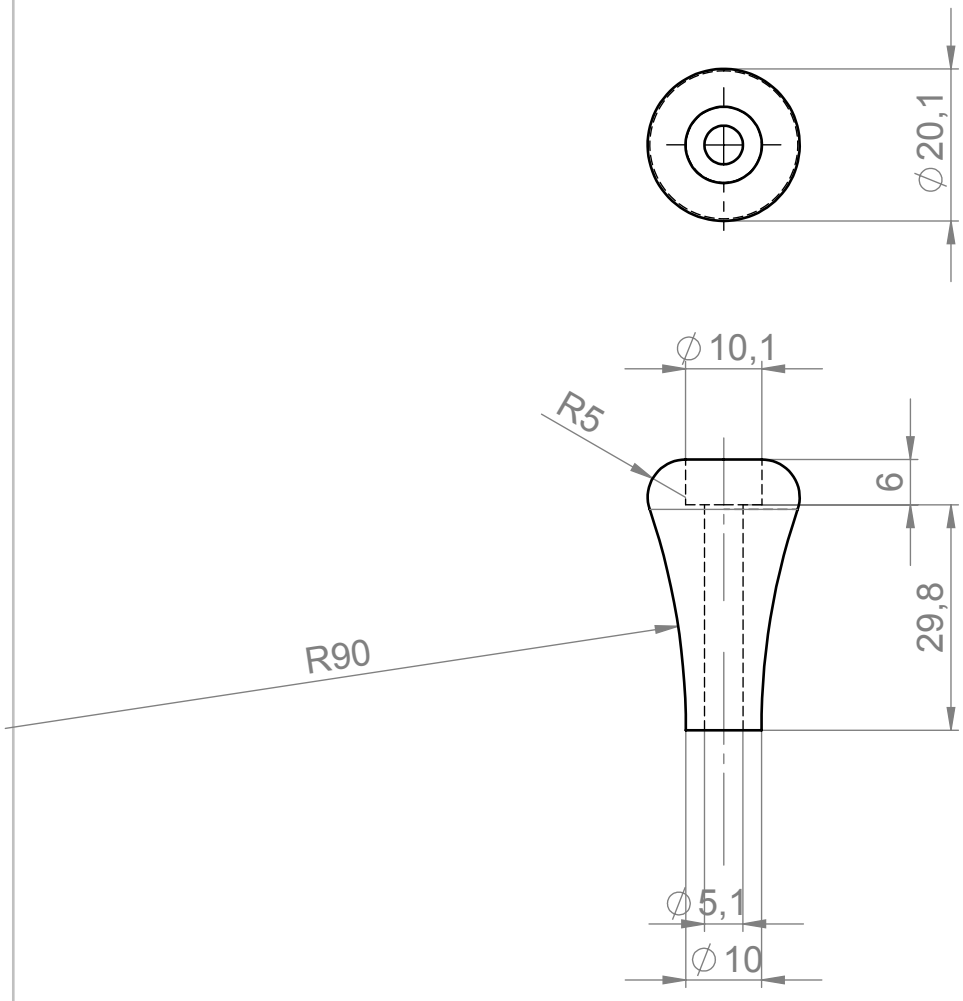

benaming Sling			maateenheid mm
		formaat A4	tekeningnummer 10
schaal 1:1	datum 4-12-2019	gewicht 5 gram	
getekend Esther de Kater			groep N. A.

TU Delft
Industrial Design Engineering

D

Raw data

D.1. Research prototype

Experiment	Data set	Straight/Curve	Sample	Transport rate [mm/5 cycles]
Material test A	1	Straight	Gelatin (12.5 mass%)	sample 1: 15.5, 13, 13, 13.5, 11.5 sample 2: 13, 13.5, 14, 14, 14.5
	2	Straight	Gelatin (10 mass%)	sample 1:10.5, 10.5, 13, 13.5, 14 sample 2: 16, 15, 15, 16, 17
	3	Straight	Gelatin (7.5 mass%)	sample 1:13, 11.5, 14, 13, 14 sample 2: 15, 15.5, 15, 19, 18.5
Material test B	4	Straight	Gelatin (12.5 mass%) with particles	sample 1:13, 11, 12.5, 11, 12 sample 2: 11, 11, 10.5, 9.5, 11
	5	Straight	Gelatin (10 mass%) with particles	sample 1:9, 13, 10.5, 11, 8.5 sample 2:11.5, 11, 11, 12.5, 10.5
	6	Straight	Gelatin (7.5 mass%) with particles	sample 1:15.5, 14.5, 13.5, 11.5, 14 sample 2: 9.5, 10.5, 10, 11, 10
Curve test	7	Curve (R=59 mm)	Gelatin (12.5 mass%)	sample 1: 8.5, 13.5, 14.5, 11.5, 10.5 sample 2: 14.5, 14, 14.5, 12.5, 10.5
	8	Curve (R=59 mm)	Gelatin (10 mass%)	sample 1: 4, 3, 3.5, 4, 4.5 sample 2: 11, 13, 13.5, 13, 11.5
	9	Curve (R=59 mm)	Gelatin (7.5 mass%)	sample 1:15, 8, 9, 12, 10 sample 2: 11, 10, 12.5, 13, 15.5

D.2. Final prototype

Data set	Straight/Curve	Sample	Number of cycles [-]
1	Straight	Gelatin (12.5 mass%)	65, 64, 56, 66, 71, 75, 73, 84, 60, 59
2	Curve (R=59 mm)	Gelatin (12.5 mass%)	71, 68, 57, 86, 64, 66, 72, 58, 61, 91

E

Flexural rigidity

The flexural rigidity of the flexible shaft is measured in the following manner.

E.1. Experiment

E.1.1. Experimental goal

The goal of this experiment is to identify the flexural rigidity of the flexible shaft.

E.1.2. Experimental variables

The dependent variables are the applied force and deflection of the endpoint. This is the point where the force is applied.

E.1.3. Experimental facility

The flexible shaft and handle will be clamped. By elevating the load cell the tip is deflected, and the force needed for this deflection can be measured. The flexible shaft is assumed to be behave as an Euler-Bernoulli beam. This means that the flexural rigidity can be calculated with Equation E.1.

$$EI = \frac{FL^3}{3\delta} \tag{E.1}$$

With $F\,[N]$ is the applied force, $L\,[m]$ is the length between the fixation and the tip of the flexible shaft and $\delta\,[m]$ is the deflection of the endpoint. A Futek load cell (250 g) is used to measure the applied force. The load cell is calibrated to read 9.9 Volt when a force of 1.98 Newton is applied. A Scaime CPJ analog transmitter is used to amplify the voltage. The voltage is measured by using a Fluke 114 multi-meter. A schematic graph showing the measurement setup can be found in Figure E.1

E.1.4. Experimental protocol

The handle and the end of the flexible shaft are clamped. The distance between the horizontal reference and the tip of the shaft is measured. This is indicated as m_0 in Figure E.1. The output voltage of the load cell is noted. The load cell is elevated, resulting in a deflection of the tip of the shaft. The distance between a horizontal reference and the tip of the shaft is measured. This is indicated as m_1 in Figure E.1. Again the output voltage of the load cell is noted. This cycle in repeated multiple times until a deflection of approximately 30 mm is achieved. From there on the load cell is lowered is steps. For each step the distance between the horizontal reference and the tip is measured as well as the output voltage.

E.1.5. Data analysis

The data analysis will be performed in MATLAB 2015B.

E.2. Results

A force-deflection curve is generated which shows the hysteresis in the flexible shaft, see Figure E.2. The measured flexural rigidity determined based on the measurements is $3.7 * 10^{-3} \pm 3.2 * 10^{-4} [Nm^2]$

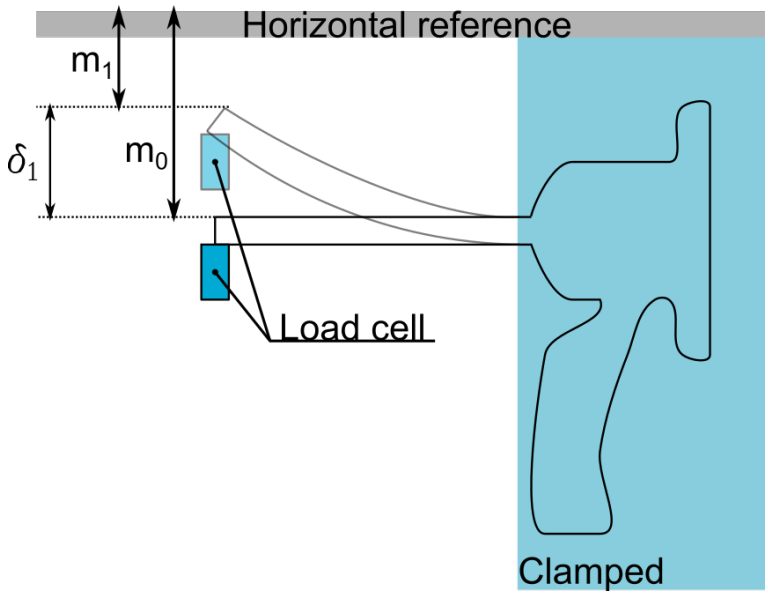

Figure E.1: Schematic representation of the measurement set up to measure both the applied force as well as the deflection. This measurement setup is used to determine the flexural rigidity of the flexible shaft.

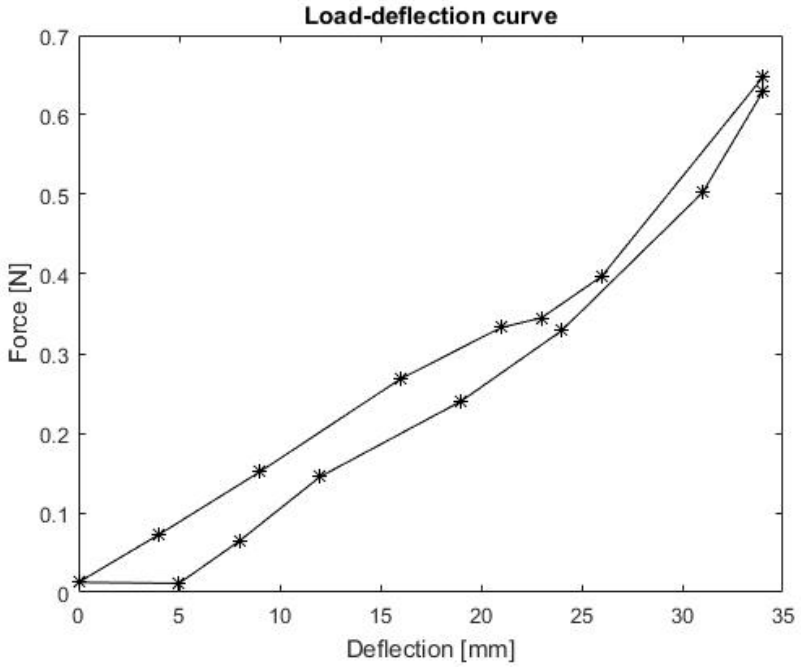

Figure E.2: Force-deflection curve showing the hysteresis present in the flexible shaft.

F

Bending effects

The flexible shaft is able to bend, but when bend, the blade at the inside of the curve spans a shorter path than the blade following the outer curve, as shown in Figure F.1. This difference in distance can, depending on the diameter of the flexible shaft and the angle of curvature, be big enough to complicate the transportation. Different solutions to eliminate this problem will be discussed below.

Counter bending

A curve in the flexible shaft results is a length difference in the path for each of the blades. This can be counter acted with a second curve in the opposite direction. This principle can be used in the flexible shaft and is schematically shown in Figure F.1 B. Part of the flexible shaft will not be inside the patients body and could thus be used to facilitate this 'counter bend'. This however also introduces complications. For instance, it is not priory known what curves the system will have to make. Therefore the compensating curves must be made during the procedure which will elongate the procedure time. Furthermore, the flexible shaft must be longer to leave enough space for the compensating curves. For the curve compensation extra space is needed while the space in an operation room is limited. In extreme cases the flexible shaft of the transport mechanism might get intertwined with other tubes and cables present in the OR. This cannot only result in problems for the transport mechanism but can also cause problems in other systems.

Spring

Springs can elongate easily. The elongation of a spring can be used to compensate for the length difference of the blades introduced due to curvature of the flexible shaft, see Figure F.1 C. The stiffness of the spring will influence the flexural rigidity of the transport mechanism. The stiffer the spring the more force is needed to achieve the same elongation of the spring therefore the flexible shaft will behave more stiff. Another disadvantage of adding a spring to the flexible shaft is that a spring needs more space than for instance a wire rope, while the space in the flexible shaft is limited.

Fixation

To avoid the problems caused by curves in the transport system, it can also be chosen to fixate the blades of the transport mechanism after it is placed in the correct position, see Figure F.1 D. This way there will be no length differences between the blades during the transportation of the tissue. The fixation of the blades requires an additional action during the procedure which elongates the procedure. Furthermore, for re-positioning of the transport mechanism, the blades must be loosened. After re-positioning the blades must be fixated again such that the transport mechanism is functional again.

wire rope loop

The length difference in the path between the wire ropes is dependent on the bending angle and the distance between the wire ropes. The wire ropes opposite each other will always have the same bending angle, which means that during bending one wire rope will have to be shorter and the other wire rope should be longer. By connecting the opposite wire ropes, the shortening of one wire rope can be compensated for with the elongation of the other wire rope, see Figure F.1 E. In order for this principle to work the wire ropes must be able to slide easily around. The friction-based transport is based on translating motion of the blades. To

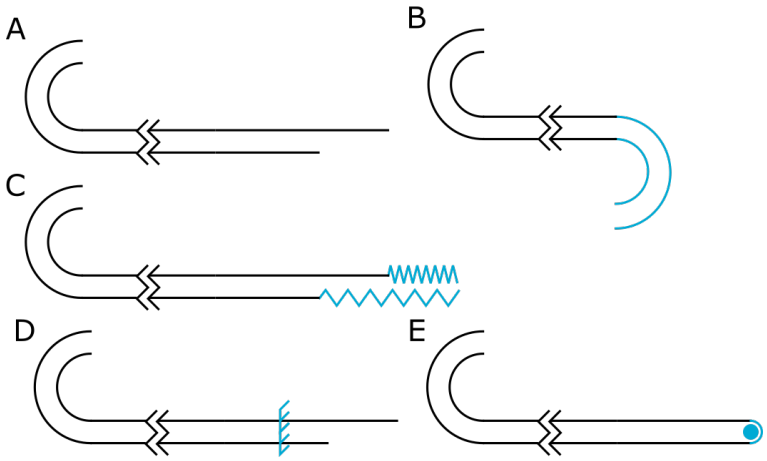

Figure F.1: Schematic representation of different solutions to compensate for the length difference between the blades that will occur during bending of the transport mechanism. A: Length difference between the blades that occurs during bending. B: Counter bending to compensate for the length difference. C: Use of springs to eliminate the length difference. D: Fixation of the blades after bending. E: Loop the blades such that the elongation of the first blade will compensate for the shortening of the opposite blade.

actuate the looped wire rope in a translating fashion while still allowing the wire rope to slide, a pulley could be used.

Bibliography

[1] *Acta Radiologica: Diagnosis*, 5(sup260):11–22, 1966.

[2] T. Ahmed, T. Zhang, K. He, S. Bai, and Z. Wang. Sense organs on the ovipositor of macrocentrus cingulum brischke (hymenoptera: Braconidae): their probable role in stinging, oviposition and host selection process. *Journal of Asia-Pacific Entomology*, 16(3):343–348, 2013.

[3] Mark N Appleyard, Charles A Mosse, Timothy N Mills, G Duncan Bell, Fortunato D Castillo, and C Paul Swain. The measurement of forces exerted during colonoscopy. *Gastrointestinal endoscopy*, 52(2):237–240, 2000.

[4] A. D. Austin and T. O. Browning. A mechanism for movement of eggs along insect ovipositors. *International Journal of Insect Morphology and Embryology*, 10(2):93–108, 1981.

[5] C. R. Calladine. *Theory of shell structures*. Cambridge University Press, 1989.

[6] William Dickey and Daphne Garrett. Colonoscope length and procedure efficiency. *The American journal of gastroenterology*, 97(1):79–82, 2002.

[7] A. E. Filippov, J. Klafter, and M. Urbakh. Friction through dynamical formation and rupture of molecular bonds. *Physical Review Letters*, 92(13):135503, 2004.

[8] Ying Han, Yoshiharu Uno, and Akihiro Munakata. Does flexible small-diameter colonoscope reduce insertion pain during colonoscopy? *World journal of gastroenterology*, 6(5):659, 2000.

[9] David Hellier, Faris Albermani, Brendon Evans, Hans De Visser, Clayton Adam, and Josh Passenger. Flexural and torsional rigidity of colonoscopes at room and body temperatures. *Proceedings of the Institution of Mechanical Engineers, Part H: Journal of Engineering in Medicine*, 225(4):389–399, 2011.

[10] Nicolae Lobontiu and Ephrahim Garcia. Two-axis flexure hinges with axially-collocated and symmetric notches. *Computers & structures*, 81(13):1329–1341, 2003.

[11] Loos and Co. Recommended bend radius. URL `https://www.loosco.com/resource-library/technical-information/recommended-bend-radius/`.

[12] James D Luketich, Miguel Alvelo-Rivera, Percival O Buenaventura, Neil A Christie, James S McCaughan, Virginia R Litle, Philip R Schauer, John M Close, and Hiran C Fernando. Minimally invasive esophagectomy: outcomes in 222 patients. *Annals of surgery*, 238(4):486, 2003.

[13] Liza Pelyhe, Anna Kertész, and Eszter Bognár. Flexibility of diagnostic catheters. 2014.

[14] P Posthoorn. The design of a self-propelling mechanism for an endoluminal robot. 2017.

[15] *Aspiration Catheters*. QualiMed Innovative Medizinprodukte GmbH.

[16] Maria Tiikkaja, Tommi Alanko, Harri Lindholm, Maila Hietanen, Juha Hartikainen, and Lauri Toivonen. Experimental study on malfunction of pacemakers due to exposure to different external magnetic fields. *Journal of interventional cardiac electrophysiology*, 34(1):19–27, 2012.

[17] I. A. van de Steeg. The design of the endo-tubular friction carrier, 2018.

[18] Xiaoming Zhang, Bo Qiang, and James Greenleaf. Comparison of the surface wave method and the indentation method for measuring the elasticity of gelatin phantoms of different concentrations. *Ultrasonics*, 51(2):157–164, 2011.